AWARD NUMBER: W81XWH-11-1-0250

TITLE: Tibial Bowing and Pseudarthrosis in Neurofibromatosis Type 1

PRINCIPAL INVESTIGATOR: Dr. David Stevenson

CONTRACTING ORGANIZATION: University of Utah
SALT LAKE CITY, UT 84112-9023

REPORT DATE: January 2015

TYPE OF REPORT: Final

PREPARED FOR: U.S. Army Medical Research and Materiel Command
Fort Detrick, Maryland 21702-5012

REPORT DOCUMENTATION PAGE

Form Approved
OMB No. 0704-0188

1. REPORT DATE	2. REPORT TYPE	3. DATES COVERED
January 2015	Final	04/01/2011-12/31/14

4. TITLE AND SUBTITLE
Tibial Bowing and Pseudathrosis in Neurofibromatosis Type 1

5a. CONTRACT NUMBER
W81XWH-11-1-0250

5b. GRANT NUMBER

5c. PROGRAM ELEMENT NUMBER

6. AUTHOR(S)
David Stevenson, MD

E-Mail: david.stevenson@hsc.utah.edu

5d. PROJECT NUMBER

5e. TASK NUMBER

5f. WORK UNIT NUMBER

7. PERFORMING ORGANIZATION NAME(S) AND ADDRESS(ES)

UNIVERSITY OF UTAH
201 PRESIDENTS CIR RM 4008
SALT LAKE CITY UT 84112-9023

8. PERFORMING ORGANIZATION REPORT NUMBER

9. SPONSORING / MONITORING AGENCY NAME(S) AND ADDRESS(ES)

U.S. Army Medical Research and Materiel Command
Fort Detrick, Maryland 21702-5012

10. SPONSOR/MONITOR'S ACRONYM(S)

11. SPONSOR/MONITOR'S REPORT NUMBER(S)

12. DISTRIBUTION / AVAILABILITY STATEMENT

Approved for Public Release; Distribution Unlimited

13. SUPPLEMENTARY NOTES

14. ABSTRACT

Anterolateral tibial bowing is a morbid skeletal manifestation observed in 5% of children with neurofibromatosis type 1 (NF1), typically identified in infancy. The majority of NF1 individuals with tibial bowing will sustain a fracture that will not heal (i.e. pseudarthrosis) resulting in multiple surgeries, poor limb function, and amputation. Some NF1 individuals with tibial bowing, however, do not fracture and the bowing improves over time. Clinical predictors to help drive management are lacking, and the pathophysiology of tibial bowing and pseudarthrosis is not well understood. Our objective was to identify clinical predictors of tibial pseudarthrosis and better understand its pathophysiology. The data showed that quantitative bone ultrasound was able to distinguish an affected leg in individuals with neurofibromatosis type 1 (NF1). This further confirms a decrease of bone mineralization of the bowed tibia. The importance of this finding is that this can now be used as an outcome measure for clinical trials.. We also confirmed the molecular etiology of tibial dysplasia as double inactivation of the NF1 gene. In addition, we provide evidence that the periosteum likely harbors the somatic mutation.

15. SUBJECT TERMS
Neurofibromatosis type 1, bone, pseudarthrosis

16. SECURITY CLASSIFICATION OF:			17. LIMITATION OF ABSTRACT	18. NUMBER OF PAGES	19a. NAME OF RESPONSIBLE PERSON
a. REPORT	b. ABSTRACT	c. THIS PAGE			USAMRMC
Unclassified	Unclassified	Unclassified	Unclassified	77	19b. TELEPHONE NUMBER *(include area code)*

Table of Contents

Tibial Bowing and Pseudarthrosis in Neurofibromatosis Type 1

(PI: David Stevenson, MD)

Introduction

Anterolateral tibial bowing is a morbid skeletal manifestation observed in 5% of children with neurofibromatosis type 1 (NF1), typically identified in infancy (Friedman and Birch, 1997). The majority of NF1 individuals with tibial bowing will sustain a fracture that will not heal (i.e. pseudarthrosis) resulting in multiple surgeries, poor limb function, and amputation. Some NF1 individuals with tibial bowing, however, will not fracture and the bowing improves over time (Stevenson et al., 2009). Clinical predictors to help drive management are lacking, and the pathophysiology of tibial bowing and pseudarthrosis is not well understood. Our objective was to identify clinical predictors of tibial pseudarthrosis and better understand its pathophysiology. Our integrative proposal helped gain novel information about the pathophysiology of tibial bowing and pseudarthrosis using techniques innovative in respect to their application to NF1 tibial dysplasia. As part of the study we made progress toward validation of the use of an imaging modality for tibial bowing for clinical trials and clinical practice. We will also described osteoclast function in individuals with tibial bowing. Additionally we provided novel information on genetic modifiers and pathophysiology of the skeletal phenotype of NF1. Ultimately, as described below, our proposal helped in the development of methods to create personalized treatment protocols based on an NF1 individual's quantitative ultrasound measurements, osteolytic activity, and somatic mutation profile.

Body

The following section will describe the research accomplishments associated with each task outlined in the approved Statement of Work.

The individual tasks are underlined below followed by a description of accomplishments related to the task.

Task 1. Plan Development, Patient Recruitment, and Institutional Review (Months 0-6):

a. Train a clinical coordinator to identify potential subjects and contact appropriate providers to offer enrollment.

-We trained Heather Hanson as a clinical coordinator on the project. Heather met personally with the investigators to discuss the project and critical areas including timing of shipment of blood, consenting, number of participants needed and enrollment criteria.

The clinical coordinator investigated and made contact with organizations that were likely to have contact with individuals who have neurofibromatosis type 1 and tibial bowing prior to fracture. We continued to send out recruitment flyers to NF support groups and orthopedic agencies. In

addition, Dr. Stevenson spoke and gave presentations at several NF support group functions and attempted to provide wider knowledge of the study.

b. Review current research registries to identify and prioritize individuals for recruitment with primary focus in first 6 months on recruitment of individuals with tibial bowing.

-We have an NF Registry in which individuals with NF1 were recruited and consented to be contacted for future studies. As part of the NF Registry clinical information is contained in our database. We searched our NF registries for individuals with long bone bowing and NF1 individuals who could serve as controls who have agreed to be contacted for future research. We previously identified these individuals who are potential study participants for future contact. We focused on those with tibial bowing primarily.

We also recruited individuals coming to the University of Utah for clinical or research purposes for convenience to the family.

c. Arrange requests, procedures and transfer of prospectively acquired tissue from the NF1 Orthopedic Core Facility (NOCF) for analysis for Specific Aim 3.

-We previously received samples from the NOCF that were located at the Shrine Hospital in SLC and the samples are now at the University of Utah.

d. Assure compliance with USAMRMC and home institutional guidelines on research involving human subjects.

-This was done.

Task 2. Data Collection, QUS Imaging, and Molecular Analysis (Months 6-42):

a. Continue to recruit subjects for all specific aims. A projected 150 individuals with NF1 will be recruited over the course of the 3-year period (35 individuals for Specific Aim 1).

-We enrolled 23 individuals with NF1 with tibial bowing. We enrolled 93 individuals with NF1 without tibial bowing to function as controls. To help in recruitment primarily of NF1 individuals with bowing, Dr. Stevenson previously traveled to the Children's Tumor Foundation (CTF) NF Forum for advertisement to the US clinic coordinators and chapter leaders and the study was highlighted by CTF on their website. In addition the study was advertised through the CTF Registry. However, given the rarity of the condition we were unable to recruit the desired number of individuals, although we do not think this dramatically hindered the results (see analyses below).

Examples of the radiographs of a few of the NFI individuals with tibia bowing who have enrolled are shown in **Fig.1** and document the anterolateral

bowing that is typically seen in individuals with NF1. However, the radiographs also show that there is variability in the radiographic features of each individual with NF1 in terms of the tibial structure. This suggests that not all individuals with NF1 who have tibial dysplasia will have the same bone architecture and may result in varying clinical outcomes.

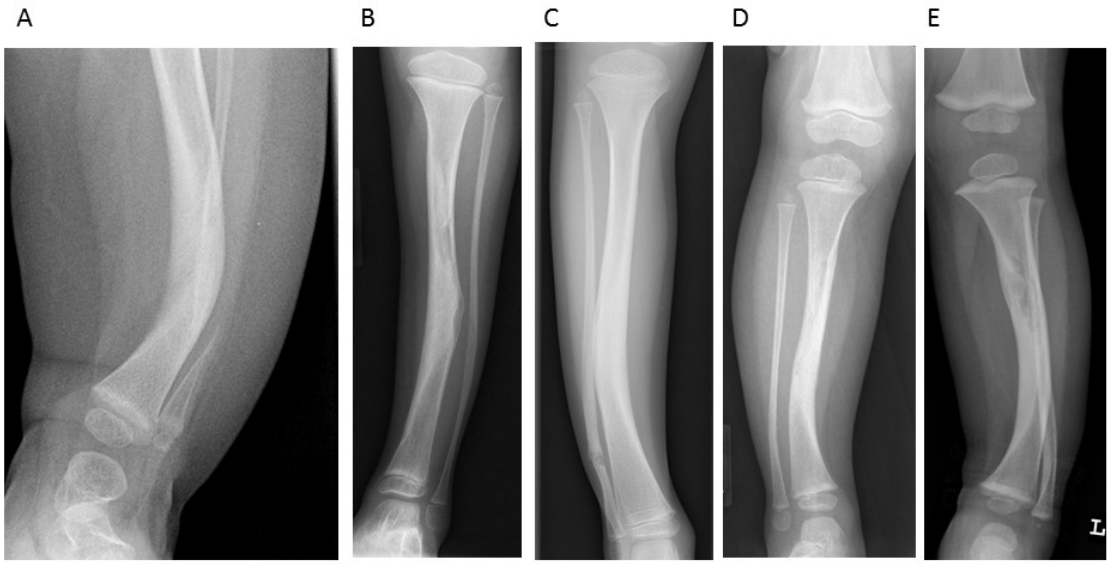

Figure 1. Examples of radiographs (A-E) of the bowed leg of different individuals with NF1 with tibial dysplasia who have enrolled.

b. Document findings from physical examinations and medical histories on NF1 exam forms for data entry upon enrollment.

-All affected individuals were personally examined by Dr. Stevenson and the subjects filled our releases of information to obtain radiographs and medical reports to ensure appropriate diagnosis and categorization. Findings were documented through standardized exam forms and entered into spreadsheets by the research coordinator.

c. Biannual phone interviews with individuals with tibial bowing enrolled in Specific Aim 1.

-We performed biannual phone interviews for individuals with tibial bowing who have reached their required time for phone interviews. In addition we have informed all subjects and their families to contact us for any fracture or surgical intervention.

To date, 3 individuals have sustained a tibial fracture and one individual underwent elective surgery prior to fracture. One individual (Participant #1) sustained a fracture of the tibia and had an intramedullary rod placed. The second individual (Participant #9) sustained a fracture of the tibia and had an external fixator placed. The third individual (participant #14) sustained a tibial fracture and also had an intramedullary rod placed. Another individual

(Participant #12) elected to undergo surgical procedures to correct the bowing prior to fracture (See **Fig. 2).**

Fig. 2. Radiograph of Participant #12 who had surgical intervention to try and decrease the degree of bowing.

d. Obtain QUS at baseline on all NF1 individuals with anterolateral tibial bowing (Specific Aim 1).

-We obtained quantitative ultrasound measurements on both legs of participants with tibial bowing. Decreased z-scores for speed of sound as measured by the quantitative ultrasound machine were observed in the affected tibia in 19/23 participants (see results in **Table 1**), and in 2 of the individuals with positive or neutral z-score differences we think that these individuals had physiologic bowing and not pathologic tibial dysplasia (see **Figures 3,4**).

Statistical analysis showed significant differences in the speed of sound (SOS) [mean -187, SD 239, p=0.001], and z-score [mean -2.07, SD 2.67; p=0.001] between the mean differences of the affected vs. unaffected leg. The statistical significance increased dramatically when the 2 individuals with what we think are physiologic bowing are excluded [SOS mean -219, SD 222, p=0.0002; Z-score mean -2.43, SD 2.49, p=0.0002].

Since only a few of the individuals have yet fractured, we are unable to determine if the degree of difference in the speed of sound z-scores as measured by quantitative ultrasound between the bowed and non-bowed tibia can help predict who will fracture. However, two of the three individuals who fractured had the largest negative difference of z-score between the bowed and non-bowed tibia (z-scores of -8.0 and -5.0). Future longitudinal follow up beyond the scope of this proposal will help in determining the ultimate clinical utility of bone ultrasound.

Table 1. Mean Z-scores of Speed of Sound from Quantitative Ultrasound of Bowed and Non-bowed Tibia in NF1 Individuals

	Tibia Affected	Z-score Right Tibia	Z-score Left Tibia	Difference between bowed and non-bowed tibia
Participant #1	Left	-0.7	-1.0	-0.3
Participant #2	Left	-3.3	-2.4	+0.9
Participant #3	Left	+1.3	-1.0	-2.3
Participant #4	Right	-3.7	-0.7	-3.0
Participant #5	Right	-0.5	+0.3	-0.7
Participant #6	Right	-4.2	-1.7	-2.5
Participant #7	Left	-0.3	-1.0	-0.7
Participant #8	Left	-0.3	-3.9	-3.6
Participant #9	Right	-7.5	+0.5	-8.0
Participant #10	Right	-4.5	-0.7	-3.2
Participant #11	Right	-3.2	-2.4	-0.8
Participant #12	Left	+3.2	-5.2	-8.4
*Participant #13	Left	0	+2.6	+2.6*
Participant #14	Right	-5.2	-0.2	-5.0
*Participant #15	Right	-0.1	-0.8	+0.7*
Participant #16	Left	-2.3	-3.9	-1.6
Participant #17	Right	-2.2	-0.5	-1.7
Participant #18	Left	+0.7	-2.8	-3.5
Participant #19	Left	0.9	-2.8	-3.7
Participant #20	Right	-0.4	-0.2	-0.2
Participant #21	Left	-0.5	-0.5	0
Participant #22	Right	-1.0	+0.2	-1.2
Participant #23	Left	+1.1	-1.4	-2.5

*These two individuals had very minimal lateral vs. anterolateral bowing without radiographic findings of tibial dysplasia (ie. cortical thickening and medullary canal narrowing) – see **Figure 3 and 4** and although these individuals were initially included in the study as they were referred and being treated as tibial dysplasia, we think given the young age when the bowing was noted is most consistent with probably physiologic bowing of infancy and hence an indicator that bone ultrasound is helpful in differentiating pathologic tibial bowing vs. physiologic bowing. Longitudinal follow-up will help clarify this question.

A. 

B. 
C. 

D. 

Fig. 3. Radiograph of Participant #13 with minimal anterior bowing on left (B,C) compared to right (A), and no significant lateral bowing without cortical thickening or medullary canal narrowing. This was very difficult to discern on examination (D).

A. 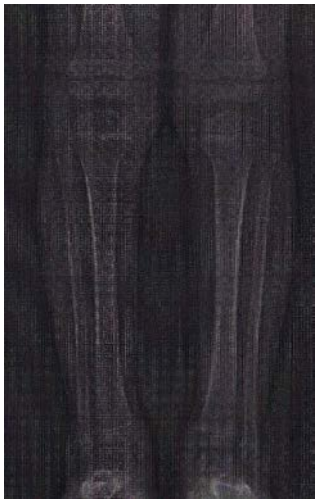
B. 

Fig. 4. (A) Radiograph of Participant #15 with history per parent of tibial bowing that was thought to be bilateral with possible increase on the right. Bracing was used bilaterally for 6 months and then stopped. (B) Upon our examination we could not see any anterior bowing and only mild bilateral bowing which we thought was likely within normal limits and most consistent with physiologic bowing.

Examples of photos of the bowed tibia of each NF1 individual with tibial bowing that have been enrolled are shown below in **Fig. 5**.

Figure 5. Photographs of the bowed leg of the 23 individuals with NF1 with tibial dysplasia.

e. Obtain urine samples for urinary crosslink measurements to be performed at the University of Utah (Specific Aim 2).

-We have obtained urine samples from NF1 individuals who have enrolled and the urine was frozen prior to being sent for analysis. Urine samples were sent to Dr. Pasquali's laboratory for pyridinium crosslink analysis. Results of the pyridinium crosslinks for affected individuals are shown in Table 2. The average DPD/PYD ratio was 0.32, which is well above the mean that we have previously reported in children without NF1 (i.e. approximately 0.22) (Stevenson et al. 2010). Some individuals did not return urine samples and hence the number of individuals with results are smaller than the number enrolled. A general linear model controlling for age and sex was used. However, there were no statistically significant differences between NF1 individuals with and without tibial bowing. This suggests that pyridinium crosslinks may not be optimal surrogate markers for clinical trials of tibial bowing.

Table 2. Urine Pyridinium Crosslink in individuals with Tibial Bowing.

NF1 individuals with Tibial Bowing	Pyridinoline (PYD) umol/mol creatinine	Deoxy-pyridinoline (DPD) umol/mol creatinine	DPD/PYD Ratio
NF1-07	408	141	0.35
NF1-211	524	150	0.29
NF1-217	127	33	0.26
NF1-223	250	65	0.26
NF1-225	211	54	0.26
NF1-229	508	128	0.25
NF1-231	290	93	0.32
NF1-232	290	90	0.32
NF1-243	412	147	0.36
NF1-246	357	107	0.30
NF1-254	358	147	0.41
NF1-257	507	174	0.35
NF1-260	654	201	0.31
NF1-265	448	166	0.37
NF1-269	387	122	0.36
NF1-266	220	71	0.33
NF1-270	532	211	0.39
NF1-271	347	122	0.36
NF1-175	256	95	0.37
NF1-274	54	18	0.34
NF1-275	314	119	0.38
NF1-279	86	30	0.36

*Measurements are average of two consecutive first morning voids.

f. Obtain blood samples for pit resorption assays to be shipped and performed at Indiana University (Specific Aim 2).

-Blood samples for pit resorption assays were obtained on individuals with tibial bowing and NF1 individuals without tibial bowing. Samples were shipped via FedEx to Dr. Yang at Indiana University.

After osteoclast culture, the number of osteoclasts per field were analyzed. Individuals with NF1 had larger multinucleated osteoclasts with an increase in the osteloclast area per field compared to healthy control cohort. However, there was no significant difference between NF1 individuals with and without tibial bowing (Fig. 6).

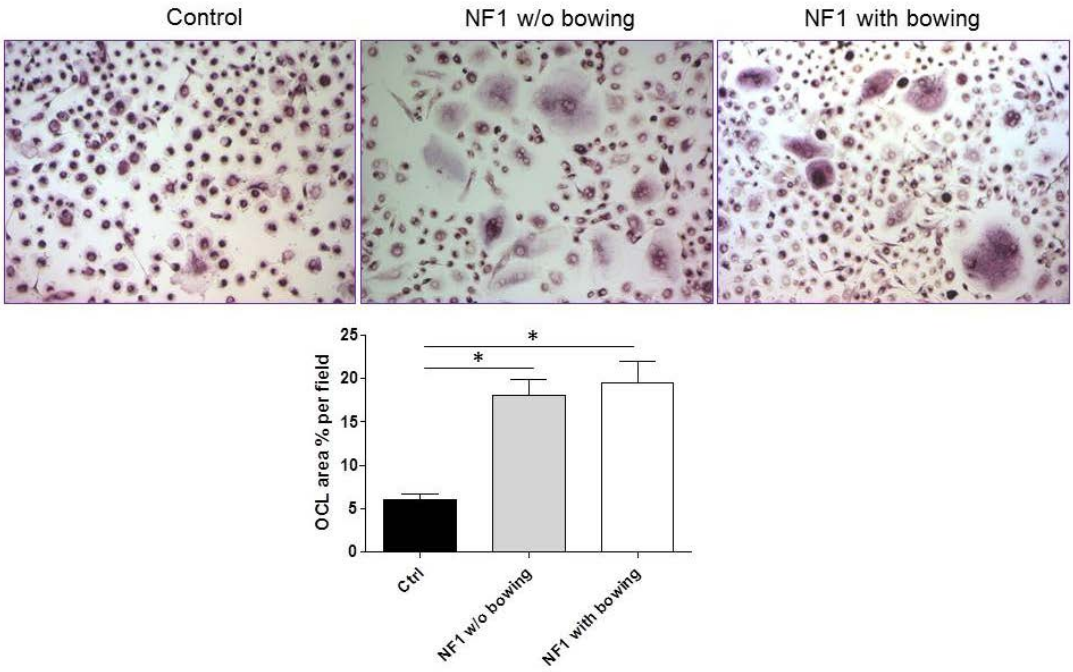

Figure 6. Top panel: Example of osteoclast area per field in an individual without NF1, NF1 individual without tibial bowing, and an individual with NF1 with tibia bowing. **Bottom panel:** Percent of osteoclast area per field is increased in the NF1 individuals compared to controls but no significant difference between NF1 individuals with and without tibial bowing.

In **Figure 7** we show data that osteoclast activity is increased in NF1 compared to controls as we have previously described (Stevenson et al., 2011), and that pit resorption in individuals with NF1 with bowing compared to NF1 individuals without bowing is increased.

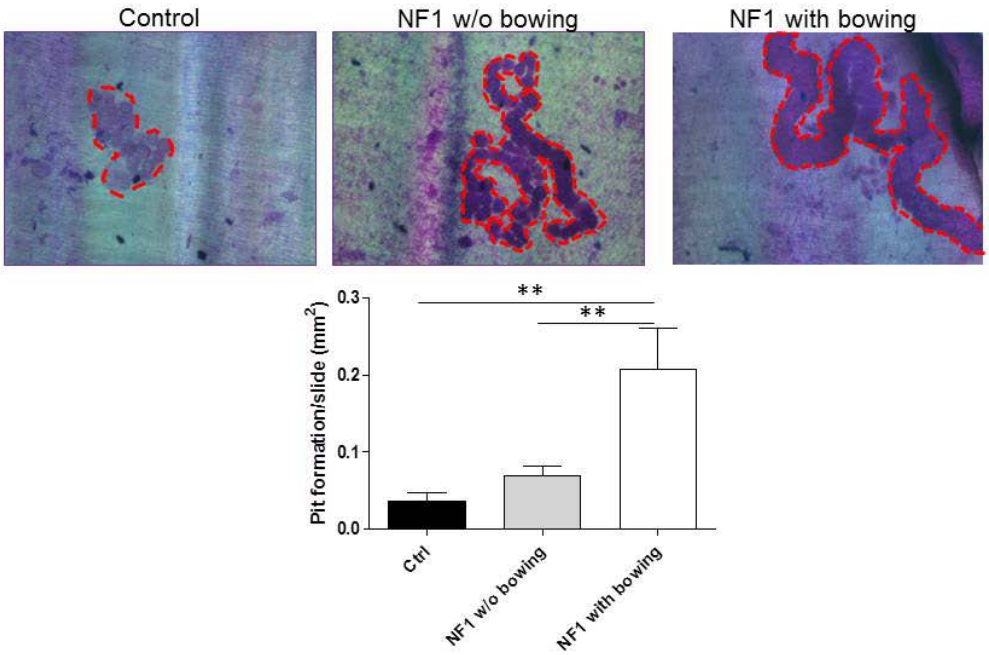

Figure 7. Top panel: Example of resorption area (outlined in dotted red line) of an individual without NF1, NF1 individual without tibial bowing, and an individual with NF1 with tibia bowing. **Bottom panel:** Percent of pit resorption area per low power field is increased in the NF1 individuals with bowing compared to NF1 individuals without bowing and controls.

g. <u>Perform genetic analyses (next-generation sequencing and confirmation Sanger sequencing) and histologic evaluations on osseous tissue specimens obtained at the University of Utah. These analyses will take place with prioritized fashion with first analyses on prospectively acquired tissue and subsequently analyze archived tissues beginning in the second year of the proposal (Specific Aim 3).</u>

-We have continued to collect tissue samples from individuals with tibial pseudarthrosis. We have collected discarded tissue from surgical procedures of two of the individuals with tibial bowing proceeded to fracture in March 2014, and we are currently processing the sample (example of tissue shown **Fig. 8**).

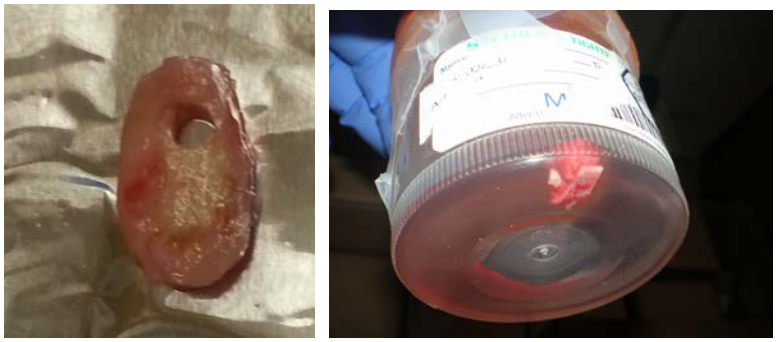

Figure 8. Tissue sample from surgery of two different participants (A and B) who developed fracture of the bowed tibia.

We have extracted DNA from peripheral blood of all individuals with tibial bowing and will continue to monitor them for development of fracture. For the individuals who have fractured in which we have tissue (see Fig. 7), we extracted DNA from bone for exome sequencing. Whole genome amplification was also performed on the DNA extracted from several other individuals with stored pseudarthrosis tissue. Given the advances in next generation sequencing we utilized exome sequencing for our analyses. As mentioned in the task above these analyses took place in a prioritized fashion given the cost of next generation sequencing (i.e. exome sequencing).

DNA extraction from bone and whole genome amplification (WGA): DNA extraction from bone is challenging. There are three key facts which affect the yield of the DNA extraction; 1) There are low cell numbers (e.g. osteocytes) in bone, 2) release of DNA from osteocytes nucleus is difficult, 3) calcium precipitation. A Qiagene kit was used for DNA extraction from bone tissue. Figure 9 is gel picture for the DNA extractions from four different pieces of the bone from tibial dysplasia. 10 ug of bone has been used for each extraction. The yield of DNA is between 50ng and 1000ng/ per sample. Due to the low yield of DNA whole genome amplification was pursued to meet the requirement for exome sequencing (200 ug of DNA required from Illumina TrueSeq Exome capture, 1.5ug of DNA for Nimblegen Exome and 3ug of DNA for Agilent Exome capture). Whole genome amplification has been performed on some of the samples with low yield of DNA using GenomePlex® (Sigma-Aldrich Co.). Please see the gel pic show below showing post amplification. The fist WGA yielded 981.3ng/ul in 100 ul of DNA and the second WGA (lane 2) yielded 983.7 ng/ul in 100 ul of DNA, see Figure 9.

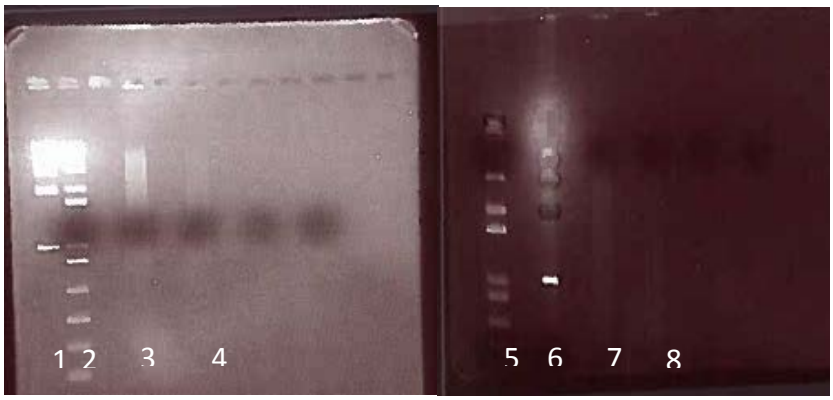

Figure 9. DNA extractions from four pieces of bone tissue from a patient. Lane 1,2,5,6 are the molecular weight markers. Lane 3,4,7,8 are DNA from different extractions.

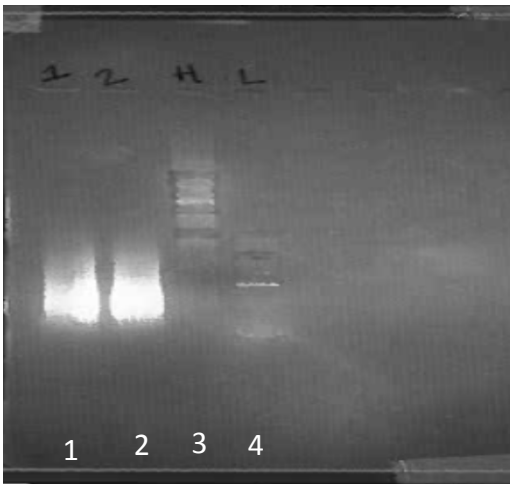

Figure 10. Lane 1 and 2 are whole genome amplifications from the same sample. Lane 3 is high molecular weight marker, Lane 4 is 50bp molecular weight marker.

Exome Sequencing: Our amended approach from our initial proposal was to use exome sequencing to examine the entire coding region of the genome. A significant finding is that we have been able to identify a second hit in 6/8 individuals, and in the one individual without a confirmed somatic *NF1* mutation there is still the question of a possible second hit (IVS+1,ex15) (Table 3). This dramatically shifts the thought that mutations in other genes are the causative factor for tibial dysplasia in NF1. In communication with collaborators from a different institution (Dr. Rios – personal communication), this is further confirmed and hence we think that double inactivation of *NF1* is necessary for development of tibial dysplasia in NF1. These results have

been published in the Journal of Bone and Mineral Research (Paria et al., 2014).

Table 3. *NF1* Mutations in Pseudarthrosis Tissue vs. Germline

Age at Diagnosis/Presentation	**NF1 Inherited**	**NF1 Somatic**
Birth (bowing); fracture 18 month	p.R1849Q	17q LOH
Bowing noticed at 2 months; 7 years of age sx for PA	IVS-2, ex15	p.N45fs
Pseudarthrosis at 10 years (amputation at 18 years)	p.V7155fs	? IVS+1,ex15
Bowing noted at birth; fracture at 3 mo	IVS-2,ex2	p.E1192X
Fracture at 2 weeks	n.d.	p.R1276X
Bowing at birth; fracture at ~3 years	p.585Lfs	n.d.
Bowing noted as infant; fracture at ~3 year	p.1152Lfs	17q LOH
Birth (bowing); never fractured but surgery and bone removed due to degree of bowing	p.1061Vfs	p.1199Tfs

It is still unknown what cell type harbors the specific *NF1* second hit. Based on our results of the samples analyzed in Table 3, there is low level mosaicism providing evidence of a mixed cellular population. This may be the reason for the ambiguity of whether or not there is a somatic mutation in the single case in Table 3. However, in one individual we were able to perform analysis of 4 samples (blood, combination of bone and hypercellular pseudarathrosis tissue, and separated cortical bone and pseudarthrosis tissue from the same surgical site). The results showed that the pseudarthrosis tissue harbored the somatic mutation while the cortical bone portion did not (see **Figure 11**). This suggests that the somatic mutation likely arises from progenitor cells that give rise to the hypercellular proliferating tissue and very likely from the periosteal region. These results have been submitted and accepted for publication in the Journal of Medical Genetics. We envision future studies to analyze separate sections from tissue blocks of individuals with tibial pseudarthrosis to further determine the specific tissue in which the second hit occurred (i.e. cortical bone, periosteum, etc.).

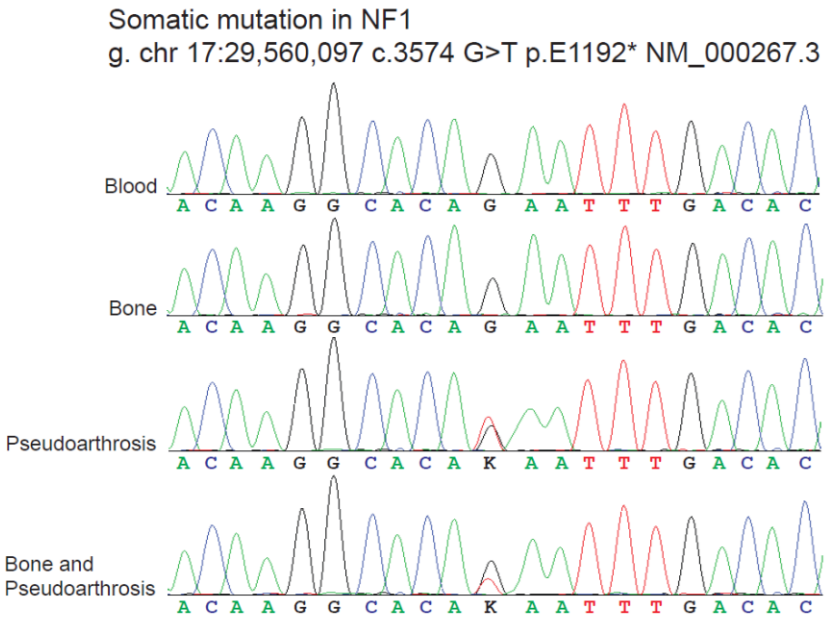

Figure 11. Comparison of the somatic mutation in an individual with neurofibromatosis type 1 (NF1) and tibial pseudathrosis. The top panel show sequence from DNA extracted from blood. The bottom 3 panels show sequence from DNA extracted from different sections of the surgical sample. The somatic mutation is not shown in DNA extracted from the sample that was purely bone and lower levels of the mutation seen in the mixed bone and pseudoarthrosis sample suggesting that the somatic mutation arises from the hypercellular proliferating tissue in between the bone segments likely from the periosteum.

We also performed exome sequencing on matched blood and tibial pseudarthrosis samples of 2 individuals with tibial pseudarthrosis without NF1 clinically. In these two individuals we did not identify a pathogenic germline NF1 mutation, which is to be expected given the lack of other NF1 clinical features. However, we also did not identify a pathogenic somatic mutation in the bone tissue. This provides further evidence that the tibial pseudarthrosis in individuals without NF1 are due to a different molecular process.

Even though our data are quite convincing that the salient factor for tibial dysplasia development is double inactivation of *NF1*, there is still a possibility of modifier genes impacting the subsequent natural history of tibial bowing, as not all individuals with tibial bowing fracture and there is variable expressivity. We first used a tier analysis to first analyze the 16 genes in RAS/MAPK Pathway as initially proposed. Using a variant analysis for the whole blood sample compared to bone tissue, the mutations in only bone tissue were considered as secondary events and more likely to play a role as genetic modifiers of pseudarthrosis. We identified a number of variants in other genes using exome sequencing, but none that were consistent between individuals or that had significant relevance to the RAS/MAPK pathway or dramatic

biologic plausibility. However, future studies may shed light on modifying effects of these variants.

However, in one sample we identified a germline variant in *PTPN11* which is involved in the RAS/MAPK signal transduction pathway (see **Figure 12**). However, this variant is not a somatic event, although it could still provide a modifying event and the child had severe bowing and pseudarthrosis that required amputation. These data have been submitted and accepted for publication in the Journal of Medical Genetics (Sant et al., 2015).

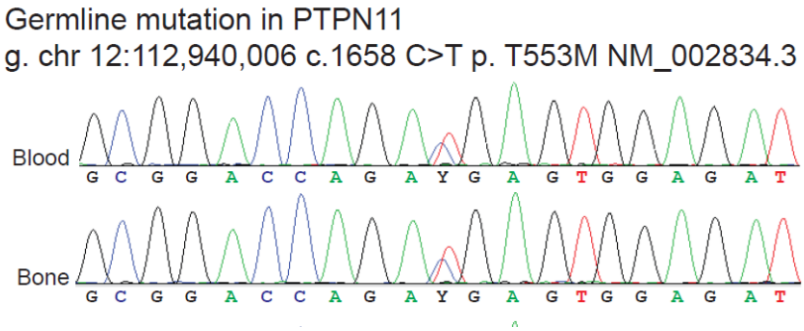

Figure 12. Comparison of Sanger sequencing of variant identified in *PTPN11* from exome sequencing showing *PTPN11* variant in both blood and bone tissue.

h. <u>Interim analyses and manuscripts.</u>
-Interim analyses and manuscripts were performed and submitted as stated in previous annual reports.

i. <u>Annual reports will be written.</u>
-Annual reports were written and submitted previously.

Task 3. Data Analysis (Months 42-48):

a. Review the data entered and updates fracture and surgical history from biannual phone interviews.
-This has been performed as described above.
b. Perform statistical analysis of data from QUS, urine crosslinks, and osteoclast pit resorption assays.
-This has been done and described above in the respective sections.
c. Summarize the results of genetic and histologic analyses of osseous tissue.
-This is described above.
d. A final report will be written.
-This is the final report.

Key Research Accomplishments

- Enrollment of 116 individuals with NF1.
- Twenty-three individuals with NF1 with tibial bowing without fracture have been recruited and medical histories and examinations documented and followed prospectively.
- Quantitative ultrasound measurements show decreases in the speed of sound of the affected leg compared to the unaffected leg in 19/23 individuals, and in 2 of the 4 individuals with positive or neutral z-score differences we think that the individuals have physiologic bowing rather than tibial dysplasia. This is a key finding as it will allow for future surrogate marker for clinical trials focused on therapeutics to improve bone quality prior to fracture in a non-invasive and age specific manner
- DNA extraction from peripheral blood for somatic mutation comparison in tibial tissue.
- Successful whole genome amplification of pseudarthrosis tissue.
- Documentation of double inactivation in *NF1* in tissue samples as the primary event leading to tibial dysplasia.
- Data showing absence of somatic mutation in the cortical bone but presence of somatic mutation in hyperproliferative pseudathrosis tissue.
- Confirmation of increased bone resorption in NF1.

Reportable Outcomes
Given that this proposal is primarily prospective in which we are following NF1 individuals with tibial bowing over time to see who will fracture, reportable outcomes and research accomplishments will be limited within the timeframe of the grant. However the following manuscripts have been accepted/published.

Plotkin SR, Albers AC, Babovic-Vuksanovic D, Blakeley JO, Breakefield XO, Dunn CM, Evans DG, Fisher MJ, Friedman JM, Giovannini M, Gutmann DH, Kalamarides M, McClatchey AI, Messiaen L, Morrison H, Parkinson DB, Stemmer-Rachamimov AO, Van Raamsdonk CD, Riccardi VM, Rosser T, Schindeler A, Smith MJ, **Stevenson DA**, Ullrich NJ, van der Vaart T, Weiss B, Widemann BC, Zhu Y, Bakker AC, Lloyd AC. Update from the 2013 International Neurofibromatosis Conference. Am J Med Genet A 2014;164A:2969-78.

Paria N, Cho TJ, Choi IH, Kamiya N, Keyembe K, Mao R, Margraf RL, Obermosser G, Oxendine I, Sant DW, Song MH, **Stevenson DA**, Viskochil DH, Wise CA, Kim HKW, Rios JJ. Neurofibromin Deficiency-Associated Transcriptional Dysregulation Suggests a Novel Therapy for Tibial Pseudoarthrosis in NF1. J Bone Miner Res 2014;29:2636-42.

de la Croix Ndong J, Makowski AJ, Uppuganti S, Vignaux G, Ono K, Perrien DS, Joubert S, Baglio SR, Granchi D, **Stevenson DA,** Rios JJ, Nyman JS, Elefteriou F. Asfotase-α improves bone growth, mineralization and strength in mouse models of neurofibromatosis type-1. Nat Med 2014;20:904-10.

Sant DW, Margraf RL, **Stevenson DA**, Grossmann AH, Viskochil DH, Hanson H, Everitt MD, Rios JJ, Elefteriou F, Hennessey T, Mao R. Evaluation of somatic mutations in tibial pseudarthrosis samples in neurofibromatosis type 1. J Med Genet (2015 – in press).

The following abstracts and presentations were given in which aspects of the current study supported some of the rationale for discussion:

> **Stevenson DA**, Allen S, Tidyman WE, Carey JC, Viskochil DH, Stevens A, Hanson H, Sheng X, Thompson GA, Okumura M, Reinker K, Johnson B, Rauen KA. Peripheral muscle weakness in RASopathies. Oral presentation at the Western Society for Pediatric Research, Carmel, California, January, 2012.
>
> *Bone Health in NF1*. Invited speaker at the Children's Tumor Foundation NF Forum. New Orleans, Louisiana (June, 2012)
>
> *Physical Fitness and Muscle in NF1*. Invited speaker at the Children's Tumor Foundation NF Forum. Nashville, TN, April, 2013.

Comparison of the Musculoskeletal Findings in RASopathies. Invited speaker at the Bone Series, Vanderbilt University, Nashville, TN, April, 2013.

Muscle in NF1. Invited speaker at the Children's Tumor Foundation International NF Conference, Monterrey, CA, June, 2013.

Andresen BS, Hartung AM, Swensen J, Uriz IE, Lapin M, Carey JC, Calhoun A, Yu P, Vaughn CP, Dobrowolski SF, Larsen MR, Hanson H, **Stevenson DA**. Splicing of HRAS exon 2 is vulnerable: The splicing efficiency of activating mutations in codons 12 and 13 determines Costello syndrome phenotype. ASHG, Boston, MA, Oct. 2013.

Stevenson DA, Slater H, Hanson H, Stevens A, Carey JC, Viskochil DH. Use of quantitative ultrasound for tibial dysplasia in neurofibromatosis type 1. ASHG, Boston, MA, Oct. 2013.

The Musculoskeletal Findings in NF1. Invited speaker at the BC Neurofibromatosis Foundation Conference in Vancouver, Canada, October, 2013.

Neurofibromatosis and the Rasopathies. Pediatric Grand Rounds at the University of Iowa, Iowa City, Iowa, May, 2014.

Physical Fitness in NF1. Invited speaker at the NF Forum in Iowa City, Iowa, May, 2014.

Tibial Pseudarthrosis in NF1. Invited speaker at the University of Minnesota NF symposium. St. Paul, MN, May, 2014.

Conclusion

Our integrative proposal helped gain novel information about the pathophysiology of tibial bowing and pseudarthrosis. The data show that quantitative bone ultrasound is able to distinguish an affected leg in individuals with neurofibromatosis type 1 (NF1). This further confirms a decrease of bone mineralization of the bowed tibia. The importance of this finding is that this can now be used as an outcome measure for clinical trials. Our data also confirm that individuals with NF1 have increased bone resorption markers, but there was no difference of individuals with NF1 with and without tibial dysplasia. Osteolytic activity was increased in individuals with NF1. We also confirmed the molecular etiology of tibial dysplasia as double inactivation of the NF1 gene. In addition, we provide evidence that the periosteum likely harbors the somatic mutation.

References

1. Friedman JM, Birch PH. Type 1 Neurofibromatosis: A descriptive analysis of the disorder in 1728 patients. Am J Med Genet 1997;70:138-143.
2. Stevenson DA, Carey JC, Viskochil DH, Moyer-Mileur LJ, Slater H, Murray MA, D'Astous JL, Murray KA. Analysis of radiographic characteristics of anterolateral bowing of the lower leg prior to fracture in neurofibromatosis type 1. J Pediatr Orthop 2009;29:385-92.
3. Stevenson DA, Yan J, He Y, Li H, Liu Y, Jing Y, Guo Z, Zhang Q, Zhang W, Yang D, Wu X, Hanson H, Li X, Staser K, Viskochil DH, Carey JC, Chen S, Miller L, Roberson K, Moyer-Mileur L, Yang FC. Multiple increased osteoclast functions in individuals with neurofibromatosis type 1. Am J Med Genet A 2011;155:1050-9.
4. Stevenson DA, Schwarz EL, Carey JC, Viskochil DH, Hanson H, Bauer S, Weng HYC, Greene T, Reinker K, Swensen J, Chan RJ, Yang FC, Senbanjo L, Yang Z, Mao R, Pasquali M. Bone resorption in syndromes of the Ras/MAPK Pathway. Clin Genet 2010 [Epub ahead of print].
5. Paria N, Cho TJ, Choi IH, Kamiya N, Keyembe K, Mao R, Margraf RL, Obermosser G, Oxendine I, Sant DW, Song MH, Stevenson DA, Viskochil DH, Wise CA, Kim HKW, Rios JJ. Neurofibromin Deficiency-Associated Transcriptional Dysregulation Suggests a Novel Therapy for Tibial Pseudoarthrosis in NF1. J Bone Miner Res 2014;29:2636-42.
6. Sant DW, Margraf RL, Stevenson DA, Grossmann AH, Viskochil DH, Hanson H, Everitt MD, Rios JJ, Elefteriou F, Hennessey T, Mao R. Evaluation of somatic mutations in tibial pseudarthrosis samples in neurofibromatosis type 1. J Med Genet (2015 – in press).

List of Personnel

David A. Stevenson
Heather Hanson
Rong Mao
David Viskochil
Xiaoming Sheng
Laurie Moyer-Mileur
Feng-Chun Yang

Appendices

Appendix #1:
Manuscript (Plotkin et al. Update from the 2013 International Neurofibromatosis Conference. Am J Med Genet A 2014;164A:2969-78.)

Appendix #2:
Manuscript (Paria et al. Neurofibromin Deficiency-Associated Transcriptional Dysregulation Suggests a Novel Therapy for Tibial Pseudoarthrosis in NF1. J Bone Miner Res 2014;29:2636-42.)

Appendix #3:
Manuscript (de la Croix Ndong et al. Asfotase-α improves bone growth, mineralization and strength in mouse models of neurofibromatosis type-1. Nat Med 2014;20:904-10.)

Appendix #4:
Submitted file of accepted manuscript (Sant et al. Evaluation of somatic mutations in tibial pseudarthrosis samples in neurofibromatosis type 1. J Med Genet 2015 – in press).

CONFERENCE REPORT

AMERICAN JOURNAL OF medical genetics PART A

Update from the 2013 International Neurofibromatosis Conference

Scott R. Plotkin,[1]* Anne C. Albers,[2] Dusica Babovic-Vuksanovic,[3] Jaishri O. Blakeley,[4] Xandra O. Breakefield,[5] Courtney M. Dunn,[2] D. Gareth Evans,[6] Michael J. Fisher,[7] Jan M. Friedman,[8] Marco Giovannini,[9] David H. Gutmann,[2] Michel Kalamarides,[10] Andrea I. McClatchey,[11] Ludwine Messiaen,[12] Helen Morrison,[13] David B. Parkinson,[14] Anat O. Stemmer-Rachamimov,[11] Catherine D. Van Raamsdonk,[8] Vincent M. Riccardi,[15] Tena Rosser,[16] Aaron Schindeler,[17] Miriam J. Smith,[6] David A. Stevenson,[18] Nicole J. Ullrich,[19] Thijs van der Vaart,[20] Brian Weiss,[21] Brigitte C. Widemann,[22] Yuan Zhu,[23] Annette C. Bakker,[24] and Alison C. Lloyd[25]**

[1]Department of Neurology and Cancer Center, Massachusetts General Hospital, Harvard Medical School, Boston, Massachusetts

[2]Department of Neurology, Washington University School of Medicine, St. Louis, Missouri

[3]Department of Medical Genetics, Mayo Clinic, Rochester, Minnesota

[4]Department of Neurology, Johns Hopkins University, Baltimore, Maryland

[5]Neuroscience Center, Center for Molecular Imaging and Department of Neurology, Massachusetts General Hospital/Harvard Medical School, Boston, Massachusetts

[6]Center for Genomic Medicine, St Mary's Hospital, Manchester Academic Health Sciences Centre, University of Manchester, Manchester, UK

[7]Division of Oncology, Children's Hospital of Philadelphia, Philadelphia, Pennsylvania

[8]Department of Medical Genetics, University of British Columbia, Vancouver, Canada

[9]Center for Neural Tumor Research, House Research Institute, Los Angeles, California

[10]Department of Neurosurgery, Hopital Pitié-Salpêtriére, Paris, France

[11]Department of Pathology, Massachusetts General Hospital/Harvard Medical School, Boston, Massachusetts

[12]Department of Genetics, University of Alabama at Birmingham, Birmingham, Alabama

[13]Leibniz Institute for Age Research, Jena, Germany

[14]Centre for Biomedical Research, University of Plymouth, Peninsula College of Medicine and Dentistry, Plymouth, UK

[15]The Neurofibromatosis Institute, La Crescenta, California

[16]Department of Neurology, Children's Hospital, Los Angeles, University of Southern California, Los Angeles, California

[17]Kids' Research Institute, The Children's Hospital at Westmead, University of Sydney, Westmead, Australia

[18]Division of Medical Genetics, Department of Pediatrics, University of Utah, Salt Lake City, Utah

[19]Departments of Neurology and Pediatric Oncology, Boston Children's Hospital, Harvard Medical School, Boston, Massachusetts

[20]ENCORE – NF1 Center, Erasmus MC, Rotterdam, The Netherlands

[21]Division of Hematology/Oncology, Cincinnati Children's Hospital Medical Center, Cincinnati, Ohio

[22]Pediatric Oncology Branch, National Cancer Institute, Bethesda, Maryland

[23]Gilbert Neurofibromatosis Institute, Children's National Medical Center, Washington, District of Columbia

Conflict of interest: none

Grant sponsor: National Institutes of Health Grant Award; Grant number: 1R13NS084619-01.

*Correspondence to:
Scott R. Plotkin, MD, PhD, Massachusetts General Hospital, Yawkey 9E, 55 Fruit Street, Boston, MA 02114
E-mail: splotkin@partners.org

**Correspondence to:
Alison C. Lloyd, PhD, MRC Laboratory for Molecular Cell Biology, University College London, Gower Street, London WC1E 6BT
E-mail: alison.lloyd@ucl.ac.uk

Article first published online in Wiley Online Library (wileyonlinelibrary.com): 00 Month 2014
DOI 10.1002/ajmg.a.36754

[24]Children's Tumor Foundation, New York, New York

[25]MRC Laboratory for Molecular Cell Biology, University College London, London, UK

Manuscript Received: 23 April 2014; Manuscript Accepted: 14 August 2014

How to Cite this Article:
Plotkin SR, Albers AC, Babovic-Vuksanovic D, Blakeley JO, Breakefield XO, Dunn CM, Evans DG, Fisher MJ, Friedman JM, Giovannini M, Gutmann DH, Kalamarides M, McClatchey AI, Messiaen L, Morrison H, Parkinson DB, Stemmer-Rachamimov AO, Van Raamsdonk CD, Riccardi VM, Rosser T, Schindeler A, Smith MJ, Stevenson DA, Ullrich NJ, van der Vaart T, Weiss B, Widemann BC, Zhu Y, Bakker AC, Lloyd AC. 2014. Update from the 2013 International Neurofibromatosis Conference.
Am J Med Genet Part A. 9999:1–10.

INTRODUCTION

The 2013 Neurofibromatosis (NF) Conference took place at the Portola Hotel and Spa, Monterey, CA, from June 8–11, 2013. This international meeting is sponsored annually by the Children's Tumor Foundation (CTF), with the goal of bringing together NF researchers and clinicians from disparate fields of expertise. The conference agenda included a range of preclinical topics with a focus on signaling pathways and mouse models and a number of clinical topics, including a symposium on the interaction of academics, government, and industry in NF clinical trials.

Neurofibromatosis is a group of inherited genetic disorders–NF1, NF2, and schwannomatosis–that together affect about 100,000 persons in the US. NF1 is the most common, with an estimated birth prevalence of 1:3,000 [Friedman, 1999; Lammert et al., 2005]; for NF2 and schwannomatosis, the estimated birth prevalence is 1:25,000 and 1:40,000, respectively [Antinheimo et al., 2000; Evans et al., 2005]. NF1, NF2, and schwannomatosis have in common that they predispose affected individuals to develop Schwann cell tumors such as neurofibromas and schwannomas. At a lower frequency, they also predispose to the development of a number of other benign and malignant tumor types, as well as some developmental abnormalities including learning disabilities (in NF1). The disorders arise from mutations in different genes, each of which plays a key role in regulating cellular function. The *NF1* gene on human chromosome 17 encodes an intracellular signaling molecule that functions as a GTPase activating protein for Ras proteins, whereas the *NF2* gene on human chromosome 22 encodes a cytoskeletal-membrane linking protein with reported roles in the suppression of several different growth-associated signaling pathways. The biology of schwannomatosis remains understudied despite the identification of germline *SMARCB1* mutations in schwannomatosis patients in 2007.

NEUROFIBROMATOSIS 1

Basic Science

Neurobiology. Approximately 30–70% of individuals with neurofibromatosis type 1 (NF1) have learning disabilities, representing the most significant cause of lifetime morbidity associated with this disease. Moreover, recent findings indicate that signaling proteins within the Ras and the extracellular-signal regulated kinase (ERK) subfamily of mitogen-activated protein kinases (MAPK) pathway are mutated and hyperactivated in a number of human genetic syndromes (known as RASopathies) associated with varying levels of cognitive dysfunction substantiating the view that these pathways are important in regulating brain function [Rauen, 2013].

Yuan Zhu (University of Michigan) presented evidence that biallelic, but not monoallelic, inactivation of *Nf1* in developing neural stem cells increased the number of glial lineage cells but by distinct mechanisms depending on the region of the brain. In the dorsal forebrain *Nf1* loss in neural stem and progenitor cells altered their fate-specification resulting in increased numbers of glial cells in the corpus callosum at the expense of neurogenesis in the olfactory bulb. In contrast, in the ventral forebrain, overproduction of glial cells resulted from increased proliferation of glial-restricted progenitors. Importantly, both of these glial defects appeared to be caused by hyperactivation of Ras/ERK signaling, as a MEK inhibitor rescued the deficits. Yuan Wang (University of Michigan) presented data on the effects of biallelic loss of the *Nf1* gene in the cerebellum of mice and provided further evidence for the importance of the ERK pathway showing that hyperactivity of ERK underlies the defects seen in both neurons and glia of these mice, disrupting cerebellum structure and causing motor defects.

William Snider (University of North Carolina) performed both loss-of-function and gain-of-function studies on MEK1/2 in developing neural stem cells and post-mitotic neurons and showed that while loss of MEK1 and MEK2 impaired the generation of glial cells, hyperactive MEK/ERK signaling promoted gliogenesis during development. These results provide further genetic evidence that supports the observations of the Zhu group and others that accurate regulation of Ras signaling through the MEK/ERK pathway is critical for normal brain development.

Alcino Silva (University of California, Los Angeles) described the possible mechanisms by which loss of one allele of *Nf1* can cause deficits in long-term potentiation (LTP) and learning in adult mice. Dr. Silva also presented evidence that mutations in *SHP2* (identified in Noonan syndrome) cause similar deficits in LTP and learning. However, he emphasized that what appeared to be a similar phenotype occurred via distinct mechanisms, as the genetic mutations caused their effects in distinct cell types.

Freda Miller (University of Toronto, Canada) and her colleagues investigated signaling proteins within the Ras pathway and their

activating mutations in embryonic neural stem cells of the murine cortex, and arrived at two major conclusions. First, each protein, including SHP2, B-Raf, and Ras, plays an important role in regulating the genesis of neurons and astrocytes from developing neural precursors. Second, that when these proteins are hyperactivated, as in the Rasopathies, they deregulate cell genesis by distinct mechanisms.

Debra Mayes (Cincinnati Children's Hospital Medical Center) presented an analysis of the histological and behavioral changes of mice with hyperactive RAS signaling in oligodendrocytes. She hypothesized that upregulation of nitrous oxide plays a critical role in the phenotypes, which could be reversed with antioxidant treatment.

Tumor models. Thomas De Raedt (Brigham and Women's Hospital) presented work characterizing a more severe NF1 phenotype associated with microdeletions of the *NF1* region. He identified an additional gene within the deletion and, in a mouse model, recapitulated a more severe NF1 phenotype when this gene was lost in conjunction with the *NF1* gene. Nancy Ratner (Cincinnati Children's Hospital Medical Center) presented further work using the DhhCre; $NF1^{fl/fl}$ mouse model to test the requirement of specific signaling pathways for tumor growth. The studies verified the MEK/ERK pathway as a therapeutic target and identified STAT-3 as a potential new target. In studies of NF1-associated low grade gliomas, David Gutmann (Washington University) presented evidence that human tumors are monoclonal and have no other mutations other than loss of *NF1* gene expression [Gutmann et al., 2013]. However, in a genetically engineered mouse optic glioma model, loss of *Nf1* gene expression in glial cells alone is not sufficient to drive tumorigenesis but requires signals from $Nf1^{+/-}$ microglia in the surrounding microenvironment [Pong et al., 2013].

Luis Parada (UT Southwestern) presented work on a novel glioma mouse model in which stem cells are labeled and can be ablated following ganciclovir treatment. A stem cell population was found to be labeled in glioblastomas in these mice and was relatively quiescent. Following treatment of the tumor however, these stem-like cells differentially proliferated and were responsible for the regrowth of the tumor. These results reinforce the importance of targeting the stem-like cells found in many tumors. Dinorah Friedmann-Morvinski (The Salk Institute) presented a different model of glioblastoma in which tumors were induced from fully differentiated cortical neurons rather than from stem cells, demonstrating that the cell-of–origin may not always be obvious.

MPNST is the primary cause of early mortality in NF1 patients [Evans et al., 2011]. Using a Sleeping Beauty genetic screen, Adrienne Watson (University of Minnesota) identified Wnt signaling as a driver of Schwann cell tumorigenesis. Induction of Wnt signaling was sufficient to induce a transformed phenotype in human Schwann cells, while inhibition of both Wnt signaling and mTOR synergistically induced apoptosis of MPNST cell lines. Rebecca Dodd (Duke University) described a mouse model of soft tissue sarcoma in which *Nf1* and *lnk4a* were knocked out by the injection of a Cre-expressing adenovirus into either muscle or sciatic nerve. Treatment with a MEK inhibitor decreased sarcoma growth in these mice.

Clinical Research

Cognitive issues and clinical trials. Up to two-thirds of individuals with NF1 demonstrate signs of cognitive dysfunction, ranging from deficits in attention, visual-spatial memory and executive function, to language problems, learning disabilities, and academic underachievement. Nicole Ullrich (Boston Children's Hospital, Harvard Medical School) summarized the major challenges in clinical trial design for neurocognitive interventions, including trial design, selection of ideal outcome measures, selection of the appropriate drug and duration for intervention, dose-finding and appropriate inclusion criteria.

Maria Ribeiro (Coimbra University, Portugal) presented data using magnetic resonance spectroscopy to measure brain metabolites such as the inhibitory neurotransmitter GABA in the visual cortex of children and adolescents with NF1. Mouse models have implicated increased release of GABA in the pathophysiology of cognitive issues [Cui et al., 2008]. Children with NF1 have lower measured levels of unbound GABA, which might reflect depletion of GABA from synaptic vesicles [Violante et al., 2013]. Within the NF1-group, higher overall GABA-levels correlated with slower reaction times.

Thijs van der Vaart (Erasmus MC, The Netherlands) reported on the final results of the NF1-SIMCODA trial, a 12-month randomized placebo-controlled trial in 84 NF1-children aged 8–16 years. Earlier work had shown positive effects of lovastatin, a cholesterol-lowering drug, in a mouse model of NF1 [Li et al., 2005]. The NF1-SIMCODA trial aimed to detect beneficial effects of simvastatin on cognitive and behavioral problems in children with NF1. The current randomized controlled trial (RCT) was based on a previous 12-week pilot RCT with 61 NF1-children in the same age range, in which only one secondary outcome measure, the IQ-subtest "object assembly", demonstrated a positive effect of simvastatin over placebo [Krab et al., 2008]. The results of NF1-SIMCODA were disappointing, showing no benefit of simvastatin over placebo for treating cognitive and behavioral problems [van der Vaart et al., 2013].

Kristina Hardy (Children's National Medical Center) presented data on the use of a computerized training program, CogMed, in children with NF1. CogMed has been proposed as a neurocognitive intervention in an upcoming clinical trial through the NF Clinical Trials Consortium.

Recognizing that clinical trials for NF1 learning disability are currently underway, the Response Evaluation in Neurofibromatosis and Schwannomatosis (REiNS) group has been working to recommend a standardized set of outcome measures in clinical trials for NF. Karin Walsh (Children's National Medical Center) summarized the progress of the REiNS working group on neurocognitive outcome measurements. One concern of commonly utilized neuropsychological measures is that they are not designed to detect change over time. The ideal outcome measures for cognitive interventions should measure constructs of interest that are relevant to individuals with NF1, should detect change over time, and should be generalizable.

Optic pathway glioma. Peter de Blank (Rainbow Babies & Children's Hospital, Case Western Reserve University) retrospectively evaluated the ophthalmologic records and diffusion tensor imaging measurements of the optic pathway in children with NF1

and optic pathway gliomas. He found that a decrease in fractional anisotropy of the optic radiations was associated with abnormal visual acuity and could be a predictor of visual acuity loss in the following year [de Blank et al., 2013].

Autism spectrum disorder. Susan Huson (Oxford, UK) presented a study evaluating the prevalence of autistic features in a large population of children 4–16 years of age with NF1. In this population-based study, she found that approximately 30% of subjects met the diagnostic criteria for an autistic spectrum disorder [Garg et al., 2013]. These findings build on previous reports suggesting that autistic symptoms are common in NF1 patients but contrasts with a prior report in adult NF1 patients. [van Eeghen et al., 2013; Walsh et al., 2013].

Clinical efficiency. Amanda Bergner (Johns Hopkins School of Medicine) presented the results of a pilot project evaluating the use of a dedicated adult intake clinic at the Johns Hopkins Comprehensive NF Center in improving the efficiency of care. The intake clinic significantly reduced patient wait time, allowed for more effective time to be spent with NF providers, and generated new revenue for the clinic.

NF1 Clinical Trials Update

Brian Weiss (Cincinnati Children's Hospital Medical Center) presented the results from a 2-stratum phase II clinical trial of the mTOR inhibitor sirolimus for plexiform neurofibroma (PNF) in subjects with NF1. This trial specifically sought to determine whether sirolimus either: (a) increases time to progression (TTP) in progressive PNF (stratum 1) or; (b) results in objective radiographic responses in inoperable PNFs in the absence of documented radiographic progression at trial entry (stratum 2). Disease status was evaluated using volumetric MRI analysis at regular intervals; pain reduction and quality of life (QOL) outcomes were also assessed. No patients on stratum 2 experienced a radiographic response. [Weiss et al., 2013] In contrast, patients in stratum 1 had an estimated median TTP of 15.4 months, compared to 11.9 months in a control group from a completed NCI-sponsored study with near identical eligibility criteria.

Brigitte Widemann (National Cancer Institute) reported the preliminary results of an ongoing phase 1 trial of selumetinib, a MEK inhibitor, in children 3–18 years of age with NF1 and inoperable PNFs. Selumetinib is administered orally BID on a continuous dosing schedule. The maximally tolerated dose will be determined based on toxicities observed in the first three courses. Disease status is evaluated using volumetric MRI analysis at regular intervals. Nine subjects had enrolled to date (median age 15 years; range, 5–18 years). No dose limiting toxicities (DLTs) were observed at the 20 mg/m^2 dose, but one of three initial subjects developed a DLT at 30 mg/m^2 which was reversible and asymptomatic. This dose level has since been expanded to six subjects, with no additional DLTs to date. Decreases in PNF volume have been observed in all subjects who have undergone at least one restaging MRI, and partial response ($\geq$ 20% shrinkage in tumor volume) has been achieved in four of the six subjects. Chronic dosing of selumetinib has been tolerated by children with NF1 and PNF, and enrollment of this study is ongoing.

David Viskochil (University of Utah) presented the results of a phase II trial of chemotherapy in sporadic and NFI-associated high-grade malignant peripheral nerve sheath tumors (MPNSTs). Ifosfamide and doxorubicin followed by 2 cycles of ifosfamide and etoposide were used. The objective response rate was lower in NF1 than in sporadic MNST patients, which is consistent with retrospective literature reports.

NEUROFIBROMATOSIS 2

Basic Science

NF2 signaling. Merlin interacts with the E3 ubiquitin ligase CRL4-DCAF1 in the nucleus and inhibits its function [Li et al., 2010]. Filippo Giancotti (Memorial Sloan-Kettering Cancer Center) described a functional link between Merlin, CRL4-DCAF1, and LATS in human Schwann cells. These results provide a mechanism for Merlin's activation of Lats and the Hippo tumor suppressor pathway in the nucleus of Schwann cells. In addition, they indicate that YAP/TEAD inhibitors, which are undergoing preclinical testing, may be effective for the treatment of NF2.

Duojia Pan (Johns Hopkins University) discussed recent efforts in targeting the Hippo pathway as a potential strategy against NF2. He presented findings showing that loss of *NF2* mimics inactivation of Hippo signaling in the liver, the lens of the eye, and ependymal cells, suggesting that *NF2* is a physiological regulator of Hippo signaling in multiple mammalian tissues. Disruption of the YAP-TEAD complex, the nuclear effector of the Hippo pathway, potently suppresses hepatomegaly/tumorigenesis resulting from *Nf2* inactivation in the mouse liver. Screening of a library of drugs approved by the U.S. Food and Drug Administration (FDA) identified verteporfin as a small molecule that inhibits TEAD-YAP association and YAP-induced liver overgrowth, providing proof of principle for YAP inhibitors as molecular-targeted therapeutics for NF2 [Liu-Chittenden et al., 2012].

Joe Kissil (The Scripps Research Institute) detailed the identification of a novel Merlin-interacting protein–angiomotin (Amot)–associated with tight and adherens junctions and an interactor of several small G-protein modulators. Amot directly associates with Yap, a transcriptional activator regulated by the Hippo pathway. Moreover, Amot is required for hepatic "oval cell" response and tumorigenesis in response to toxin-induced injury or *Nf2* loss in a liver-specific Amot knockout mouse. In these studies, Amot appears to regulate Yap at multiple levels, both in the cytoplasm and in the nucleus. These studies implicate Amot as a critical downstream effector of Merlin and the Hippo/Yap pathway.

Dominique Lallemand (Curie Institute, France) reported the use of a combination of proteomic approaches to evaluate the expression, activity, and link to tumor cell proliferation of several of the signaling pathways regulated by Merlin in a large series of human schwannoma biopsies. They found that Her3, Her2, PDGFR-β, and Axl are the most frequently activated receptor tyrosine kinases (RTKs) in schwannomas and could represent key therapeutic targets. Using Reverse Phase Protein Array, they showed that the expression of the Ki67 proliferation marker is strongly associated with levels of Yap, activated Her3, and PDGFR-β. Also, the expression of PDGFR-β and Her3 can be stimulated by Yap in

schwannoma cells in culture suggesting that a signaling network under the control of Yap may be involved in tumor growth. Finally, they observed remarkable heterogeneity in the expression of all the proteins assessed by immunohistochemistry on tumor sections, indicating that the response to targeted treatments will likely be variable from patient to patient.

Alizee Boin (Curie Institute, Paris, France) presented data indicating that Merlin and YAP directly interact, with the possibility that Merlin sequesters YAP in the cytosol, preventing it from transactivating expression. Lastly, Alexander Schulz (Leibniz Institute, Germany) presented data showing how loss of Merlin in PNS axons leads to reduced expression of the myelin regulator, neuregulin 1 type III. They are currently studying the effects upon PNS myelination and the implications for the polyneuropathies seen in patients with NF2.

Preclinical Science

NF2 mouse models. Andrea McClatchey (Massachusetts General Hospital/Harvard Medical School) started off this session by presenting her studies of the origin of the *Alb-Cre;Nf2*$^{flox/flox}$ model of liver progenitor expansion and tumorigenesis. Surprisingly, this analysis uncovered a novel, proliferation-independent function for Merlin during liver development.

Michel Kalamarides (Hopital Pitié-Salpêtriére, Paris, France) presented an update on mouse models of human meningioma [Peyre et al., 2013] showing an important role of PDGF-β for the initiation and malignant progression of meningiomas associated with *NF2* gene inactivation. Two recent papers showed that recurrent mutations in SMO and AKT1 are mutually exclusive with *NF2* loss in meningioma initiation [Brastianos et al., 2013; Clark et al., 2013]. The lab's current strategy to reproduce these genetic events in mice was presented.

Charles Yates (Indiana University School of Medicine) described a genetically engineered NF2 mouse model with excision of the *Nf2* gene driven by Cre expression under control of a tissue-restricted 3.9 kb Periostin promoter element. By 10 months of age, 100% of these *Postn-Cre;Nf2*$^{flox/flox}$ mice develop spinal, peripheral, and cranial nerve tumors that are histologically identical to human schwannomas. In addition, the development of cranial nerve VIII tumors in these mice may correlate with functional impairments in hearing and balance, as measured by auditory brainstem response and vestibular testing. Embryonic analyses suggest an early Schwann cell progenitor tumor cell of origin.

Screening and Compound Testing

Cristina Fernandez-Valle (University of Central Florida) discussed the high-throughput screening of a 1280 compound library (LOPAC) using Merlin-null mouse Schwann cells in order to identify probes that reduced cell viability. Dr. Fernandez-Valle identified two compounds from an initial 40 "hits" that selectively reduced viability of Merlin-null mouse Schwann cells as compared to normal mouse Schwann cells. In a joint project, Cenix Bioscience validated a number of compounds from the drug screen as well as those in clinical trials for NF2. This demonstrated the validity of the cell line and high-throughput screening approach to identify candidate drugs for human studies.

Marco Giovannini (House Research Institute) reported on efficacy testing of HSP90 inhibitors for NF2. The antiproliferative activity of NXD30001 was tested in NF2-deficient cell lines and in human primary schwannoma and meningioma cultures in vitro, and in two allograft models and in one Nf2 transgenic model in vivo [Tanaka et al., 2013]. They found that NXD30001 induced degradation of client proteins and suppressed proliferation of NF2-deficient cells. In addition, differential expression analysis using a global transcriptome approach identified subsets of genes implicated in cell proliferation, cell survival, vascularization, and Schwann cell differentiation whose expression was altered by NXD30001 treatment. Overall, results showed that NXD30001 in NF2-deficient schwannoma suppressed multiple pathways necessary for tumorigenesis.

Dina Stepanova (Fox Chase Cancer Center) reported that *Nf2* null mouse cells exhibit higher levels of acetyl CoA and fatty acid synthase (Fasn) and that the Fasn inhibitor, cerulenin, selectively inhibits cell proliferation in xenografts. In humans, the treatment of *NF2* null vestibular tumors with anti-VEGF therapy (bevacizumab) alone has shown promise. Using a mouse xenograft model, Lei Xu (Massachusetts General Hospital, Harvard Medical School) showed promising results using a combination of radiotherapy and anti-VEGF therapy.

Clinical Research

Rosalie Ferner (Guy's and St. Thomas' NHS Foundation Trust, UK) presented the results of her multi-center longitudinal study of quality of life (QOL) in 288 patients with NF2 using the NF2 Impact on QOL (NFTI-QOL) questionnaire [Hornigold et al., 2012]. This measure was quick and easy to administer, and demonstrated good reliability and ability to detect significant QOL changes over time in this patient population.

Vanessa Merker (Massachusetts General Hospital) analyzed prospective data from the NF2 Natural History Consortium Study, using new endpoint measures recommended by the Response Evaluation in NF and Schwannomatosis (REiNS) committee. Vestibular schwannomas were evaluated for volumetric progression and hearing was assessed with word recognition scores. The median time to tumor progression was 14 months. A significant number of patients experienced tumor progression and hearing decline over 3 years [Plotkin et al., 2014].

NF2 Clinical Trials Update

Jaishri Blakely (Johns Hopkins University) presented the results of a multi-institutional study of bevacizumab, a VEGF-A antibody, in subjects >12 years of age with NF2 and symptomatic vestibular schwannomas (VS). Subjects were given bevacizumab every 3 weeks for 1 year, with hearing evaluations performed during treatment and twice after completion of treatment. The primary endpoint was a statistically-significant increase in word recognition score (WRS) compared with baseline. Brain MRI, whole body MRI, and QOL outcomes were also assessed. Fourteen subjects (median age 30 years; range, 14–79 years) were enrolled. No subjects had progressive hearing loss while on treatment. Thirty-six percent of (5/14) subjects had significant improvement in WRS maintained

for three consecutive months, and improvement was maintained off bevacizumab for those subjects. Four of five subjects with an improved WRS also had significant reduction in tumor volume on MRI. These prospective data confirm that bevacizumab is well tolerated in this patient population and that bevacizumab can reverse hearing loss due to NF2-related VS in select patients, independent of tumor volume.

Michel Kalamarides (Hopital Pitié-Salpêtriére, Paris, France) presented the intermediate results of a prospective trial of the mTOR inhibitor everolimus for progressive VS in NF2 patients. The rationale for the trial was based on preclinical results in a NF2 genetically engineered mouse schwannoma model and encouraging and consistent results in an index patient [Giovannini et al., 2014]. To date, no tumor shrinkage has been observed. However, preliminary analysis suggests that mTORC1 inhibition may delay time to tumor progression. In the second year of the trial, patients who experience tumor growth after discontinuation of everolimus will be allowed to restart the drug. This design is intended to determine whether stable disease on everolimus represents a true clinical response to treatment.

Matthias Karajannis (New York University) reported the results of a separate clinical trial using everolimus in ten patients with NF2 and progressive vestibular schwannomas. No objective improvement in hearing or imaging response was seen [Karajannis et al., 2014].

SCHWANNOMATOSIS

Preclinical Science

Xandra Breakefield (Massachusetts General Hospital/Harvard Medical School) described her collaboration with Gary Brenner and Giulia Fulci to develop an AAV1-PO-ICE vector that has a Schwann cell-specific promoter driving caspase-1. Intratumoral injection of the vector causes regression of schwannomas and a reduction in schwannoma-induced pain in NF2-derived human xenograft mice in sciatic nerve. This effect may occur via a process of pyroptosis and therefore has the potential to control growth of tumors that are not directly exposed to the vector.

Larry Sherman (Oregon Health and Science University) discussed the underlying mechanisms of pain in schwannomatosis. He described a SMARCB1 conditional knockout mouse with nerves that showed a similar expression profile and morphology to wild type cells, but which were quicker to respond to painful stimuli. An expression array from cultured dorsal root ganglia of these mice showed elevated VR1 capsaicin receptors (TRPV1) suggesting that this pathway could be considered for therapeutic intervention.

Clinical research. Miriam Smith (University of Manchester, England) presented exome sequencing data showing that multiple spinal meningiomas can be inherited as a distinct genetic condition, caused by mutations in the chromatin remodeling complex subunit *SMARCE1*. Theo Hulsebos (Academic Medical Center, Netherlands) presented an analysis of mutant SMARCB1 protein expression in schwannomas from schwannomatosis patients, showing that mutant forms of SMARCB1 can be found in these tumors and that the type of mutation influences the amount of protein present. However, the type of mutation does not influence the presence of the typical mosaic pattern of staining in tissue preparations. Alvaro Pinto (Massachusetts General Hospital) presented his research correlating *SMARCB1* mutation analysis and SMARCB1 immunohistochemical expression patterns in syndromic and sporadic schwannomas. He found a discrepancy between the high rate of altered, mosaic SMARCB1 expression in syndromic schwannomas (familial schwannomatosis, sporadic schwannomatosis, NF2) and low rates of mutations in the *SMARCB1* gene, suggesting other mechanisms may play a role in tumor development. In addition, despite a high rate of mosaic pattern of SMARCB1 expression in NF2 tumors, *SMARCB1* mutations were not present in any of the NF2-associated tumors.

Judith Eelloo (Central Manchester University Hospitals Foundation Trust, UK) presented a case report of a patient with SMARCB1-associated schwannomatosis with three independent malignancies (lymphoma, neuroendocrine tumor, and sarcoma). This further highlighted the clinical overlap between syndromes and stressed the importance of seeking care in an expert center as well as the need for on-going genetic and phenotypic characterization of schwannomatosis. Amanda Bergner presented the progress of the International Schwannomatosis Database (ISD). The ISD is a medically curated, anonymous database of schwannomatosis patients, and was designed as a resource to identify people who would be suitable candidates for clinical trials or research studies. The ISD is being contributed to by 10 academic centers around the globe and recently, a remote patient entry mechanism was added to allow patients not affiliated with an enrolling center to participate (www.schwannomatosis.com).

NOVEL SESSIONS AT THE 2013 CONFERENCE

The 2013 conference incorporated novel sessions including educational sessions, small group sessions, and an industry/academia/government symposium.

Clinical Phenotypes: What do They Tell Us?

NF1, NF2, and schwannomatosis are characterized by wide clinical variability. Making a clinical diagnosis can be challenging due to the overlap in tumor types encountered in the neurofibromatoses and in the clinical presentation with a variety of other conditions.

Ludwine Messiaen (University of Alabama, Birmingham) discussed clinical and molecular characteristics of skin hyper pigmentation in NF1 and in Legius syndrome. In addition, an array of other conditions associated with multiple cafe-au-lait macules (CALM) were reviewed, including NF2, McCune-Albright syndrome, ring chromosomes (ch. 7, 11, 12, 15, 17, 22), LEOPARD syndrome, constitutive mismatch repair deficiency, Cowden, Fanconi anemia, tuberous sclerosis complex, Silver-Russell, and piebaldism. She noted that the NIH diagnostic criteria for NF1 are not specific, as some patients with pigmentary signs only (CALM and skinfold freckling) have Legius syndrome, due to mutations in *SPRED1*, instead of *NF1*.

Gareth Evans (Saint Mary's Hospital, United Kingdom) discussed the lack of sensitivity of the current NIH diagnostic consensus criteria for NF1 patients with "spinal neurofibromatosis". These patients present with multiple spinal tumors but few, if any, CALMs, skinfold freckling, or cutaneous neurofibromas [Burkitt

Wright et al., 2013]. Dr. Evans recommended testing of both *NF1* and *SMARCB1* genes in blood and, in selected cases, in tumor biopsies in order to distinguish between NF1, mosaic NF2, and schwannomatosis.

Anat Stemmer-Rachamimov (Massachusetts General Hospital, Harvard Medical School) discussed that hybrid tumors are peripheral nerve sheath tumors that have mixed pathological features of two or more types of peripheral nerve sheath tumors and are therefore difficult to classify. However, their presence in a patient is highly suggestive of one of the syndromic forms of neurofibromatosis [Harder et al., 2012].

Dusica Babovic-Vuksanovic (Mayo Clinic) presented a recently published series of patients with multiple orbital neurofibromas, painful peripheral nerve tumors, distinctive face, and marfanoid habitus [Babovic-Vuksanovic et al., 2012]. Four unrelated patients have been described with this condition, and this is thought to be a new syndrome, as none of the known genes associated with predisposition to develop neurofibromas or schwannomas were mutated in any of these patients.

Small Group Sessions

NF-related neuropathy. Neuropathies are a significant problem in many patients with NF1, NF2, and schwannomatosis. Susan Huson (NF Centre, Manchester, UK) reviewed the clinical aspects of neuropathy in NF2, including length dependant peripheral neuropathy and focal amyotrophy/mononeuropathy [Trivedi et al., 2000; Sperfeld et al., 2002]. In the latter group, the diagnosis can be made only after exclusion of a causative tumor. Gareth Evans (personal communication) identified 77/396 (19%) NF2 patients in the UK registry with amyotrophy/mononeuropathy; the most common symptom is sudden unilateral facial weakness (40/77) followed by foot drop (23/77); 8.6% (34/396) of patients have a peripheral neuropathy.

In another study of NF2 peripheral neuropathy [Sperfeld et al., 2002], 7/15 patients were found to have a clinically detectable neuropathy and a further three had nerve conduction abnormalities. Sural nerve biopsies in NF2 neuropathy cases have shown diffuse Schwann cell proliferation and small endoneurial tumorlets of schwannomas and perineuriomas associated with a reduction in nerve fiber density. Electron microscopy demonstrated de-differentiated Schwann cells isolated, or in complexes, and multiple interdigitating cell processes compatible with merlin malfunction [Sperfeld et al., 2002]. Three hypotheses were suggested as to the cause of the neuropathy: nerve compression by multiple tumorlets, an unknown local toxic effect of abnormal endoneurial cells, or the inability of NF2 Schwann cells to adhere to nerve sheath axons. Support for the compression hypothesis came from a MRI study of peripheral nerves in NF2 patients that demonstrated accumulation of non- compressive fascicular lesions with the clinical severity being proportional to the number of lesions [Baumer et al., 2013].

Helen Morrison (Leibniz Institute for Age Research, Germany) highlighted that NF2-neuropathy is likely of multifactorial origin. She reported a novel merlin-specific function in maintaining axonal integrity and proposed that reduced axonal *nf2* gene dosage influences NF2-associated polyneuropathy. Genetically engineered mice that specifically lack neuronal merlin display abnormal axons and these mice suffer from polyneuropathy-like symptoms of axonal origin. This finding is of clinical interest because, in addition to the observed Schwann cell tumorlets, reduced merlin expression in axons may contribute to NF2-polyneuropathy [Schulz et al., 2013].

The clinical and biological aspects of NF1 associated neuropathies were reviewed by Rosalie Ferner (Guy′s and St. Thomas′ NHS Foundation Trust, UK). NF1 neuropathy is a length-dependent, predominantly axonal sensorimotor neuropathy. It occurs less frequently than the NF2 neuropathy and the symptoms and neurological signs are usually mild and non–progressive. The pathogenesis of NF1 neuropathy has not been determined but there is a putative abnormality in signaling between Schwann cells, fibroblasts, and perineurial cells.

Neuropathy associated with schwannomatosis was reviewed by Gareth Evans (University of Manchester, UK). Typically, schwannomatosis is characterized by painful schwannomas with minimal deficit in motor or sensory function. Tumor morphology is discrete rather than invasive and therefore peripheral neuropathy and amyotrophy are rare. The main clinical challenge is treating neuropathic pain.

Musculoskeletal biology and metabolism in NF. While the skeletal complications associated with NF1 are well described, several research groups have begun to explore the prevalence and impact of muscle weakness. Reductions in the muscle compartment in NF1 individuals have been documented by peripheral quantitative computed tomography, which initiated a number of studies examining muscle performance.

David Stevenson (University of Utah) described studies in children with NF1 showing significant reductions in total motor composite scores and strength. In addition, preliminary data from 16 individuals with NF1 suggest that energy expenditure/metabolism may also be abnormal in NF1 muscles. He theorized that impaired muscle function may be a feature common to RASopathies, suggesting an underlying importance of RAS signaling in muscle function [Stevenson et al., 2012]. These clinical findings were supported by hand-held dynamometry results from the lab of Joshua Burns (Children's Hospital, Westmead, Sydney, Australia) showing mean reductions of 30–45% in strength in a range of muscle movements. Juliana de Souza (Federal University of Minas Gerais, Belo Horizonte, Brazil) presented data showing that a range of muscle outcomes in NF1 patients were affected (aerobic capacity [de Souza et al., 2013], handgrip strength, 6 minute walk, respiratory muscle force) and were not affected (cardiac function, myocardial mass and pulmonary function). As researchers and clinicians increasingly recognize that weakness and reduced muscle tone are features of NF1, research has turned to exploring the benefits of physical therapy and discovering the underlying molecular mechanism.

Kate Quinlan (University of Sydney, Australia) described how mouse models were used to understand metabolic changes associated with α-actinin deficiency, a common inherited polymorphism [Quinlan et al., 2010] and then documented an underlying metabolic deficiency in NF1 mouse models. [Sullivan et al., 2014] in the *MyoD:Nf1*$^{-/-}$ mice lacking *Nf1* expression in muscles, a neonatal lethal phenotype with intramyocellular fat inclusions was observed. Examination of the *Prx1:Nf1*$^{-/-}$ mice, which lack Nf1 expression in

the developing limbs, showed reduced muscle mass and strength [Kossler et al., 2011], and increased muscle triglycerides.

Integrative Management of Children With NF1

The Washington University NF Center described a multidisciplinary approach to the management of children with NF1. A patient coordinator assists in scheduling same day appointments, especially for families who travel long distances. A physical therapist completes standardized testing of general development in children younger than eight years, and gross and fine motor skills for older children. Based on these and other assessments performed during the clinic visit, individualized recommendations for home activities are provided. In addition, an occupational therapist integrates haptic technology into daily activities and school routines to improve achievement in children with NF1. A pediatric neuropsychologist performs early screening of academic skills in children with NF1.

Multiple Phases of Neurofibroma Progression

In this session, the group led by Vincent Riccardi (Neurofibromatosis Institute, La Crescenta, CA) discussed the initiation and progression of neurofibromas and characterized the stages of progression. The main discussion centered around whether loss of the second *NF1* allele in Schwann cells was always the initiating event in neurofibroma formation and the role of macrophages, pericytes and CD34+ cells in tumor progression.

Using Genetically Engineered Mouse Models for Preclinical Drug Screening

Chaired by David Gutmann (Washington University), the discussion leveraged the expertise of investigators versed in clinical trial design and execution as well as those leading preclinical small-animal model discovery and evaluation efforts. The panel emphasized the successes that have directly resulted from generating and intelligently using genetically-engineered mouse (GEM) strains. Important concerns raised included the timely access of drugs in the clinical pipeline to preclinical GEM researchers and the need to collect biospecimens from individuals participating in human clinical trials. In addition, members of the panel emphasized the importance of matching GEM models with specific subtypes of NF-associated clinical features to best reflect the inherent heterogeneity of these conditions as well as the need to obtain detailed pharmacokinetic, pharmacodynamic, and long-term toxicity data from GEM preclinical studies relevant to the treatment of both adults and children with NF1 and NF2.

Industry/Academia/Government Symposium

In this session, leaders from industry, governmental agencies, and academia discussed the pathways to accelerate the development of effective therapies for NF1, NF2, and schwannomatosis. Salvatore LaRosa (Children's Tumor Foundation) described three CTF-sponsored preclinical initiatives: (1) NF Therapeutics Consortium (formerly the NF Preclinical Consortium, also funded by the Neurofibromatosis Therapeutic Accelerations Program), a collaborative effort amongst leading NF mouse model laboratories focusing on the evaluation of new or repurposed drugs for NF tumors; (2) Synodos, a new pre-clinical effort to fund new approaches to the diagnosis and treatment of NF2-related vestibular schwannomas and meningiomas; and (3) Drug Discovery Initiative, which since its launch in 2006 has provided >$1.4 million in funding for rapid screening of new drugs for manifestations of NF.

Roger Packer (Children's National Medical Center) reviewed the current and future clinical trials of the DOD NF Clinical Trials Consortium, which has been expanded to include 13 sites. He also discussed some of the clinical and therapeutic challenges the consortium has faced, including selection of appropriate outcome measures and study design, and the limitations imposed based on the geographic location of the consortium members.

Helen Chen (CTEP, National Cancer Institute) reviewed the CTEP program, which sponsors clinical trials to evaluate new anticancer agents. CTEP has a broad list of agents in clinical development including agents targeting specific signaling pathways, apoptosis, and the cell cycle. In addition to supplying drug, CTEP provides data infrastructure and regulatory support for clinical trials. In the past, CTEP has sponsored several clinical trials directed at NF1-related plexiform neurofibromas and NF2-related vestibular schwannomas. Dr. Chen commented on the challenges in selecting drug combinations including the potential for increased toxicity and the challenge in defining the optimal dose and schedule of the agents.

Gregory Reaman (Center for Drug Evaluation and Research, FDA) reviewed the Orphan Drug Act, which promotes the development of products that demonstrate promise for the diagnosis and/or treatment of rare diseases. He commented that while orphan products are held to the same approval standards as products for common diseases by requiring substantial evidence of safety and effectiveness for approval, regulations allow for "flexibility" and "scientific judgment" in how this is achieved. He also discussed the FDA Safety and Innovation Act and the Prescription Drug User Fee Act, both of which aim to bring critical new medicines to the market for patients and to support industry in their pursuit of innovative treatments for rare diseases.

ACKNOWLEDGMENTS

We thank all speakers and attendees who contributed to the 2013 Children's Tumor Foundation Neurofibromatosis Meeting and to this summary, and to the staff of the Children's Tumor Foundation for the outstanding organization of the meeting. The 2013 NF Conference was supported in part by National Institutes of Health Grant Award 1R13NS084619-01 to Dr. Scott Plotkin.

REFERENCES

Antinheimo J, Sankila R, Carpen O, Pukkala E, Sainio M, Jaaskelainen J. 2000. Population-based analysis of sporadic and type 2 neurofibromatosis-associated meningiomas and schwannomas. Neurology 54:71–76.

Babovic-Vuksanovic D, Messiaen L, Nagel C, Brems H, Scheithauer B, Denayer E, Mao R, Sciot R, Janowski KM, Schuhmann MU, Claes K, Beert E, Garrity JA, Spinner RJ, Stemmer-Rachamimov A, Gavrilova R, Van CF, Mautner V, Legius E. 2012. Multiple orbital neurofibromas, painful

peripheral nerve tumors, distinctive face and marfanoid habitus: A new syndrome. Eur J Hum Genet 20:618–625.

Baumer P, Mautner VF, Baumer T, Schuhmann MU, Tatagiba M, Heiland S, Kaestel T, Bendszus M, Pham M. 2013. Accumulation of non-compressive fascicular lesions underlies NF2 polyneuropathy. J Neurol 260:38–46.

Brastianos PK, Horowitz PM, Santagata S, Jones RT, McKenna A, Getz G, Ligon KL, Palescandolo E, Van HP, Ducar MD, Raza A, Sunkavalli A, Macconaill LE, Stemmer-Rachamimov AO, Louis DN, Hahn WC, Dunn IF, Beroukhim R. 2013. Genomic sequencing of meningiomas identifies oncogenic SMO and AKT1 mutations. Nat Genet 45:285–289.

Burkitt Wright EM, Sach E, Sharif S, Quarrell O, Carroll T, Whitehouse RW, Upadhyaya M, Huson SM, Evans DG. 2013. Can the diagnosis of NF1 be excluded clinically? A lack of pigmentary findings in families with spinal neurofibromatosis demonstrates a limitation of clinical diagnosis. J Med Genet 50:606–613.

Clark VE, Erson-Omay EZ, Serin A, Yin J, Cotney J, Ozduman K, Avsar T, Li J, Murray PB, Henegariu O, Yilmaz S, Gunel JM, Carrion-Grant G, Yilmaz B, Grady C, Tanrikulu B, Bakircioglu M, Kaymakcalan H, Caglayan AO, Sencar L, Ceyhun E, Atik AF, Bayri Y, Bai H, Kolb LE, Hebert RM, Omay SB, Mishra-Gorur K, Choi M, Overton JD, Holland EC, Mane S, State MW, Bilguvar K, Baehring JM, Gutin PH, Piepmeier JM, Vortmeyer A, Brennan CW, Pamir MN, Kilic T, Lifton RP, Noonan JP, Yasuno K, Gunel M. 2013. Genomic analysis of non-NF2 meningiomas reveals mutations in TRAF7, KLF4, AKT1, and SMO. Science 339: 1077–1080.

Cui Y, Costa RM, Murphy GG, Elgersma Y, Zhu Y, Gutmann DH, Parada LF, Mody I, Silva AJ. 2008. Neurofibromin regulation of ERK signaling modulates GABA release and learning 1. Cell 135:549–560.

de Blank PM, Berman JI, Liu GT, Roberts TP, Fisher MJ. 2013. Fractional anisotropy of the optic radiations is associated with visual acuity loss in optic pathway gliomas of neurofibromatosis type 1. Neuro Oncol 15:1088–1095.

de Souza JF, Araujo CG, de Rezende NA, Rodrigues LO. 2013. Exercise capacity impairment in individuals with neurofibromatosis type 1. Am J Med Genet A 161A:393–395.

Evans DG, Moran A, King A, Saeed S, Gurusinghe N, Ramsden R. 2005. Incidence of vestibular schwannoma and neurofibromatosis 2 in the North West of England over a 10-year period: Higher incidence than previously thought. Otol Neurotol 26:93–97.

Evans DG, O'Hara C, Wilding A, Ingham SL, Howard E, Dawson J, Moran A, Scott-Kitching V, Holt F, Huson SM. 2011. Mortality in neurofibromatosis 1: In North West England: An assessment of actuarial survival in a region of the UK since 1989. Eur J Hum Genet 19:1187–1191.

Friedman JM. 1999. Epidemiology of neurofibromatosis type 1. Am J Med Genet 89:1–6.

Garg S, Lehtonen A, Huson SM, Emsley R, Trump D, Evans DG, Green J. 2013. Autism and other psychiatric comorbidity in neurofibromatosis type 1: Evidence from a population-based study. Dev Med Child Neurol 55:139–145.

Giovannini M, Bonne NX, Vitte J, Chareyre F, Tanaka K, Adams R, Fisher LM, Valeyrie-Allanore L, Wolkenstein P, Goutagny S, Kalamarides M. 2014. mTORC1 inhibition delays growth of neurofibromatosis type 2 schwannoma. Neuro Oncol 16:493–504.

Gutmann DH, McLellan MD, Hussain I, Wallis JW, Fulton LL, Fulton RS, Magrini V, Demeter R, Wylie T, Kandoth C, Leonard JR, Guha A, Miller CA, Ding L, Mardis ER. 2013. Somatic neurofibromatosis type 1 (NF1) inactivation characterizes NF1-associated pilocytic astrocytoma. Genome Res 23:431–439.

Harder A, Wesemann M, Hagel C, Schittenhelm J, Fischer S, Tatagiba M, Nagel C, Jeibmann A, Bohring A, Mautner VF, Paulus W. 2012. Hybrid neurofibroma/schwannoma is overrepresented among schwannomatosis and neurofibromatosis patients. Am J Surg Pathol 36:702–709.

Hornigold RE, Golding JF, Leschziner G, Obholzer R, Gleeson MJ, Thomas N, Walsh D, Saeed S, Ferner RE. 2012. The NFTI-QOL: A Disease-Specific Quality of Life Questionnaire for Neurofibromatosis 2. J Neurol Surg B Skull Base 73:104–111.

Karajannis MA, Legault G, Hagiwara M, Giancotti FG, Filatov A, Derman A, Hochman T, Goldberg JD, Vega E, Wisoff JH, Golfinos JG, Merkelson A, Roland JT, Allen JC. 2014. Phase II study of everolimus in children and adults with neurofibromatosis type 2 and progressive vestibular schwannomas. Neuro Oncol 16:292–297.

Kossler N, Stricker S, Rodelsperger C, Robinson PN, Kim J, Dietrich C, Osswald M, Kuhnisch J, Stevenson DA, Braun T, Mundlos S, Kolanczyk M. 2011. Neurofibromin (Nf1) is required for skeletal muscle development. Hum Mol Genet 20:2697–2709.

Krab LC, de Goede-Bolder A, Aarsen FK, Pluijm SM, Bouman MJ, van der Geest JN, Lequin M, Catsman CE, Arts WF, Kushner SA, Silva AJ, de Zeeuw CI, Moll HA, Elgersma Y. 2008. Effect of simvastatin on cognitive functioning in children with neurofibromatosis type 1: A randomized controlled trial. JAMA 300:287–294.

Lammert M, Friedman JM, Kluwe L, Mautner VF. 2005. Prevalence of neurofibromatosis 1 in German children at elementary school enrollment. Arch Dermatol 141:71–74.

Li W, Cui Y, Kushner SA, Brown RA, Jentsch JD, Frankland PW, Cannon TD, Silva AJ. 2005. The HMG-CoA reductase inhibitor lovastatin reverses the learning and attention deficits in a mouse model of neurofibromatosis type 1. Curr Biol 15:1961–1967.

Li W, You L, Cooper J, Schiavon G, Pepe-Caprio A, Zhou L, Ishii R, Giovannini M, Hanemann CO, Long SB, Erdjument-Bromage H, Zhou P, Tempst P, Giancotti FG. 2010. Merlin/NF2 suppresses tumorigenesis by inhibiting the E3 ubiquitin ligase CRL4(DCAF1) in the nucleus. Cell 140:477–490.

Liu-Chittenden Y, Huang B, Shim JS, Chen Q, Lee SJ, Anders RA, Liu JO, Pan D. 2012. Genetic and pharmacological disruption of the TEAD-YAP complex suppresses the oncogenic activity of YAP. Genes Dev 26:1300–1305.

Peyre M, Stemmer-Rachamimov A, Clermont-Taranchon E, Quentin S, El-Taraya N, Walczak C, Volk A, Niwa-Kawakita M, Karboul N, Giovannini M, Kalamarides M. 2013. Meningioma progression in mice triggered by Nf2 and Cdkn2ab inactivation. Oncogene 32:4264–4272.

Plotkin SR, Merker VL, Muzikansky A, Barker FG, Slattery W III. 2014. Natural history of vestibular schwannoma growth and hearing decline in newly diagnosed neurofibromatosis type 2 patients. Otol Neurotol 35: e50–e56.

Pong WW, Higer SB, Gianino SM, Emnett RJ, Gutmann DH. 2013. Reduced microglial CX3CR1 expression delays neurofibromatosis-1 glioma formation 2. Ann Neurol 73:303–308.

Quinlan KG, Seto JT, Turner N, Vandebrouck A, Floetenmeyer M, Macarthur DG, Raftery JM, Lek M, Yang N, Parton RG, Cooney GJ, North KN. 2010. Alpha-actinin-3 deficiency results in reduced glycogen phosphorylase activity and altered calcium handling in skeletal muscle. Hum Mol Genet 19:1335–1346.

Rauen KA. 2013. The RASopathies. Annu Rev Genomics Hum Genet 14:355–369.

Schulz A, Baader SL, Niwa-Kawakita M, Jung MJ, Bauer R, Garcia C, Zoch A, Schacke S, Hagel C, Mautner VF, Hanemann CO, Dun XP, Parkinson DB, Weis J, Schroder JM, Gutmann DH, Giovannini M, Morrison H. 2013. Merlin isoform 2 in neurofibromatosis type 2-associated polyneuropathy. Nat Neurosci 16:426–433.

Sperfeld AD, Hein C, Schroder JM, Ludolph AC, Hanemann CO. 2002. Occurrence and characterization of peripheral nerve involvement in neurofibromatosis type 2. Brain 125:996–1004.

Stevenson DA, Allen S, Tidyman WE, Carey JC, Viskochil DH, Stevens A, Hanson H, Sheng X, Thompson BA, Okumura MJ, Reinker K, Johnson B, Rauen KA. 2012. Peripheral muscle weakness in RASopathies. Muscle Nerve 46:394–399.

Sullivan K, El-Hoss J, Quinlan KG, Deo N, Garton F, Seto JT, Gdalevitch M, Turner N, Cooney GJ, Kolanczyk M, North KN, Little DG, Schindeler A. 2014. NF1 is a critical regulator of muscle development and metabolism 1. Hum Mol Genet 23:1250–1259.

Tanaka K, Eskin A, Chareyre F, Jessen WJ, Manent J, Niwa-Kawakita M, Chen R, White CH, Vitte J, Jaffer ZM, Nelson SF, Rubenstein AE, Giovannini M. 2013. Therapeutic potential of HSP90 inhibition for neurofibromatosis type 2. Clin Cancer Res 19:3856–3870.

Trivedi R, Byrne J, Huson SM, Donaghy M. 2000. Focal amyotrophy in neurofibromatosis 2. J Neurol Neurosurg Psychiatry 69:257–261.

van der Vaart T, Plasschaert E, Rietman AB, Renard M, Oostenbrink R, Vogels A, de Wit MC, Descheemaeker MJ, Vergouwe Y, Catsman-Berrevoets CE, Legius E, Elgersma Y, Moll HA. 2013. Simvastatin for cognitive deficits and behavioural problems in patients with neurofibromatosis type 1 (NF1-SIMCODA): A randomised, placebo-controlled trial. Lancet Neurol 12:1076–1083.

van Eeghen AM, Pulsifer MB, Merker VL, Neumeyer AM, van Eeghen EE, Thibert RL, Cole AJ, Leigh FA, Plotkin SR, Thiele EA. 2013. Understanding relationships between autism, intelligence, and epilepsy: A cross-disorder approach. Dev Med Child Neurol 55:146–153.

Violante IR, Ribeiro MJ, Edden RA, Guimaraes P, Bernardino I, Rebola J, Cunha G, Silva E, Castelo-Branco M. 2013. GABA deficit in the visual cortex of patients with neurofibromatosis type 1: Genotype-phenotype correlations and functional impact. Brain 136:918–925.

Walsh KS, Velez JI, Kardel PG, Imas DM, Muenke M, Packer RJ, Castellanos FX, Acosta MT. 2013. Symptomatology of autism spectrum disorder in a population with neurofibromatosis type 1. Dev Med Child Neurol 55:131–138.

Weiss B, Widemann BC, Wolters P, Dombi E, Vinks AA, Cantor A, Korf B, Perentesis J, Gutmann DH, Schorry E, Packer R, Fisher MJ. 2013. Sirolimus for non-progressive NF1-associated plexiform neurofibromas: An NF clinical trials consortium phase II study. Pediatr Blood Cancer 61:982–986.

Original Article

Neurofibromin Deficiency-Associated Transcriptional Dysregulation Suggests a Novel Therapy for Tibial Pseudoarthrosis in NF1†

Authors: Nandina Paria PhD,[1] Tae-Joon Cho MD,[2] In Ho Choi MD/PhD,[2] Nobuhiro Kamiya MD/PhD,[1,3] Kay Kayembe,[4] Rong Mao MD,[5,6] Rebecca L. Margraf PhD,[5] erlinde Obermosser MD,[4] Ila Oxendine,[1] David W. Sant,[5] Mi Hyun Song MD,[7] David Stevenson MD,[8] David H. Viskochil MD,[8] Carol A. Wise PhD,[1,9,10,3] Harry K.W. Kim MD,[1,3] and Jonathan J Rios PhD[1,9,10,3,*]

Author Affiliations: [1]Sarah M. and Charles E. Seay Center for Musculoskeletal Research, Texas Scottish Rite Hospital for Children, Dallas, Texas, 75219 USA; [9]Department of Pediatrics, [10]Eugene McDermott Center for Human Growth and Development and [3]Department of Orthopaedic Surgery, UT Southwestern Medical Center, Dallas, TX, 75390 USA; [2]Division of Pediatric Orthopaedics, Seoul National University Children's Hospital, Seoul, Republic of Korea; [4]Baylor Institute for Immunology Research, Dallas, Texas 75204 USA; [5]ARUP Institute for Clinical and xperimental Pathology, ARUP Laboratories, [6]Department of Pathology, University of Utah Medical School, and [8]Department of Pediatrics, Division of Medical Genetics, University of Utah, Salt Lake City, Utah, 84103 USA; [7]Department of Orthopaedic Surgery, Jeju National University Hospital, Jeju, Republic of Korea;

Corresponding Author: [*]Jonathan J. Rios (email: Jonathan.Rios@tsrh.org)

†This article has been accepted for publication and undergone full peer review but has not been through the copyediting, typesetting, pagination and proofreading process, which may lead to differences between this version and the Version of Record. Please cite this article as doi: [10.1002/jbmr.2298]

Additional Supporting Information may be found in the online version of this article.

Initial Date Submitted April 11, 2014; Date Revision Submitted June 9, 2014; Date Final Disposition Set June 12, 2014

Journal of Bone and Mineral Research

DOI 10.1002/jbmr.2298

ABSTRACT:

Neurofibromatosis type 1 (NF1) is an autosomal dominant disease caused by mutations in *NF1*. Among the earliest manifestations is tibial pseudoarthrosis and persistent nonunion after fracture. To further understand the pathogenesis of pseudoarthrosis and the underlying bone remodeling defect, pseudoarthrosis tissue and cells cultured from surgically resected pseudoarthrosis tissue from NF1 individuals were analyzed using whole-exome and whole-transcriptome sequencing as well as genomewide microarray analysis. Genomewide analysis identified multiple genetic mechanisms resulting in somatic bi-allelic *NF1* inactivation; no other genes with recurring somatic mutations were identified. Gene expression profiling identified dysregulated pathways associated with neurofibromin deficiency, including phosphoinositol-3-kinase (PI3K) and mitogen-activated protein kinase (MAPK) signaling pathways. Unlike aggressive NF1-associated malignancies, tibial pseudoarthrosis tissue does not harbor a high frequency of somatic mutations in oncogenes or other tumor-suppressor genes, such as p53. However, gene expression profiling indicates pseudoarthrosis tissue has a tumor-promoting transcriptional pattern, despite lacking tumorigenic somatic mutations. Significant over-expression of specific cancer-associated genes in pseudoarthrosis highlights a potential for receptor tyrosine kinase inhibitors to target neurofibromin-deficient pseudoarthrosis and promote proper bone remodeling and fracture healing.

Keywords: Tumor-induced bone disease, Molecular pathways – Development, Cell/Tissue Signaling – Transcription factors, Human association studies, Diseases and Disorders Related to Bone - other

INTRODUCTION

Neurofibromatosis type 1 (NF1) is a common autosomal dominant disorder caused by mutations in *NF1*, a tumor suppressor gene that encodes neurofibromin, a GTPase-activating protein that negatively regulates RAS signaling (1,2). *NF1* haploinsufficiency constitutively activates the RAS signaling cascade, predisposing patients to secondary clinical sequelae such as neurofibromas and malignant peripheral nerve sheath tumors (MPNSTs). Often, tumors in these patients harbor a somatic mutation of the normal *NF1* allele or loss of heterozygosity (LOH), resulting in bi-allelic inactivation of *NF1* and neurofibromin deficiency, in addition to other somatic events (3).

Among the earliest clinical manifestations in individuals with NF1 is long bone dysplasia, usually affecting a single tibia (4,5). About 5% of individuals with NF1 will present with anterolateral bowing (dysplasia) leading to fracture that fails to achieve proper union, often after repeated surgical correction. A significant proportion (~16%) of individuals with NF1 and tibial pseudoarthrosis require amputation of the affected limb (6), or elect for amputation as the primary treatment. Long bone dysplasia and pseudoarthrosis were previously proposed to result from localized bi-allelic inactivation of *NF1* due to somatic LOH (7). However, subsequent studies reported inconsistent or inconclusive results in additional patients and the genomewide spectrum of somatic mutations in pseudoarthrosis tissue was never investigated (7,8).

How tibial pseudoarthrosis compares to other NF1-associated manifestations such as neurofibromas and MPNSTs, including the frequency of somatic mutation or gene expression profile, is unknown. Adjuvant therapies (i.e. bone morphogenetic proteins, bisphosphonates) have been attempted anecdotally based on data from preclinical models and current clinical understanding of the pathophysiology of tibial pseudarthrosis (5). However, a general lack of a

detailed biological understanding of NF1-associated tibial pseudoarthrosis has hindered progress in developing effective therapies to enhance bone healing and avoid amputation in these individuals. To understand the molecular mechanisms leading to tibial pseudoarthrosis, we comprehensively characterized genomewide somatic mutations and transcriptional dysregulation in tibial pseudoarthrosis in sixteen individuals with NF1.

MATERIALS AND METHODS

Genomic analyses. All samples were collected from individuals after obtaining written informed consent approved by the Institutional Review Board of the University of Texas Southwestern Medical Center, the University of Utah, or Seoul National University Hospital. Five of the sixteen samples included in this study were reported previously with inconsistent results after genotyping four polymorphic markers (D17S1863, GXALU, IN38, and 3*NF1*-1) near the *NF1* locus (8). In this study, no sample showed evidence of LOH across all markers in the pseudoarthrosis compared to matched blood/saliva, and this method is unable to distinguish copy-neutral LOH from LOH caused by somatic gene deletion.

DNA was extracted from blood or saliva samples (N=16), tissue harvested during surgical procedures performed as standard of care (N=11) or from cells cultured from surgical tissue (N=6); DNA was extracted from tissue and cultured cells for individual NF#10. Whole-exome capture was performed using either the SeqCap EZ Human Exome Library (Nimblegen, Basel, Switzerland) or TruSeq Exome kit (Illumina, San Diego, CA) and sequenced using the paired-end 100bp protocol (SeqCap) or the paired-end 150bp (TruSeq) protocol on the Illumina HiSeq 2000/2500. Sequence reads were mapped using the Burrow-Wheeler aligner (9) and final alignments generated after multiple quality controls steps applied using the Genome Analysis

Toolkit (10), Samtools (11) and Picard. Somatic mutations were identified after comparison to matched blood, saliva or iliac crest samples, amplified by PCR and confirmed by Sanger sequencing. When necessary, PCR amplicons were cloned into pcDNA3.1 vector (Life Technologies, CA, USA) to Sanger sequence individual alleles.

Expression profiling. Whole-transcriptome profiling (RNA-seq) was performed using RNA extracted from cells cultured from tissue harvested during surgery, including iliac crest tissue haploinsufficient for *NF1* mutations and pseudoarthrosis tissue representing a mixed-cell population including *NF1*-deficient cells. Sequence reads were mapped to the human reference genome (b37) using TopHat. Low quality reads were filtered using Samtools and duplicates marked using Picard. Gene expression levels were calculated using BEDtools software. Differential expression analysis was performed using EdgeR software (12) implemented in the R statistical framework. Gene Ontology and Pathway enrichment were performed using Partek Genomics Suite software (Partek, St. Louis, MO).

Quality measures of RNA-sequencing were investigated. Pairwise correlation of gene expression between control samples calculated using counts per million (CPM) ranged from 0.60 to 0.85 (**Supplemental Fig. 20)**. To measure reproducibility between sequence runs, technical replicates were re-sequenced for a single iliac/pseudoarthrosis pair (NF#6). Pearson correlation for gene expression was high for both iliac (r=0.9861) and pseudoarthrosis (r=0.9846) samples (**Supplemental Fig 21**). As well, gene expression in both iliac samples from two individuals (NF#6 and NF#7) were highly correlated, with r=0.98 (**Supplemental Fig 22**). Multi-dimensional scaling of all samples clearly distinguished control samples from all NF1 samples, and both iliac samples with *NF1* haploinsufficiency clustered together and separate from all tibia

samples, which were less well clustered together (**Supplemental Fig. 23**). Pseudoarthrosis samples clustered more variably, likely from differences in the fraction of *NF1*-deficient cells making up the total RNA pool (mixed cell population) or possibly due to true biological differences. Regarding the latter, we were unable to identify a somatic *NF1* mutation for the distantly clustered tibia samples (NF#8 and NF#9); these samples were excluded from further analyses.

Cell culture. The surgically removed iliac crest and pseudoarthrosis tissues from individuals with NF1 were digested overnight with collagenase at 37º C followed by removal of undigested tissue. Cells were pelleted and re-suspended in Minimum Essential Medium (MEM) Alpha (Life Technologies, CA, USA) supplemented with 10% fetal bovine serum (Sigma, MO, USA) and 1% antibiotic (penicillin/streptomycin) (Life Technologies, CA, USA) and cultured as primary cells. Cultured cells reached confluence with spindle-shaped morphology, consistent with fibroblasts. Confluent cells were washed with 1X PBS and harvested by trypsinization. Cell morphology was indistinguishable between control, iliac crest and pseudoarthrosis samples.

Flow cytometry. Cells were cultured to ~90% confluence and harvested by trypsinization. The cell suspensions were fixed using 16% paraformaldehyde (PFA) (Electron Microscopy Sciences, PA, USA) at room temperature for 10 minutes. After fixation cells were re-suspended in 100% ice-cold methanol, incubated on ice for 10 minutes and stored at -80º C. The fixed and permeabilized cells were thawed and washed with FACS buffer (0.5% BSA/PBS) and re-suspended at a final concentration of approximately $5X10^5$ cells in 100ul. The cells were labeled with Alexa Fluor 647-conjugated anti-phospho-ERK1/2 primary antibody (Cell Signaling

Technology, MA, USA) using 1:50 dilution and incubated at room temperature for 30 minutes protected from light with occasional shaking every 10 minutes. Following incubation, cells were washed and re-suspended in approximately 500µl FACS buffer (0.5% BSA/PBS) and analyzed by flow cytometry. Flow cytometry was performed using an INFLUX cell sorter (BD Biosciences, CA, USA). A 640 nm laser operating at 120mW was used for excitation. Fluorescence signals were detected using bandpass filters 670/30 nm set into Alexa Fluor 647 channel.

RESULTS

Sixteen individuals with a clinical diagnosis of NF1 and tibial pseudoarthrosis were included in the study. Age at tibial fracture in these individuals ranged from shortly after birth to 13 years (**Table 1**). Genomic analyses including whole-exome sequencing (WES) and genomewide microarray SNP genotyping were performed using DNA extracted from tibial pseudoarthrosis tissue harvested during surgery and/or from cells cultured from pseudoarthrosis tissue. While pseudoarthrosis occurs in individuals without NF1, all individuals included in this study were diagnosed with NF1 using standard diagnostic criteria. To identify the constitutional *NF1* change and to confirm the pseudoarthrosis change was somatic, individual-matched samples from peripheral blood, saliva or cells cultured from iliac crest harvested during surgery were also included. WES identified the constitutional *NF1* mutation in 15 of 16 individuals, which predicted missense (n=3), nonsense (n=4), frameshift (n=3) and splice-site (n=5) changes (**Table 1**). The constitutional mutation was not identified in individual NF#16.

To comprehensively investigate genomewide LOH, we used high-density genomewide SNP genotyping in samples from eleven individuals. The sensitivity of this method to detect

LOH was expected to vary between pseudoarthrosis samples, as they likely represented mixed cell populations. However, SNP analysis identified a single recurring large region of LOH in five individuals (NF#1, NF#4, NF#7 and NF#10) that spanned the entire long-arm of chromosome 17 (17qLOH) and included *NF1* (example in **Fig. 1a**). Complete LOH was not observed for any sample but was represented as a split signal compared to the normal 17p region, reflecting the mixed-cell population in the analysis. In a fifth individual (NF#12), 17qLOH was detected by WES, which also confirmed somatic homozygosity of the mutant *NF1* allele (**Supplemental Fig. 1**). Homozygosity of the mutant allele was also confirmed in one individual (NF#7) by allele-specific expression analysis using whole-transcriptome profiling (RNA-seq) of cells cultured from iliac crest and tibial pseudoarthrosis. Expression of the mutant allele was higher (78% of reads) than the normal allele in cells from the pseudoarthrosis tissue, but only 35% of reads in the individual-matched iliac crest cells, suggesting that the mutant allele was homozygous in the pseudoarthrosis tissue (**Fig. 1b**).

Additional somatic sequence mutations, including three nonsense, two frameshift and one splice-site changes, were confirmed in six additional individuals. One individual (NF#6) harbored a somatic deletion spanning exons 14 to 46 (c.1642_6999del; p.Asn510_Lys2333del). The deletion was not identified using microarray genotyping, likely due to the mixed population sample, but was evident in multiple split-reads from RNA-seq. A junction fragment spanning the deletion was amplified from pseudoarthrosis but not the individual-matched control sample, and Sanger sequencing confirmed the deletion occurred on the normal allele, resulting in somatic bi-allelic inactivation (**Supplemental Fig. 2**).

Results for *NF1* mutations discovered in all individuals are shown in **Table 1** and details of the genomic analyses for all individuals, including those described above, are found in

Supplemental Fig. 1-16. We did not detect somatic mutations in pseudoarthrosis samples from four individuals (NF#3, NF#8, NF#9 and NF#14).

To further characterize the global gene dysregulation resulting from bi-allelic inactivation of *NF1*, we performed RNA-seq of cells cultured from pseudoarthrosis tissue harvested during surgery (NF#6-11), individual-matched cells cultured from iliac crest harvested during surgery (NF#6 and NF#7) and cells from bone tissue of three unrelated controls without NF1. To identify genes with altered expression associated with neurofibromin deficiency, we separately compared gene expression of pseudoarthrosis and iliac samples from individuals with NF1 to control samples. Differentially expressed genes with greater than 2-fold expression difference in pseudoarthrosis samples compared to control samples were identified with false discovery rate (FDR)-adjusted FDRp<0.05. These genes were then filtered to exclude those with differential expression (no fold change requirement) between iliac and control samples with nominal ($p<0.05$) significance. This analysis identified 258 genes with differential expression associated with bi-allelic *NF1* inactivation (**Supplemental Table 1**).

Gene-set enrichment analysis using Gene Ontology (GO) annotations of the 258 genes identified significant enrichment for genes involved in "positive regulation of MAPK activity" ($p=9.16e^{-5}$, GO:0043406) (**Supplemental Table 2)**. The 38 genes annotated with this GO term (amigo.geneontology.org) were investigated further using Hierarchical Clustering methods, which successfully distinguished control, iliac and pseudoarthrosis samples (**Supplemental Fig. 17**).

Hierarchical clustering analysis of the 258 differentially expressed genes identified 76 upregulated and 182 downregulated genes in pseudoarthrosis samples (**Fig. 2a**). We subjected the upregulated genes to pathway enrichment analysis to more broadly assess biological

functions and pathways significantly upregulated in NF1-associated tibial pseudoarthrosis (**Supplemental Table 3**). This analysis identified three pathways implicated in cancer ("PI3K-Akt Signaling", "MAPK Signaling" and "Pathways in Cancer"). Eight genes in these pathways were upregulated in neurofibromin-deficient pseudoarthrosis samples, and several are known to promote NF1-associated tumor progression (**Fig 2b**). Of the eight, epidermal growth factor receptor (encoded by the *EGFR* gene) was of particular interest, as it is a multi-functional receptor tyrosine kinase that promotes cellular proliferation and tumorigenesis (13). Matched-pair analysis of iliac-pseudoarthrosis pairs from two individuals with NF1 (NF#6 and NF#7) identified 42 of the 258 genes with significant differential expression (**Supplemental Fig. 18**). Interestingly, of the 42 genes, the second-most statistically significant gene (FDRp=1.09e-27) and the second-most upregulated gene (34-fold increase) was *EREG*, which encodes the EGFR ligand epiregulin.

Previous studies focused on ERK activation resulting from *Nf1* deficiency in mouse models of tibial pseudoarthrosis (15). We sought to determine whether transcriptional changes observed in pseudoarthrosis cells were driven by quantitative differences in ERK activation compared to individual-matched haploinsufficient iliac crest cells. Using fluorescent-activated flow cytometry, we detected no quantitative increase in ERK activation (phosphorylation) in pseudoarthrosis cells compared to individual-matched iliac crest cells, suggesting transcriptional changes in pseudoarthrosis are associated with neurofibromin deficiency independent of ERK activation (**Supplemental Fig. 19**). Interestingly, we found that cells from pseudoarthrosis tissue displayed significant upregulation of the *KITLG* gene encoding KIT ligand (also known as stem cell factor (SCF)) and *RAC2*.

DISCUSSION

We describe the genetic and transcriptional mechanisms underlying tibial pseudoarthrosis occurring in individuals with NF1. Similar to other secondary sequelae in these patients (e.g. cutaneous neurofibroma), tibial pseudoarthrosis manifests, at least in part, from bi-allelic inactivation of *NF1*. The combination of WES, microarray analysis and RNA-seq identified somatic variants in 12 of 16 pseudoarthrosis samples; no somatic variants were identified in the remaining four samples. It is possible these samples harbor somatic mutations other than in *NF1* that lead to tibial dysplasia and pseudoarthrosis. More likely, the proportion of cells with a somatic *NF1* mutation was below the level of detection for either WES or RNA-seq, or these individuals harbor changes not detectable by our methods, such as deep intronic mutations affecting splicing or changes in methylation that affect expression. The transcriptional changes in pseudoarthrosis cultured cells suggest an underlying tumor-promoting expression profile with upregulated *EGFR*, *EREG* and *KITLG* (SCF). Transcriptional analyses were performed using plastic-adherent bone marrow stromal cells, rather than directly from pseudoarthrosis tissue. While it is possible to introduce artifacts from culture procedures, multiple quality-control analyses suggest the differences in gene expression are not due to such artifacts. However, it will be important to similarly investigate changes in gene expression in mouse models of *Nf1* deficiency as well as directly from patient tissue. Taken together, the changes in gene expression described here are associated with pseudoarthrosis-specific neurofibromin deficiency. This raises the intriguing question of why NF1 patients with tibial pseudoarthrosis do not develop bone tumors. Our genomewide analyses found that tibial pseudoarthrosis lacks oncogenic mutations driving transformation, such as p53 mutations frequent in MPNSTs. Additionally, tissue-specific events or changes in the local microenvironment (17) may be required for tumorigenesis. Despite

the lack of bone tumor formation in these patients, our results suggest studies using receptor tyrosine kinase inhibitors are warranted in existing mouse models and may improve future patient outcomes.

Currently, off-label use of recombinant human bone morphogenic protein (BMP)-2 (rhBMP-2) is used to stimulate bone formation, although its efficacy and complication rate are widely debated, particularly in spine surgery (18). The results presented here provide mechanistic context to the use of rhBMP-2 in tibial pseudoarthrosis with NF1. In mouse embryonic fibroblasts, fibroblast growth factor (FGF)-2-induced MAPK activation inhibited the osteogenic response to BMP2 (19). Additionally, FGF2 inhibited osteoblast differentiation of hMSCs (20). These studies, with the significant *FGF2* upregulation in pseudoarthrosis (**Fig. 2**), suggest a mechanism by which the osteogenic effects of rhBMP-2 treatment may be inhibited in tibial pseudoarthrosis in individuals with NF1. Our data alternatively suggest that use of FDA-approved receptor tyrosine kinase inhibitors may be more therapeutically effective for promoting bone formation and union in these patients by specifically targeting neurofibromin-deficient cells.

In the context of NF1-associated tumors, *EGFR* is frequently amplified in malignant peripheral nerve sheath tumors (MPNST), and *EGFR* expression was shown to confer tumorigenic potential in *NF1*-deficient neurofibroma cells (21,22). A potential role for *EGFR* expression in development of pseudoarthrosis and subsequent chronic nonunion is intriguing and suggests the potential for targeted therapy using EGFR-inhibitors to promote proper bone formation. Multiple inhibitors of receptor tyrosine kinases, including EGFR, are clinically available, and several effectively limited proliferation/survival of MPNST cells (23,24). In metastatic colorectal cancer (mCRC) with normal *KRAS*, high *EREG* expression, which encodes

for an EGFR ligand, was shown to predict response to the EGFR inhibitor Cetuximab (14). The association of mCRC response to Cetuximab coupled with elevated expression of *EREG/EGFR* in pseudoarthrosis samples suggests EGFR or other receptor tyrosine kinase inhibitors should be investigated as alternative therapies in these patients.

Mouse models of *Nf1* deficiency previously demonstrated an essential role for neurofibromin in regulating proper bone development. Although the specific cell type involved in development of tibial pseudoarthrosis remains unknown, multiple cell type-specific conditional mutants displayed tibial dysplasia and insufficient bone formation after fracture that was attributed to altered Ras/Erk signaling (15,25,26). However, changes in global gene expression are not described. In two mouse models of neurofibromin deficiency, pharmacologic MEK inhibition improved fracture healing, although a significant proportion (~35%) of fractures failed to achieve bone union despite treatment (15). In a study of *Nf1*-deficient bone marrow-derived mast cells stimulated with murine SCF, phosphoinositide-3-kinase (PI3K)-induced Rac activation co-regulated the Ras/Mek/Erk signaling pathway (16). Therefore, inhibition of PI3K, rather than Mek, had a greater effect in limiting mast cell proliferation. Upregulation of both *KITLG* and *RAC2* in our pseudoarthrosis samples may suggest a feedback mechanism driving ERK activation in tibial pseudoarthrosis. With the dysregulation observed here, future studies should be performed to compare fracture healing in mice treated with MEK inhibitors to those treated with receptor tyrosine kinase inhibitors or combination therapy with MEK and PI3K inhibitors. Ultimately, these studies hope to improve treatment strategies in NF1 patients with persistent nonunion after fracture.

ACKNOWLEDGEMENTS

The authors thank all clinicians at Texas Scottish Rite Hospital for Children (Dallas, TX) and Shriners Hospital for Children (Salt Lake City, UT) for their role in collecting surgical tissues. We thank Dr. Jacques D'Astous and Dr. John Carey for their input and oversight of tissue procurement protocols, Dr. Talia Muram, Allie Grossmann, Kristen Mauldin and Vanessa Laws for sample processing, and Heather Hanson and Janice Davis for research coordination. The authors thank the Microarray and Next-Generation Sequencing core facilities at the University of Texas Southwestern Medical Center for technical assistance and Sarah Lassen for help in preparing figures. This work was supported by grants from the Pediatric Orthopaedic Society of North America, Department of Defense (award W81XWH-11-1-250), Shriners Hospital for Children (Salt Lake City, UT) and Texas Scottish Rite Hospital for Children. Portions were supported by the University of Utah Clinical Genetics Research Program (CGRP) and the National Center for Research Resources and National Center for Advancing Translational Sciences at the National Institutes of Health (UL1RR025764). Research reported in this publication was supported by the National Center for Advancing Translational Sciences of the National Institutes of Health under award Number UL1TR001105. The content is solely the responsibility of the authors and does not necessarily represent the official views of the NIH.

Data analysis: N.P, K.K, G.O, R.M, R.L.M, J.J.R, T-J. C., I.H.C, N.K., I.O. and M.H.S. Study design: D.W.S, D.A.S, D.H.V, C.A.W, H.K.W.K and J.J.R. Drafting manuscript: D.A.S, H.K.W.K, T-J. C., C.A.W and J.J.R. J.J.R takes responsibility for the integrity of the data analysis.

REFERENCES

1. Ballester R, Marchuk D, Boguski M, Saulino A, Letcher R, Wigler M, et al. The NF1 locus encodes a protein functionally related to mammalian GAP and yeast IRA proteins. Cell 1990;63(4)**:**851-9.
2. Xu GF, Lin B, Tanaka K, Dunn D, Wood D, Gesteland R, et al. The catalytic domain of the neurofibromatosis type 1 gene product stimulates ras GTPase and complements ira mutants of S. cerevisiae. Cell 1990;63(4)**:**835-41.
3. Cichowski K, Jacks T. NF1 tumor suppressor gene function: narrowing the GAP. Cell 2001;104(4)**:**593-604.
4. Stevenson DA, Little D, Armstrong L, Crawford AH, Eastwood D, Friedman JM, et al. Approaches to treating NF1 tibial pseudarthrosis: consensus from the Children's Tumor Foundation NF1 Bone Abnormalities Consortium. Journal of pediatric orthopedics 2013;33(3)**:**269-75.
5. Elefteriou F, Kolanczyk M, Schindeler A, Viskochil DH, Hock JM, Schorry EK, et al. Skeletal abnormalities in neurofibromatosis type 1: approaches to therapeutic options. American journal of medical genetics Part A 2009;149A(10)**:**2327-38.
6. Stevenson DA, Birch PH, Friedman JM, Viskochil DH, Balestrazzi P, Boni S, et al. Descriptive analysis of tibial pseudarthrosis in patients with neurofibromatosis 1. American journal of medical genetics 1999;84(5)**:**413-419.
7. Stevenson DA, Zhou H, Ashrafi S, Messiaen LM, Carey JC, D'Astous JL, et al. Double inactivation of NF1 in tibial pseudarthrosis. American journal of human genetics 2006;79(1)**:**143-8.

8. Lee SM, Choi IH, Lee DY, Lee HR, Park MS, Yoo WJ, et al. Is double inactivation of the Nf1 gene responsible for the development of congenital pseudarthrosis of the tibia associated with NF1? J Orthop Res 2012;30(10)**:**1535-40.

9. Li H, Durbin R. Fast and accurate short read alignment with Burrows-Wheeler transform. Bioinformatics 2009;25(14)**:**1754-60.

10. McKenna A, Hanna M, Banks E, Sivachenko A, Cibulskis K, Kernytsky A, et al. The Genome Analysis Toolkit: a MapReduce framework for analyzing next-generation DNA sequencing data. Genome research 2010;20(9)**:**1297-1303.

11. Li H, Handsaker B, Wysoker A, Fennell T, Ruan J, Homer N, et al. The Sequence Alignment/Map format and SAMtools. Bioinformatics 2009;25(16)**:**2078-9.

12. Robinson MD, McCarthy DJ, Smyth GK. edgeR: a Bioconductor package for differential expression analysis of digital gene expression data. Bioinformatics 2010;26(1)**:**139-40.

13. Lo HW. Nuclear mode of the EGFR signaling network: biology, prognostic value, and therapeutic implications. Discov Med 2010;10(50)**:**44-51.

14. Khambata-Ford S, Garrett CR, Meropol NJ, Basik M, Harbison CT, Wu S, et al. Expression of epiregulin and amphiregulin and K-ras mutation status predict disease control in metastatic colorectal cancer patients treated with cetuximab. J Clin Oncol 2007;25(22)**:**3230-7.

15. Sharma R, Wu X, Rhodes SD, Chen S, He Y, Yuan J, et al. Hyperactive Ras/MAPK signaling is critical for tibial nonunion fracture in neurofibromin-deficient mice. Human molecular genetics 2013;22(23)**:**4818-28.

16. Ingram DA, Hiatt K, King AJ, Fisher L, Shivakumar R, Derstine C, et al. Hyperactivation of p21(ras) and the hematopoietic-specific Rho GTPase, Rac2, cooperate to alter the

proliferation of neurofibromin-deficient mast cells in vivo and in vitro. J Exp Med 2001;194(1):57-69.

17. Le LQ, Shipman T, Burns DK, Parada LF. Cell of origin and microenvironment contribution for NF1-associated dermal neurofibromas. Cell Stem Cell 2009;4(5):453-63.

18. Carragee EJ, Hurwitz EL, Weiner BK. A critical review of recombinant human bone morphogenetic protein-2 trials in spinal surgery: emerging safety concerns and lessons learned. Spine J 2011;11(6):471-91.

19. Sapkota G, Alarcon C, Spagnoli FM, Brivanlou AH, Massague J. Balancing BMP signaling through integrated inputs into the Smad1 linker. Molecular cell 2007;25(3):441-54.

20. Biver E, Soubrier AS, Thouverey C, Cortet B, Broux O, Caverzasio J, et al. Fibroblast growth factor 2 inhibits up-regulation of bone morphogenic proteins and their receptors during osteoblastic differentiation of human mesenchymal stem cells. Biochemical and biophysical research communications 2012;427(4):737-42.

21. Perry A, Kunz SN, Fuller CE, Banerjee R, Marley EF, Liapis H, et al. Differential NF1, p16, and EGFR patterns by interphase cytogenetics (FISH) in malignant peripheral nerve sheath tumor (MPNST) and morphologically similar spindle cell neoplasms. J Neuropathol Exp Neurol 2002;61(8):702-9.

22. Williams JP, Wu J, Johansson G, Rizvi TA, Miller SC, Geiger H, et al. Nf1 mutation expands an EGFR-dependent peripheral nerve progenitor that confers neurofibroma tumorigenic potential. Cell Stem Cell 2008;3(6):658-69.

23. Kohli L, Kaza N, Lavalley NJ, Turner KL, Byer S, Carroll SL, et al. The pan erbB inhibitor PD168393 enhances lysosomal dysfunction-induced apoptotic death in malignant peripheral nerve sheath tumor cells. Neuro Oncol 2012;14(3)**:**266-77.

24. Holtkamp N, Malzer E, Zietsch J, Okuducu AF, Mucha J, Mawrin C, et al. EGFR and erbB2 in malignant peripheral nerve sheath tumors and implications for targeted therapy. Neuro Oncol 2008;10(6)**:**946-57.

25. Kolanczyk M, Kossler N, Kuhnisch J, Lavitas L, Stricker S, Wilkening U, et al. Multiple roles for neurofibromin in skeletal development and growth. Human molecular genetics 2007;16(8)**:**874-86.

26. Wang W, Nyman JS, Ono K, Stevenson DA, Yang X, Elefteriou F. Mice lacking Nf1 in osteochondroprogenitor cells display skeletal dysplasia similar to patients with neurofibromatosis type I. Human molecular genetics 2011;20(20)**:**3910-24.

FIGURE LEGENDS

Figure 1. Genomic analysis in tibial pseudoarthrosis. (A) Homozygosity plots from microarray SNP genotyping of DNA from cells cultured from tibial pseudoarthosis (top) and blood (bottom) from one individual (NF#7) are shown. Somatically acquired homozygosity of the entire q-arm of chromosome 17 was evident and does not result from chromosomal deletion (data not shown). The split signal is consistent with a mix of *NF1*-haploinsufficient and pseudoarthrosis cells. Red asterisk shows the location of *NF1*. **(B)** RNA-sequencing from cells cultured from pseudoarthrosis (top) and iliac crest (bottom) from the same individual (NF#7). The constitutional c.4537C>T (p.Arg1513*) mutation is shown, with the proportion of reads shown above for normal (blue) and mutant (red) alleles. While the mutant allele was expressed less compared to normal in the iliac crest cells, the mutant allele was expressed higher than the normal allele in the pseudoarthrosis sample, suggesting homozygosity of the mutant allele in pseudoarthrosis.

Figure 2. Expression profiling in tibial pseudoarthrosis. (A) Hierarchical clustering of 258 differentially expressed genes associated with neurofibromin deficiency identified 76 genes upregulated and 182 genes downregulated in pseudoarthrosis samples. Expression is shown as a heatmap with low (blue) to high (red) relative expression. Sample groups are shown on the left, including control (black), iliac crest (yellow) and pseudoarthrosis (green). **(B)** Venn diagram of genes significantly upregulated in pseudoarthrosis samples and annotated in the PI3K-Akt Signaling, Cancer and/or MAPK Signaling pathways.

TABLES

Table 1. Constitutional and somatic *NF1* changes in NF1 individuals with pseudoarthrosis.

Individual	Age at Tibial Fracture	Ethnicity	Constitutional *NF1* Change[a]	Somatic *NF1* Change[b]
NF#1	4 years	Korean	c.1185+1G>A	17q LOH
NF#2	1 year	Korean	c.1950_1951insA (p.Leu650fs)	c.5839C>T (p.Arg1947*)
NF#3	3 years	Korean	c.3826C>T (p.Arg1276X)	n.d.
NF#4	1 year	Korean	c.6718_6719insAGCAAACGAGTGTCTTC ; p.His2240fs	17q LOH
NF#5	2 years	Korean	c.4269+2T>C	c.7907+1G>A
NF#6	1 year	Hispanic	c.1381C>T (p.R461X)	c.1642_6999del (p.Asn510_Lys2333del)
NF#7	1 year	Hispanic	c.4537C>T (p.Arg1513*)	17q LOH
NF#8	9 months	Caucasian	c.4537C>T (p.Arg1513*)	n.d
NF#9	6 years	African-American	c.3709-2A>G	n.d.
NF#10	13 years	Caucasian	c.3827G>A (p.Arg1276Gln)	17q LOH
NF#11	6 years	Caucasian	c.2533T>C (p.Cys845Arg)	c.403_404insC (p.Leu134fs)
NF#12	1 year	Caucasian	c.5546G>A (p.Arg1849Gln)	17q LOH
NF#13	6 years	Caucasian	c.1642-2A>G	c.133_140delAATATTTC (p.Asn45fs)
NF#14	10 years	Caucasian	c.7155delT (p.Val2385fs)	n.d.
NF#15	3 months	Caucasian	c.61-2A>T	c.3574G>T (p.Glu1192*)
NF#16	2 weeks	Caucasian	n.d.	c.3826C>T (p.Arg1276*)

[a] Identified in DNA from blood, saliva or cells cultured from iliac crest bone; n.d., not detected

[b] Identified in DNA from frozen pseudoarthrosis bone or cells cultured from pseudoarthrosis bone; n.d., not detected; LOH, loss of heterozygosity

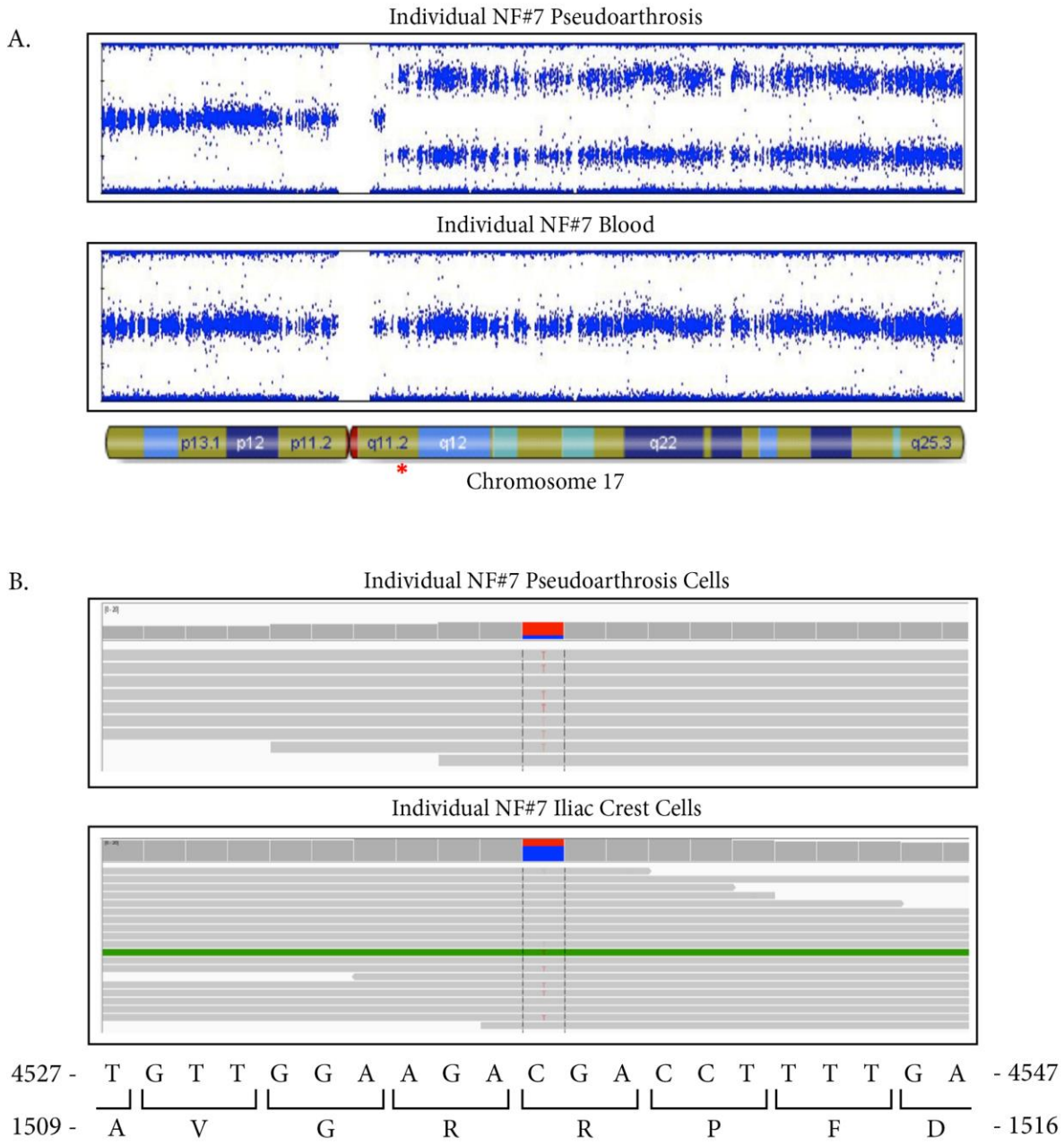
A.
Individual NF#7 Pseudoarthrosis
Individual NF#7 Blood
p13.1
p12
p11.2
q11.2
q12
q22
q25.3
Chromosome 17
B.
Individual NF#7 Pseudoarthrosis Cells
Individual NF#7 Iliac Crest Cells
4527 - T G T T G G A A G A C G A C C T T T G A - 4547
1509 - A V G R R P F D - 1516

Figure 1

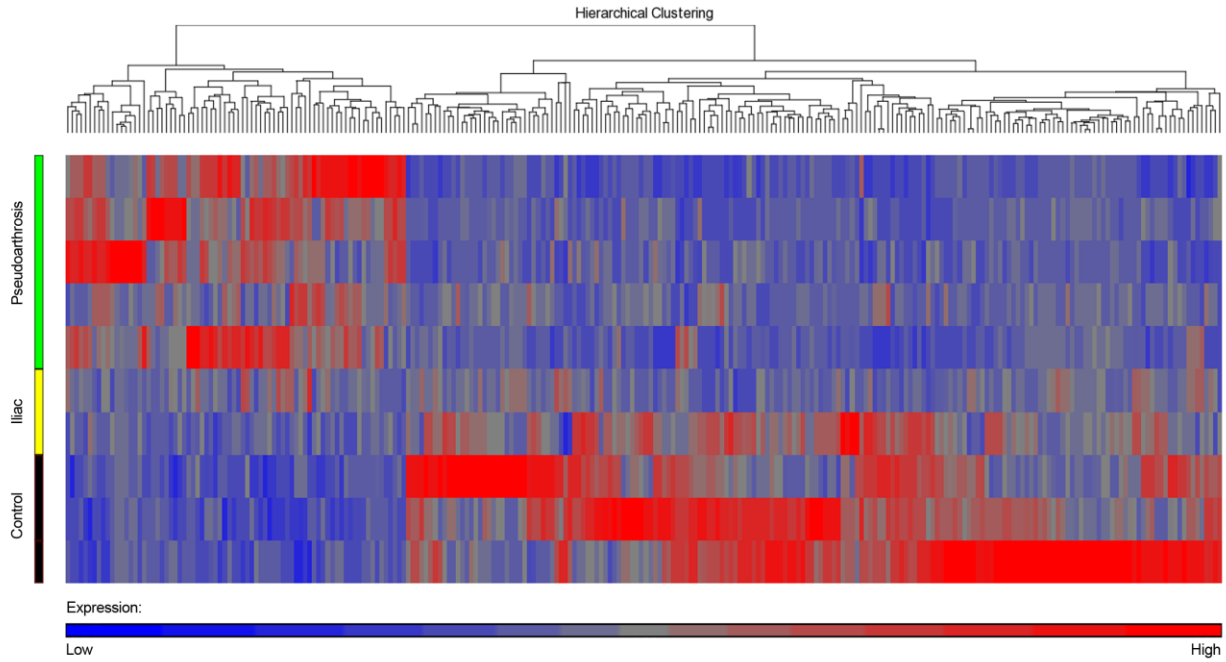
Hierarchical Clustering
Pseudoarthrosis
Iliac
Control
Expression:
Low
High

Figure 2A

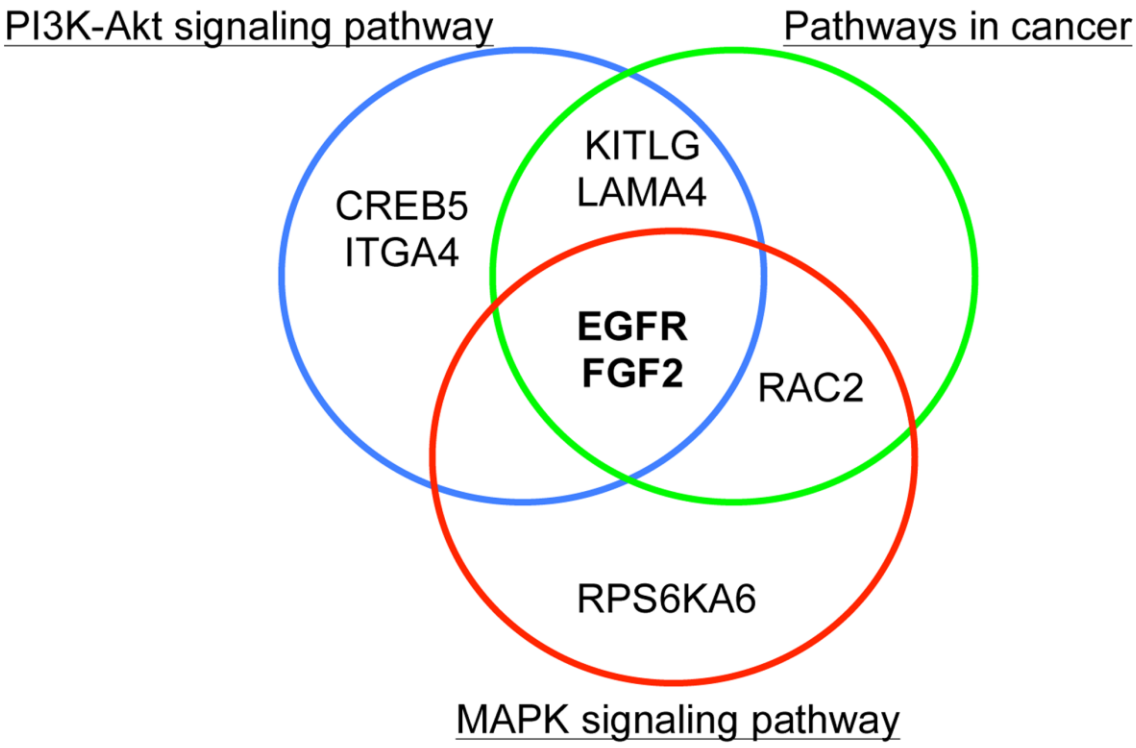
PI3K-Akt signaling pathway
Pathways in cancer
CREB5
ITGA4
KITLG
LAMA4
EGFR
FGF2
RAC2
RPS6KA6
MAPK signaling pathway

Figure 2B

nature medicine

Asfotase-α improves bone growth, mineralization and strength in mouse models of neurofibromatosis type-1

Jean de la Croix Ndong[1,2], Alexander J Makowski[1,3–5], Sasidhar Uppuganti[1,4], Guillaume Vignaux[1,2], Koichiro Ono[1,2,6], Daniel S Perrien[1,4,5,7], Simon Joubert[8], Serena R Baglio[9], Donatella Granchi[9], David A Stevenson[10], Jonathan J Rios[11–14], Jeffry S Nyman[1,3–5] & Florent Elefteriou[1,2,15,16]

Individuals with neurofibromatosis type-1 (NF1) can manifest focal skeletal dysplasias that remain extremely difficult to treat. NF1 is caused by mutations in the *NF1* gene, which encodes the RAS GTPase–activating protein neurofibromin. We report here that ablation of *Nf1* in bone-forming cells leads to supraphysiologic accumulation of pyrophosphate (PP_i), a strong inhibitor of hydroxyapatite formation, and that a chronic extracellular signal–regulated kinase (ERK)-dependent increase in expression of genes promoting PP_i synthesis and extracellular transport, namely *Enpp1* and *Ank*, causes this phenotype. *Nf1* ablation also prevents bone morphogenic protein-2–induced osteoprogenitor differentiation and, consequently, expression of alkaline phosphatase and PP_i breakdown, further contributing to PP_i accumulation. The short stature and impaired bone mineralization and strength in mice lacking *Nf1* in osteochondroprogenitors or osteoblasts can be corrected by asfotase-α enzyme therapy aimed at reducing PP_i concentration. These results establish neurofibromin as an essential regulator of bone mineralization. They also suggest that altered PP_i homeostasis contributes to the skeletal dysplasias associated with NF1 and that some of the NF1 skeletal conditions could be prevented pharmacologically.

Mutations in the *NF1* gene cause NF1, a genetic disorder with an incidence of 1/3,500 live births worldwide. This condition is characterized by malignant and nonmalignant pathologies, including skeletal manifestations[1–6]. Dystrophic scoliosis, tibia bowing, bone fragility, fracture and pseudarthrosis (nonunion following fracture) are skeletal conditions associated with high morbidity in this population[7–10]. Despite recent progress toward understanding the role of *NF1* in skeletal tissues, it is still unclear why and how these bone pathologies arise, raising uncertainty regarding optimal treatment[2,3].

Although individuals with NF1 are typically born with heterozygous mutations in *NF1*, loss of heterozygosity has been detected in pseudarthrosis biopsies[11], suggesting that local somatic *NF1* loss of function contributes to NF1 skeletal dysplasia. This point is further supported by the relative commonality of defects observed between pseudarthrosis lesions from individuals with NF1 and the skeleton of mice characterized by conditional loss of *Nf1* in osteoprogenitors. These mice indeed tend to recapitulate, in their entire skeleton, the genetic and cellular consequences of *NF1* loss of function that occurs locally in human NF1 pseudarthroses. *Nf1* inactivation in osteochondroprogenitors in $Nf1^{flox/flox}$; *Prx-cre* or $Nf1^{flox/flox}$; *Col2a1-cre* mice (herein called *Prx-Nf1* KO or *Col2-Nf1* KO mice, respectively) led to reduced stature, low bone mass, tibia bowing, diaphyseal ectopic blood vessel formation and hypomineralization associated with weakened bone mechanical properties. Bone cellular parameters also indicated that neurofibromin is required for normal osteoblast differentiation and expression of *Tnfsf11*, the gene encoding receptor activator of nuclear factor κB ligand, and hence for osteoclastogenesis[12–18]. The existence of *Nf1*-deficient osteoblasts in an *Nf1* heterozygous bone microenvironment has also been shown to cause bone loss and delayed bone healing in $Nf1^{flox/flox}$; *Col1a1-cre* (*Col1-Nf1* KO) mice via activation of transforming growth factor-β (TGF-β) signaling[19]. Notably, each of these NF1 models, as well as bone biopsies from individuals with NF1 pseudarthrosis[20], are characterized by excessive deposition of unmineralized bone matrix (osteoid) despite normal serum phosphate and calcium concentrations.

Bone matrix mineralization is a tightly regulated process that requires collagen, calcium and phosphate to form ordered crystals of hydroxyapatite, as well as tissue-nonspecific alkaline phosphatase

[1]Vanderbilt Center for Bone Biology, Vanderbilt University Medical Center, Nashville, Tennessee, USA. [2]Department of Medicine, Vanderbilt University Medical Center, Nashville, Tennessee, USA. [3]Department of Biomedical Engineering, Vanderbilt University, Nashville, Tennessee, USA. [4]Department of Orthopaedic Surgery & Rehabilitation, Vanderbilt University Medical Center, Nashville, Tennessee, USA. [5]Department of Veterans Affairs, Tennessee Valley Healthcare System, Nashville, Tennessee, USA. [6]Department of Orthopaedics, Nohon Koukan Hospital, Kawasaki, Kanagawa, Japan. [7]Vanderbilt University Institute of Imaging Sciences, Vanderbilt University Medical Center, Nashville, Tennessee, USA. [8]Alexion Pharmaceuticals, Cheshire, Connecticut, USA. [9]Laboratory for Orthopedic Pathophysiology and Regenerative Medicine, Istituto Ortopedico Rizzoli, Bologna, Italy. [10]Department of Pediatrics, University of Utah, Salt Lake City, Utah, USA. [11]Sarah M. and Charles E. Seay Center for Musculoskeletal Research, Texas Scottish Rite Hospital for Children, Dallas, Texas, USA. [12]Department of Pediatrics, UT Southwestern Medical Center, Dallas, Texas, USA. [13]Eugene McDermott Center for Human Growth & Development, UT Southwestern Medical Center, Dallas, Texas, USA. [14]Department of Orthopaedic Surgery, UT Southwestern Medical Center, Dallas, Texas, USA. [15]Department of Pharmacology, Vanderbilt University Medical Center, Nashville, Tennessee, USA. [16]Department of Cancer Biology, Vanderbilt University Medical Center, Nashville, Tennessee, USA. Correspondence should be addressed to F.E. (florent.elefteriou@vanderbilt.edu).

Received 12 December 2013; accepted 1 May 2014; published online 6 July 2014; doi:10.1038/nm.3583

(ALP) activity to hydrolyze PP_i (a potent inhibitor of mineralization) and generate inorganic phosphate[21]. Extracellular concentrations of PP_i are determined by (i) its degradation via ALP, (ii) its synthesis catalyzed by the nucleoside triphosphate pyrophosphohydrolase ENPP1/PC-1 (called ENPP1 herein) and (iii) its transport into the extracellular milieu through the PP_i channel ANK[22]. Mineralization is also controlled by Phospho1, a phosphatase that provides intracellular inorganic phosphate to generate PP_i[23], and by glycoproteins such as osteopontin, which inhibits crystal nucleation on collagen fibers in mineralizing vesicles[24,25]. Multiple growth factors such as TGF-β, activin A, bone morphogenic protein-2 (BMP2), insulin-like growth factor-1, fibroblast growth factor-2 and fibroblast growth factor-23 are involved in bone and/or cartilage mineralization[26–34]. A common signaling pathway engaged by these factors is the RAS-ERK pathway, which is constitutively activated in cells lacking neurofibromin, the RAS GTPase–activating protein (RAS-GAP) encoded by *NF1* (ref. 35). We thus hypothesized that neurofibromin, via its inhibitory action on RAS-ERK signaling in bone-forming cells, could be an important regulator of bone matrix mineralization and bone mechanical properties. We show here that neurofibromin inhibits the expression of genes increasing PP_i extracellular levels and that hydrolysis of excess PPi with a recombinant form of ALP improves bone growth and mineralization in mouse models of NF1 skeletal dysplasia. These data suggest a potential pharmacological avenue to prevent some of the skeletal abnormalities of individuals with NF1.

RESULTS

Uncontrolled PP_i production in *Nf1*-deficient bone cells

To address whether and how *Nf1* regulates bone mineralization, we first asked whether *Nf1* ablation in bone marrow stromal cells (BMSCs) affects extracellular PP_i concentrations. BMSCs from *Col2-Nf1* KO mice, lacking *Nf1* in osteochondroprogenitor cells, showed a 60–70% lower *Nf1* expression compared to those from wild-type (WT) mice (**Fig. 1a**), consistent with the heterogeneous nature of the cell populations that comprise BMSC cultures[36]. This lower *Nf1* expression level was accompanied by a significantly higher (70%) extracellular PP_i concentration in the conditioned medium of undifferentiated BMSC cultures compared to that of WT controls (**Fig. 1b**). Addition of a recombinant form of ALP, in the form of sALP-FcD10 (also known as asfotase-α, 0.5 μg ml^{-1}) to induce PP_i hydrolysis significantly reduced the amount of PP_i detected in both genotypes, confirming the validity of the PP_i measurements.

High extracellular PP_i concentration can be generated by increased production of PP_i by the ectonucleophosphatase ENPP1 and by increased cellular export through the transporter ANK. Both *Ank* and *Enpp1* mRNA (**Fig. 1c**) and protein (**Supplementary Fig. 1a**) levels were higher in *Nf1*-deficient BMSCs compared to WT BMSCs. Expression of the gene encoding osteopontin (*Spp1*) was also higher in *Nf1*-deficient BMSCs (**Fig. 1c**), consistent with the reported stimulatory effect of PP_i on *Spp1* expression[25]. We obtained similar results when comparing *Nf1*-deficient osteoprogenitor cells generated from $Nf1^{flox/flox}$ BMSC cultures infected with a Cre-expressing adenovirus to control $Nf1^{flox/flox}$ BMSC cultures infected with a GFP-expressing adenovirus (**Supplementary Fig. 1b**), which confirmed that the changes in gene expression measured in BMSCs from *Col2-Nf1* KO mice were not caused by fewer osteoprogenitors initially plated. *Ank*, *Enpp1* and *Spp1* expression was also significantly higher in long bones, calvarias and epiphyses (cartilage) from 3-week-old *Col2-Nf1* KO versus WT mice (**Fig. 1d**), whereas expression of *Runx2* and *Alpl*, two osteoblast differentiation marker genes, was lower (**Supplementary Fig. 1c**). Lastly, MEK inhibition by U0126 (1 μM, 24 h) blunted the increase in *Ank*, *Enpp1* and *Spp1* expression observed in *Nf1*-deficient BMSCs, indicating that neurofibrin controls the expression of these genes in a RAS/ERK-dependent fashion (**Fig. 1c** and **Supplementary Fig. 1b**).

To assess whether these molecular findings in mice could be replicated in humans, we obtained RNA from adherent human bone stromal cells prepared from bone biopsies from six healthy control subjects without NF1 and nine individuals with NF1 tibial pseudarthrosis, and measured *ENPP1* and *ANKH* transcript levels by quantitative PCR. Consistent with the mouse data, *ENPP1* expression was significantly higher in cultured cells from NF1 pseudarthrosis tissues (**Fig. 1e**), despite the small number of available samples and consistent with the cell heterogeneity of these cultures. *ANKH* expression, however,

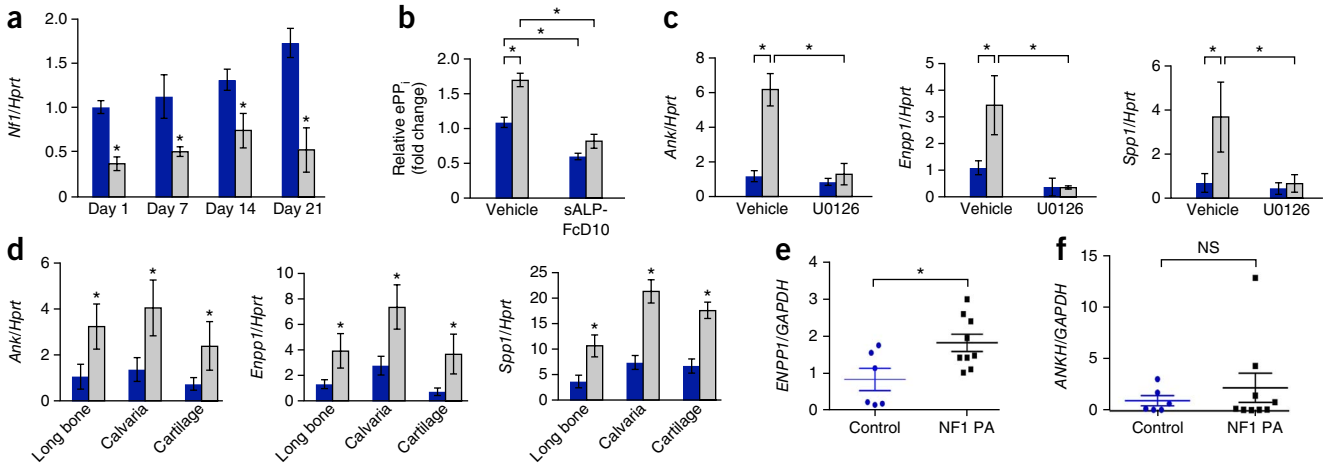

Figure 1 Uncontrolled *Ank*, *Enpp1* and *Spp1* expression and increased PP_i production in *Nf1*-deficient osteoblasts. (**a**) *Nf1* mRNA expression in mouse BMSCs differentiated for 7, 14 and 21 d ($n = 3$). (**b**) Extracellular PP_i (ePP_i) concentration in the conditioned medium of undifferentiated BMSCs ($n = 3$). Vehicle, $Na(PO_4)^{2-}$, pH 7.4. (**c**) *Ank*, *Enpp1* and *Spp1* mRNA expression in BMSCs treated with vehicle (DMSO) or U0126 for 24 h ($n = 3$). (**d**) *Ank*, *Enpp1* and *Spp1* mRNA expression in long bones, calvarias and epiphyses of 3-week-old WT (blue) and *Col2-Nf1* KO (gray) mice ($n = 6$ per group). (**e**,**f**) *ENPP1* and *ANKH* mRNA expression in human adherent bone marrow cells from control ($n = 6$ per group) and NF1-related pseudarthrosis (NF1 PA, $n = 9$ per group) biopsies. $^*P < 0.05$, determined by one-way analysis of variance (ANOVA) and Student's *t*-test. NS, nonsignificant. Data are expressed as mean ± s.d.

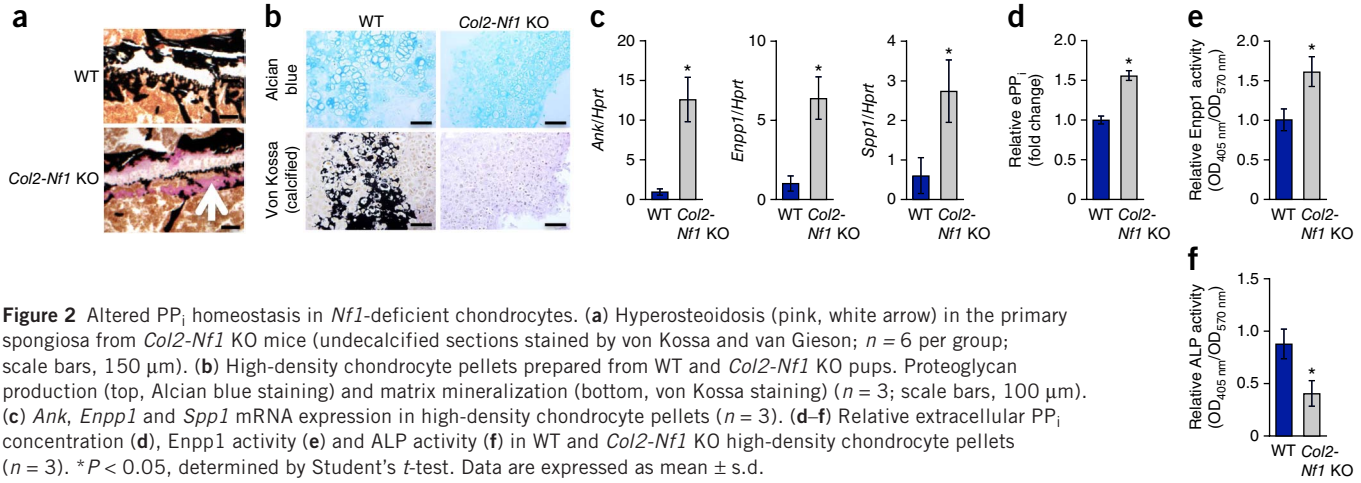

Figure 2 Altered PP_i homeostasis in *Nf1*-deficient chondrocytes. (**a**) Hyperosteoidosis (pink, white arrow) in the primary spongiosa from *Col2-Nf1* KO mice (undecalcified sections stained by von Kossa and van Gieson; $n = 6$ per group; scale bars, 150 µm). (**b**) High-density chondrocyte pellets prepared from WT and *Col2-Nf1* KO pups. Proteoglycan production (top, Alcian blue staining) and matrix mineralization (bottom, von Kossa staining) ($n = 3$; scale bars, 100 µm). (**c**) *Ank*, *Enpp1* and *Spp1* mRNA expression in high-density chondrocyte pellets ($n = 3$). (**d**–**f**) Relative extracellular PP_i concentration (**d**), Enpp1 activity (**e**) and ALP activity (**f**) in WT and *Col2-Nf1* KO high-density chondrocyte pellets ($n = 3$). $^*P < 0.05$, determined by Student's *t*-test. Data are expressed as mean ± s.d.

was variable between samples and not significantly different between cultures from normal and NF1 pseudarthrosis biopsies (**Fig. 1f**).

Mice lacking *Nf1* in mature osteoblasts (*Col1-Nf1* KO mice) have a uniform distribution of nonmineralized matrix throughout trabecular bone compartments[18], whereas mice lacking *Nf1* in osteochondroprogenitors and chondrocytes (*Col2-Nf1* KO mice) are characterized by an osteoid preferentially distributed in the primary spongiosa, where osteoblasts and chondrocytes mineralize their matrix (**Fig. 2a**). On the basis of these observations and because neurofibromin is expressed in hypertrophic chondrocytes[37,38], we hypothesized that this RAS-GAP could also contribute to cartilage mineralization, which is a process important for bone growth and ossification during development and bone healing in adults. In support of this hypothesis, *Col2-Nf1* KO chondrocyte high-density micromass cultures generated a typical Alcian blue–positive matrix but did not show signs of mineralization, in contrast to WT chondrocyte cultures (**Fig. 2b**). In addition, *Ank*, *Enpp1* and *Spp1* expression was significantly higher in *Nf1*-deficient micromass chondrocyte cultures versus WT cultures (**Fig. 2c**), in agreement with the data obtained from cartilaginous epiphyses, which contain a high proportion of chondrocytes (**Fig. 1d**). Accordingly, extracellular PP_i concentration (**Fig. 2d**) and Enpp1 enzymatic activity (**Fig. 2e**) were significantly higher, whereas ALP activity was lower (**Fig. 2f**) in *Nf1*-deficient versus WT chondrocytes.

Lack of *Nf1* in BMSCs impairs BMP2 osteogenic action

BMSCs isolated from *Col2-Nf1* KO mice displayed, compared to BMSCs isolated from WT mice, a significantly lower differentiation potential, as determined by lower osteoblast colony-forming unit (CFU-Ob) number, lower tissue-nonspecific ALP activity (**Fig. 3a**) and lower expression of osteoblast differentiation markers including *Runx2*, *Alpl* and *Bglap*, the gene encoding osteocalcin (**Fig. 3b**). We obtained similar results using $Nf1^{flox/flox}$ BMSCs infected with a Cre-expressing adenovirus (**Supplementary Fig. 1d**,**e**). However, in contrast to what we observed in the case of *Ank* and *Enpp1* expression, MEK inhibition by U0126 (1 µM), tremetinib or PD198306 (0.1 µM and 200 nM, respectively, data not shown) for 24 h did not correct the expression level of *Runx2* or *Alpl* in *Nf1*-deficient BMSCs (**Fig. 3c**), indicating that the expression of these two genes is not directly controlled by neurofibromin. Extracellular PP_i concentration, as well as *Ank*, *Enpp1* and *Spp1* expression, remained above or equal to that of WT controls throughout the differentiation period (**Fig. 3d**,**e**).

BMPs are known for their ability to promote osteoprogenitor differentiation[39] but have had limited effects on the differentiation of *Nf1*-heterozygous osteoprogenitors and on bone union in *Nf1*-heterozygous mice[40,41]. Recombinant human BMP2 (100 ng ml^{-1}) did not stimulate ALP activity or CFU-Ob formation in BMSC cultures from *Col2-Nf1* KO mice, although it did, as expected, promote

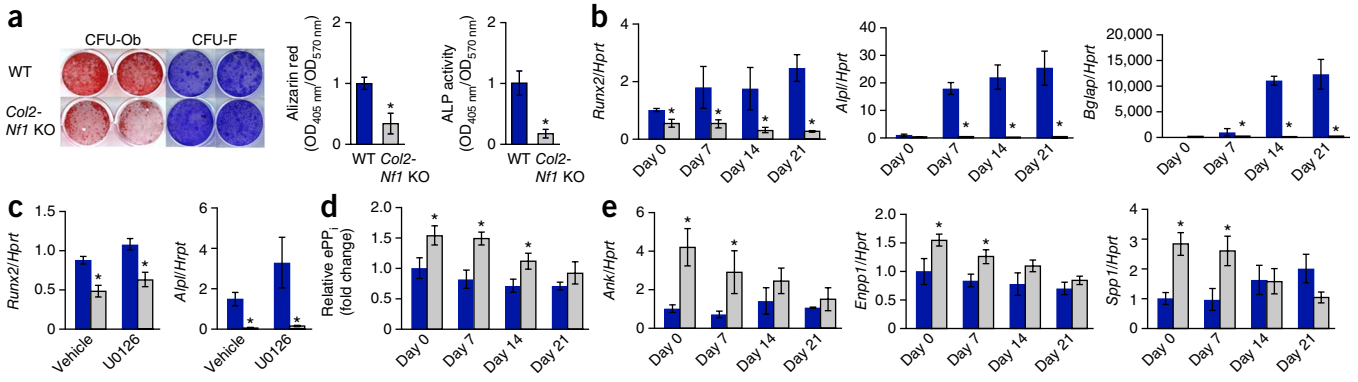

Figure 3 Blunted BMP2 response and osteoblast differentiation potential in *Nf1*-deficient osteoprogenitors. (**a**) BMSC differentiation analyzed by Alizarin red S staining (differentiation and mineralization, CFU-Ob), crystal violet staining of fibroblast CFUs (cell number, CFU-F, left), soluble Alizarin red S/crystal violet optical density ratio (middle) and ALP activity/crystal violet ratio (right) ($n = 3$). Blue, WT mice; gray, *Col2-Nf1* KO mice. (**b**) *Runx2*, *Alpl* and *Bglap* mRNA expression in BMSCs differentiated for 7, 14 and 21 d ($n = 3$). (**c**) *Runx2* and *Alpl* mRNA expression in serum-starved BMSCs treated with vehicle (DMSO) or U0126 for 24 h ($n = 3$). (**d**) Extracellular PP_i concentration/protein concentration in BMSCs differentiated for 7, 14 and 21 d ($n = 3$). (**e**) Normalized *Ank*, *Enpp1* and *Spp1* mRNA expression in BMSCs differentiated for 7, 14 and 21 d ($n = 3$). $^*P < 0.05$, determined by one-way ANOVA and Student's *t*-test. Data are expressed as mean ± s.d.

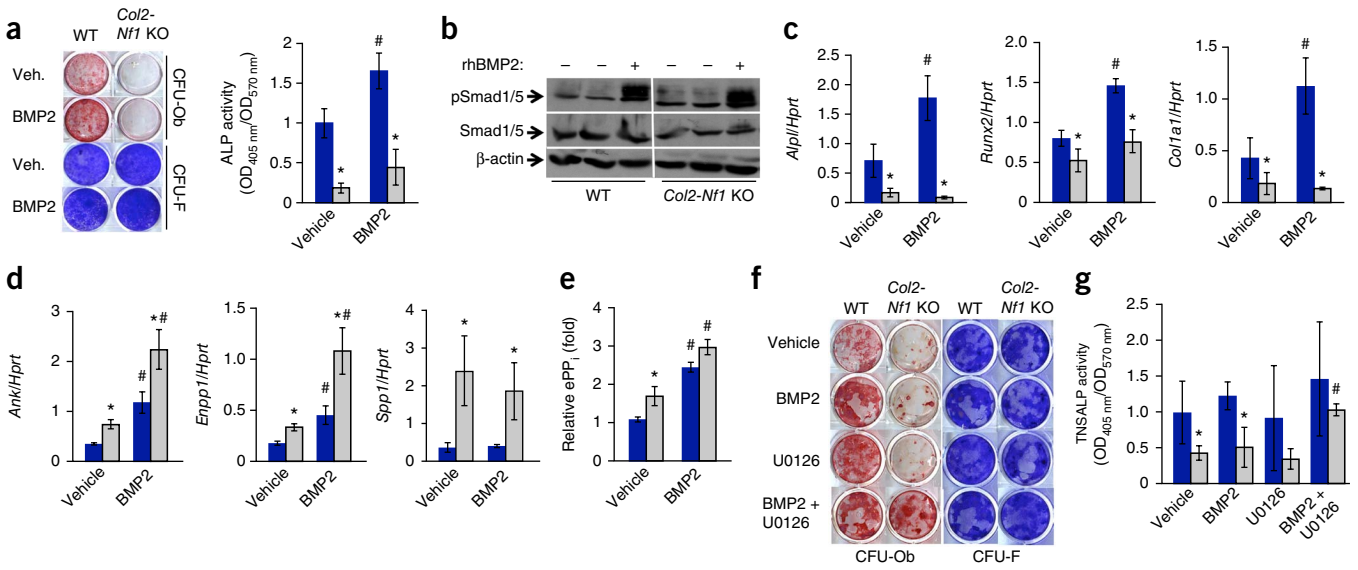

Figure 4 BMP2 does not promote differentiation in *Nf1*-deficient BMSCs but exacerbates their mineralization deficit. (**a**) BMSC differentiation analyzed by Alizarin red S (differentiation and mineralization, CFU-Ob) and crystal violet (cell number, CFU-F) staining ($n = 3$) and ALP activity ($n = 3$) following vehicle (Veh.) or BMP2 treatment. Blue, WT mice; gray, *Nf1* KO mice. (**b**) Phosphorylated Smad1 and/or Smad5 (pSmad1/5) induction in serum-starved BMSCs following recombinant human BMP2 (rhBMP2) treatment for 1 h. Smad1/5 and β-actin served as loading controls ($n = 3$). (**c**,**d**) *Alpl*, *Runx2* and *Col1a1* (**c**) and *Ank*, *Enpp1* and *Spp1* (**d**) mRNA expression following BMP2 treatment for 2 weeks ($n = 3$). (**e**) Extracellular PP_i relative concentration (normalized to protein concentration) in the conditioned medium of BMSCs treated with BMP2 for 24 h ($n = 3$). (**f**,**g**) BMSC differentiation analyzed by Alizarin red S (differentiation and mineralization, CFU-Ob) and crystal violet (cell number, CFU-F) staining (**f**, $n = 3$) and ALP activity (**g**, $n = 3$) following treatment with vehicle or BMP2 or U0126 or both for 2 weeks. $^*P < 0.05$ versus WT in the same treatment group; $^\#P < 0.05$ versus vehicle in the same genotype group, determined by one-way ANOVA and Student's *t*-test. Data are expressed as mean ± s.d.

CFU-Ob formation and ALP activity in WT BMSC cultures following 2 weeks of treatment (**Fig. 4a**). Smad1 and Smad5 phosphorylation in response to BMP2 treatment (100 ng ml^{-1}, 1 h) was not affected by *Nf1* deficiency (**Fig. 4b**), indicating that the lack of stimulatory effect of BMP2 on *Nf1*-deficient BMSC differentiation is not caused by repression of BMP2 receptor expression or by the production of factors inhibiting canonical Smad signaling. Treatment with BMP2 for 2 weeks also failed to increase the expression of *Alpl*, *Runx2* and *Col1a1* in BMSC cultures from *Col2-Nf1* KO mice (**Fig. 4c**). However, it significantly increased the expression of *Ank* and *Enpp1* (but not *Spp1*) (**Fig. 4d**) and PP_i extracellular concentration (**Fig. 4e**) in both WT and *Nf1*-deficient BMSCs. CFU-Ob formation, ALP activity (**Fig. 4f**,**g**) and the expression of *Alpl* and *Col1a1* (**Supplementary Fig. 2a**,**b**) in *Nf1*-deficient BMSC cultures were higher following a 2-week-long combined treatment with the MEK inhibitor U0126 (1 μM) and BMP2 (100 ng ml^{-1}), but not with either of these treatments alone. This combination treatment also partially reduced the increased *Ank* and *Enpp1* expression and PP_i extracellular concentration detected in vehicle-treated *Nf1*-deficient BMSC cultures, possibly owing to the antagonistic effect of these two drugs on *Ank* and *Enpp1* expression (**Supplementary Fig. 2c**,**d**).

sALP-FcD10 improves bone growth and mineral density in *Col2-Nf1* KO mice

If excessive extracellular PP_i levels cause the mineralization deficit observed in *Col2-Nf1* KO mice, then reducing PP_i concentration should have beneficial effects on matrix mineralization. This is experimentally possible by inhibiting PP_i generation or increasing its catabolism. We chose the latter approach because PP_i is a substrate for ALP, and a recombinant form of human ALP is clinically available to treat *ALPL*-deficient subjects with hypophosphatasia[42,43]. We thus treated WT and *Nf1*-deficient BMSCs with vehicle or sALP-FcD10 (0.5 mg ml^{-1}) in osteogenic conditions for 14 d and assessed matrix mineralization. As predicted, sALP-FcD10 increased matrix mineralization in both genotypes, although the relative increase was more pronounced in cultures from *Col2-Nf1* KO than in those from WT mice (**Fig. 5a**). This pronounced increase occurred despite the persistent differentiation deficit of *Nf1*-deficient BMSCs in the presence of sALP-FcD10 (**Supplementary Fig. 3a**). Treatment with sALP-FcD10 reduced *Spp1* expression in *Nf1*-deficient BMSCs (**Supplementary Fig. 3a**), in agreement with the known stimulatory effect of PP_i on *Spp1* expression[25].

On the basis of these encouraging results, we treated *Col2-Nf1* KO newborn mice daily with subcutaneous injections of sALP-FcD10 (8.2 mg per kg body weight per d) for 18 d[44,45]. *Col2-Nf1* KO mice have short stature, low bone mass, decreased bone mineralization, cortical thickness and mineral density, and high cortical porosity[37]. Following this short treatment (dictated by the relatively high death rate of these mice at weaning), we observed a significant 73% increase in the size of mutant mice (**Fig. 5b**) and a clear increase in vertebral and tibial bone mineral density on radiographs (**Fig. 5c**,**d**). Treatment with sALP-FcD10 also significantly increased mid-diaphyseal cortical bone thickness, as measured by three-dimensional microcomputed tomography (μCT) (**Fig. 5e**), partially rescued the formation of secondary ossification centers, expanded tibia metaphyseal envelopes and increased the amount of calcified matrix in the growth plate hypertrophic zone of *Col2-Nf1* KO mice (**Fig. 5f**). Despite the seemingly pronounced effects of sALP-FcD10 observed by radiography and μCT, tibia cortical tissue mineral density and mineral-to-collagen ratio (**Supplementary Fig. 3b**,**c**) were not increased following treatment.

sALP-FcD10 increases bone mineralization in *Osx-Nf1* KO mice

Because *Col2-Nf1* KO mice manifest severe developmental phenotypes that limit their survival and thus the duration of treatments,

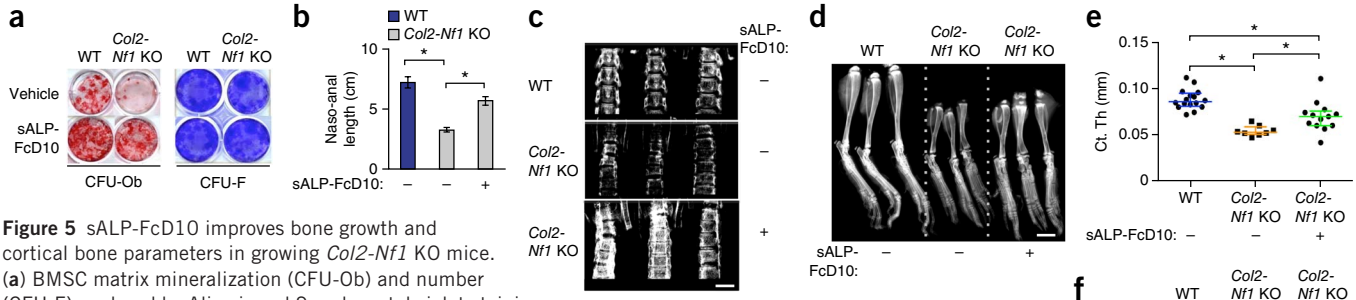

sALP-FcD10:	–	–	+
hBV/TV (%)	0.481 ± 0.1	0.340 ± 0.12*	0.548 ± 0.09#

Figure 5 sALP-FcD10 improves bone growth and cortical bone parameters in growing *Col2-Nf1* KO mice. (**a**) BMSC matrix mineralization (CFU-Ob) and number (CFU-F) analyzed by Alizarin red S and crystal violet staining, respectively ($n = 3$), following vehicle or sALP-FcD10 treatment for 2 weeks. (**b**–**f**) Bone growth (**b**, naso-anal length; WT, $n = 14$, KO + vehicle, $n = 8$, KO + sALP-FcD10, $n = 13$; P value determined by one-way ANOVA), vertebral (**c**, scale bar, 250 μm; WT, $n = 14$, KO + vehicle, $n = 8$, KO + sALP-FcD10, $n = 13$; P value determined by one-way ANOVA) and tibial (**d**, scale bar, 250 μm; WT, $n = 14$, KO + vehicle, $n = 8$, KO + sALP-FcD10, $n = 13$; P value determined by one-way ANOVA), bone mineral density (X-rays), cortical thickness (**e**, Ct.Th, μCT; WT, $n = 16$, KO + vehicle, $n = 8$, KO + sALP-FcD10, $n = 13$; P value determined by one-way ANOVA with Holm-Sidak's method), epiphyseal diameter (**f**, white arrows; scale bar, 45 μm; μCT) and hypertrophic zone von Kossa–positive calcified bone volume/tissue volume (hBV/TV, histology; WT, $n = 7$, KO + vehicle, $n = 6$, KO + sALP-FcD10, $n = 7$; P value determined by one-way ANOVA) in *Col2-Nf1* KO newborn pups treated daily with sALP-FcD10 for 18 d. *$P < 0.05$ versus WT; #$P < 0.05$ versus vehicle in the same genotype group. Data are expressed as mean ± s.d.

we generated mice in which *Nf1* can be ablated postnatally in osteoprogenitors expressing *Sp7* (also known as *Osx*) by crossing the inducible Tet-Off–based *Osx-cre* transgenic mice[46] with $Nf1^{flox/flox}$ mice[47]. This new mouse model makes it possible to dissect the mechanisms by which postnatal *Nf1* ablation impairs bone homeostasis, without complications arising from developmental phenotypes. *Osx-cre*; $Nf1_{Osx}^{flox/flox}$ mice (herein called *Osx-Nf1* KO mice) were undistinguishable in size from WT littermates upon doxycycline administration (i.e., Cre recombinase repression) from conception to day 14 (**Fig. 6a**) and had normal phosphate, calcium and 25-hydroxycholecalciferol (vitamin D) serum concentrations (**Supplementary Table 1**). *Osx-cre*–mediated *Nf1* ablation in osteoprogenitors at postnatal day 14 following doxycycline withdrawal, as seen in *Col2-Nf1* KO mice, caused hyperosteoidosis (**Fig. 6b**), lower bone mass (**Fig. 6c**), higher femoral diaphyseal cortical porosity (**Fig. 6d**) and lower cortical thickness, midshaft moment of inertia and cortical tissue mineral density compared to WT mice (**Fig. 6e**–**g**). Cortical mineral-to-collagen ratio measured by Raman spectroscopy (**Fig. 6h**)

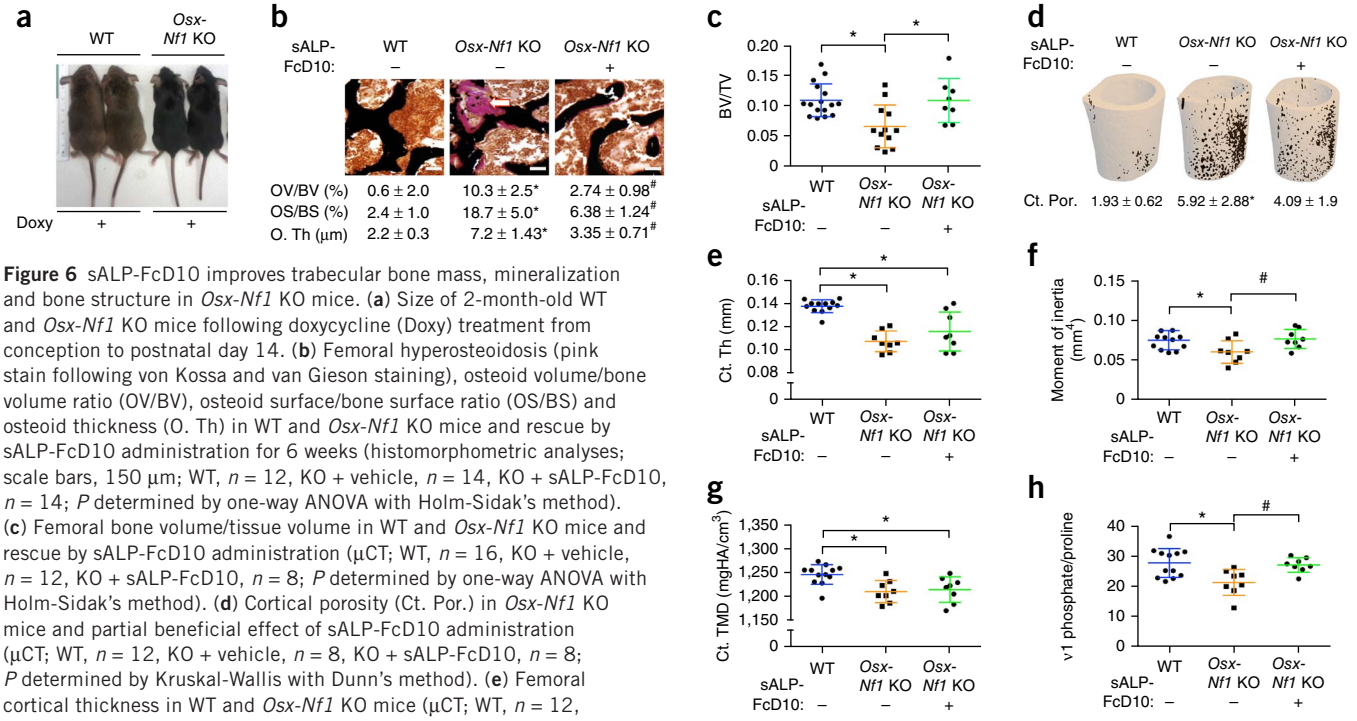

	WT	Osx-Nf1 KO	Osx-Nf1 KO
OV/BV (%)	0.6 ± 2.0	10.3 ± 2.5*	2.74 ± 0.98#
OS/BS (%)	2.4 ± 1.0	18.7 ± 5.0*	6.38 ± 1.24#
O. Th (μm)	2.2 ± 0.3	7.2 ± 1.43*	3.35 ± 0.71#

Ct. Por.	1.93 ± 0.62	5.92 ± 2.88*	4.09 ± 1.9

Figure 6 sALP-FcD10 improves trabecular bone mass, mineralization and bone structure in *Osx-Nf1* KO mice. (**a**) Size of 2-month-old WT and *Osx-Nf1* KO mice following doxycycline (Doxy) treatment from conception to postnatal day 14. (**b**) Femoral hyperosteoidosis (pink stain following von Kossa and van Gieson staining), osteoid volume/bone volume ratio (OV/BV), osteoid surface/bone surface ratio (OS/BS) and osteoid thickness (O. Th) in WT and *Osx-Nf1* KO mice and rescue by sALP-FcD10 administration for 6 weeks (histomorphometric analyses; scale bars, 150 μm; WT, $n = 12$, KO + vehicle, $n = 14$, KO + sALP-FcD10, $n = 14$; P determined by one-way ANOVA with Holm-Sidak's method). (**c**) Femoral bone volume/tissue volume in WT and *Osx-Nf1* KO mice and rescue by sALP-FcD10 administration (μCT; WT, $n = 16$, KO + vehicle, $n = 12$, KO + sALP-FcD10, $n = 8$; P determined by one-way ANOVA with Holm-Sidak's method). (**d**) Cortical porosity (Ct. Por.) in *Osx-Nf1* KO mice and partial beneficial effect of sALP-FcD10 administration (μCT; WT, $n = 12$, KO + vehicle, $n = 8$, KO + sALP-FcD10, $n = 8$; P determined by Kruskal-Wallis with Dunn's method). (**e**) Femoral cortical thickness in WT and *Osx-Nf1* KO mice (μCT; WT, $n = 12$, KO + vehicle, $n = 8$, KO + sALP-FcD10, $n = 8$; P determined by Kruskal-Wallis with Dunn's method). (**f**) Moment of inertia in WT and *Osx-Nf1* KO mice and rescue by sALP-FcD10 administration (μCT; WT, $n = 12$, KO + vehicle, $n = 8$, KO + sALP-FcD10, $n = 8$; P determined by one-way ANOVA with Holm-Sidak's method). (**g**) Cortical tissue mineral density (Ct. TMD) in WT and *Osx-Nf1* KO mice (μCT; WT, $n = 12$, KO + vehicle, $n = 8$, KO + sALP-FcD10, $n = 8$; P determined by one-way ANOVA with Holm-Sidak's method). (**h**) Mineral-to-collagen ratio (ν1 phosphate/proline) in WT and *Osx-Nf1* KO mice and rescue by sALP-FcD10 administration (Raman spectroscopy; WT, $n = 12$, KO + vehicle, $n = 8$, KO + sALP-FcD10, $n = 8$; P determined by Kruskal-Wallis with Dunn's method). *$P < 0.05$ versus WT; #$P < 0.05$ versus vehicle in the same genotype group. Data are expressed as mean ± s.d.

was also lower in *Osx-Nf1* KO mice, and femurs from *Osx-Nf1* KO mice were mechanically weaker than those from WT controls, as measured by three-point bending tests (**Supplementary Table 2**).

To assess the effect of sALP-FcD10 on the skeleton of this mouse model, we administered sALP-FcD10 daily from 2 weeks of age (at the time of *Nf1* ablation) for 6 weeks. In *Osx-Nf1* KO mice, treatment with sALP-FcD10 significantly increased trabecular bone volume/tissue volume ratio and moment of inertia, as assessed by μCT (**Fig. 6c**,**f**), as well as femoral stiffness, modulus and peak force, as measured by three-point bending (**Supplementary Table 2**), and led to a non-significant trend for increased cortical femoral thickness (**Fig. 6e**). Treatment with sALP-FcD10 also improved bone mineralization in *Osx-Nf1* KO mice, as measured by a drastic 73% reduction in osteoid volume per bone volume, a 65% reduction in osteoid surface per bone surface, a 53% decrease in osteoid thickness (**Fig. 6b**) and a 20% increase in mineral-to-collagen ratio (**Fig. 6h**).

DISCUSSION

We show here that the RAS-GAP activity of neurofibromin in the bone mesenchymal lineage restrains the expression of *Enpp1* and *Ank*, two main genes controlling PP_i homeostasis, and that increasing PP_i catabolism through enzyme therapy considerably improves bone mineralization and bone mechanical properties in mouse models of NF1 skeletal dysplasia. These results, along with suggestive evidence of conservation of function between mice and humans, support the causal role of increased PP_i levels in the etiology of NF1-related hyperosteoidosis and position neurofibromin as a critical and obligatory regulator of cartilage and bone mineralization. They also provide preclinical evidence that some of the most clinically challenging NF1-related skeletal maladies might be preventable.

Hyperactive TGF-β signaling has been proposed to cause bone loss and to delay bone healing in mice deficient for *Nf1* in mature osteoblasts and heterozygous for *Nf1* (ref. 19). TGF-β is also known to stimulate ERK activity and *Ank* and *Enpp1* expression, and to increase PP_i concentration in WT chondrocytes[48,49]. Therefore, *NF1*-deficient BMSCs may contribute cell autonomously and/or in a hyperactive TGF-β paracrine fashion to the extraphysiological skeletal accumulation of PP_i and to the impaired osteoblast differentiation and matrix mineralization observed in the setting of NF1. The beneficial effect of sALP-FcD10 on bone growth, mineralization and strength observed in this study suggests that PP_i accumulation and abnormal mineralization are important components of NF1-related bone dysplasia. However, further studies will be necessary to determine the evolution and contribution of all the cellular defects typical of *Nf1*-deficient bone cells on bone mass and strength over extended periods of treatment with sALP-FcD10, as this drug does not correct the differentiation phenotype of *Nf1*-deficient osteoblasts. Although TGF-β blockade might theoretically be used to promote bone union in children with NF1 pseudarthrosis, the cancer-prone status of this pediatric population and the known tumor-suppressor activity of TGF-β signaling limit this therapeutic approach[50]. Our results, on the other hand, suggest that stimulation of PP_i catabolism through enzyme therapy could be applied on a more chronic basis before fracture to strengthen the NF1-related dysplastic bones and prevent their mechanical failure.

The mineralization deficit of *Nf1*-deficient BMSCs could be detected in immature BMSCs before their differentiation into osteoblasts. Therefore, this phenotype cannot be attributed to the reduced differentiation potential of *Nf1*-deficient BMSCs, although the latter certainly contributes to the low bone mass phenotype observed in the two NF1 mouse models used in this study. It is also worth noting that BMP2 treatment, without the need for ERK blockade, stimulated the expression of *Ank* and *Enpp1* and increased extracellular PP_i concentration in *Nf1*-deficient BMSC cultures, as shown previously in WT cells[28]. This observation could explain why recombinant human BMP2 alone did not improve bone healing in NF1 mouse models[40,41] and bone union in individuals with NF1-related pseudarthrosis[51–53].

Our results indicate that *Nf1*-deficient BMSCs are not responsive to BMP2 with regard to their differentiation potential and suggest that this defect may in part underlie their inability to differentiate. In addition, the response of *Nf1*-deficient BMSCs to BMP2 with regard to *Ank* and *Enpp1* expression suggests that neurofibromin is not the sole negative regulator of the RAS-ERK signaling pathway upstream of these two genes. These results also indicate that the stimulatory effect of BMP2 on osteoprogenitor differentiation requires controlled ERK signaling by neurofibromin.

It is unknown to what extent poor matrix mineralization contributes to the low bone mineral density, tibia bowing, poor mechanical properties and possibly pseudarthrosis observed in children with NF1. Although local PP_i concentration could not be quantified, the observed increase in the expression of *ENPP1* in BMSCs extracted from biopsies of pseudarthroses from patients with NF1, as well as the presence of thick osteoid seams on histological sections[20], supports conservation of function between mice and humans.

Pseudarthrosis and dystrophic scoliosis can currently be treated only by invasive, and often repetitive, surgical orthopedic interventions[2,3]. Most approaches to date are corrective in nature, and only bracing techniques are available to reduce the incidence and severity of these complications. Of major interest is the possibility that sALP-FcD10, if applied preventatively, might improve mineralization, growth, architecture and mechanical properties of dysplastic bones affected by NF1 and, thus, limit their likelihood of deformation and fracture. This latter point is particularly noteworthy, as the current standard for treatment is limited to avoidance of prophylactic surgery and early long-term bracing to prevent fracture until skeletal maturity is reached. It is worth emphasizing that sALP-FcD10 targets bone and is already successfully used in the clinic to treat children with hypophosphatasia[42]. Therefore, its potential use in the context of NF1-related skeletal dysplasia has an advantage over the development of other experimental drugs that target this and other aspects of the NF1 skeletal pathologies.

METHODS

Methods and any associated references are available in the online version of the paper.

Note: Any Supplementary Information and Source Data files are available in the online version of the paper.

ACKNOWLEDGMENTS

We thank A. Bianchi and F. Cailotto for their help in establishing the PP_i measurement protocol and K.S. Campbell for editorial assistance. This work was supported by a Young Investigator Award (2012–01–028) from the Children's Tumor Foundation (J.d.l.C.N.), the US National Institute of Arthritis and Musculoskeletal and Skin Diseases and National Center for Research Resources, part of the US National Institutes of Health, under award numbers 5R01 AR055966 (F.E.) and S10 RR027631 (D.S.P.), the National Center for Advancing Translational Sciences of the National Institutes of Health under award number UL1TR001105 (J.J.R.), the Pediatric Orthopaedic Society of North America and Texas Scottish Rite Hospital for Children (J.J.R.) and the US Army Medical Research Acquisition Activity under award W81XWH–11–1–0250 (D.A.S.). The content is solely the responsibility of the authors and does not necessarily represent the official views of the US National Institutes of Health or US government.

AUTHOR CONTRIBUTIONS

F.E. and J.d.l.C.N. designed the study; J.d.l.C.N., A.J.M., S.U., G.V., K.O., J.J.R., D.A.S., S.R.B., D.G., J.S.N. performed experiments; J.d.l.C.N., D.S.P., J.S.N. and F.E. collected and analyzed data; S.J. provided reagents; F.E. and J.d.l.C.N. wrote the manuscript.

COMPETING FINANCIAL INTERESTS

The authors declare competing financial interests: details are available in the online version of the paper.

1. Huson, S.M., Compston, D.A., Clark, P. & Harper, P.S. A genetic study of von Recklinghausen neurofibromatosis in south east Wales. I. Prevalence, fitness, mutation rate, and effect of parental transmission on severity. *J. Med. Genet.* **26**, 704–711 (1989).
2. Stevenson, D.A. *et al.* Approaches to treating NF1 tibial pseudarthrosis: consensus from the Children's Tumor Foundation NF1 Bone Abnormalities Consortium. *J. Pediatr. Orthop.* **33**, 269–275 (2013).
3. Elefteriou, F. *et al.* Skeletal abnormalities in neurofibromatosis type 1: approaches to therapeutic options. *Am. J. Med. Genet. A.* **149A**, 2327–2338 (2009).
4. Kuorilehto, T. *et al.* Decreased bone mineral density and content in neurofibromatosis type 1: lowest local values are located in the load-carrying parts of the body. *Osteoporos. Int.* **16**, 928–936 (2005).
5. Stevenson, D.A. *et al.* Bone mineral density in children and adolescents with neurofibromatosis type 1. *J. Pediatr.* **150**, 83–88 (2007).
6. Duman, O. *et al.* Bone metabolism markers and bone mineral density in children with neurofibromatosis type-1. *Brain Dev.* **30**, 584–588 (2008).
7. Vitale, M.G., Guha, A. & Skaggs, D.L. Orthopaedic manifestations of neurofibromatosis in children: an update. *Clin. Orthop. Relat. Res.* **401**, 107–118 (2002).
8. Stevenson, D.A. *et al.* Descriptive analysis of tibial pseudarthrosis in patients with neurofibromatosis 1. *Am. J. Med. Genet.* **84**, 413–419 (1999).
9. Neitzschman, H.R., Costelloe, C.M., Willis, R.B. & De Mouy, E.H. Radiology case of the month. Congenital bone disorder associated with deformity, fracture, and pseudoarthrosis. Congenital tibial dysplasia–neurofibromatosis type I (NF1). *J. La. State Med. Soc.* **153**, 119–121 (2001).
10. Ippolito, E., Corsi, A., Grill, F., Wientroub, S. & Bianco, P. Pathology of bone lesions associated with congenital pseudarthrosis of the leg. *J. Pediatr. Orthop. B* **9**, 3–10 (2000).
11. Stevenson, D.A. *et al.* Double inactivation of NF1 in tibial pseudarthrosis. *Am. J. Hum. Genet.* **79**, 143–148 (2006).
12. Kolanczyk, M. *et al.* Multiple roles for neurofibromin in skeletal development and growth. *Hum. Mol. Genet.* **16**, 874–886 (2007).
13. Sullivan, K., El-Hoss, J., Little, D.G. & Schindeler, A. JNK inhibitors increase osteogenesis in Nf1-deficient cells. *Bone* **49**, 1311–1316 (2011).
14. Lee, D.Y. *et al.* Disturbed osteoblastic differentiation of fibrous hamartoma cell from congenital pseudarthrosis of the tibia associated with neurofibromatosis type I. *Clin. Orthop. Surg.* **3**, 230–237 (2011).
15. Leskelä, H.V. *et al.* Congenital pseudarthrosis of neurofibromatosis type 1: impaired osteoblast differentiation and function and altered NF1 gene expression. *Bone* **44**, 243–250 (2009).
16. Wu, X. *et al.* Neurofibromin plays a critical role in modulating osteoblast differentiation of mesenchymal stem/progenitor cells. *Hum. Mol. Genet.* **15**, 2837–2845 (2006).
17. Kühnisch, J. *et al.* Multiscale, converging defects of macro-porosity, microstructure and matrix mineralization impact long bone fragility in NF1. *PLoS ONE* **9**, e86115 (2014).
18. Elefteriou, F. *et al.* ATF4 mediation of NF1 functions in osteoblast reveals a nutritional basis for congenital skeletal dysplasiae. *Cell Metab.* **4**, 441–451 (2006).
19. Rhodes, S.D. *et al.* Hyperactive transforming growth factor-β1 signaling potentiates skeletal defects in a neurofibromatosis type 1 mouse model. *J. Bone Miner. Res.* **28**, 2476–2489 (2013).
20. Seitz, S. *et al.* High bone turnover and accumulation of osteoid in patients with neurofibromatosis 1. *Osteoporos. Int.* **21**, 119–127 (2010).
21. Johnson, K. *et al.* Linked deficiencies in extracellular PP_i and osteopontin mediate pathologic calcification associated with defective PC-1 and ANK expression. *J. Bone Miner. Res.* **18**, 994–1004 (2003).
22. Terkeltaub, R.A. Inorganic pyrophosphate generation and disposition in pathophysiology. *Am. J. Physiol. Cell Physiol.* **281**, C1–C11 (2001).
23. Macrae, V.E. *et al.* Inhibition of PHOSPHO1 activity results in impaired skeletal mineralization during limb development of the chick. *Bone* **46**, 1146–1155 (2010).
24. Harmey, D. *et al.* Concerted regulation of inorganic pyrophosphate and osteopontin by *Akp2*, *Enpp1*, and *Ank*: an integrated model of the pathogenesis of mineralization disorders. *Am. J. Pathol.* **164**, 1199–1209 (2004).
25. Addison, W.N., Azari, F., Sorensen, E.S., Kaartinen, M.T. & McKee, M.D. Pyrophosphate inhibits mineralization of osteoblast cultures by binding to mineral, up-regulating osteopontin, and inhibiting alkaline phosphatase activity. *J. Biol. Chem.* **282**, 15872–15883 (2007).
26. Sowa, H., Kaji, H., Yamaguchi, T., Sugimoto, T. & Chihara, K. Activations of ERK1/2 and JNK by transforming growth factor beta negatively regulate Smad3-induced alkaline phosphatase activity and mineralization in mouse osteoblastic cells. *J. Biol. Chem.* **277**, 36024–36031 (2002).
27. Lian, N. *et al.* Transforming growth factor β suppresses osteoblast differentiation via the vimentin activating transcription factor 4 (ATF4) axis. *J. Biol. Chem.* **287**, 35975–35984 (2012).
28. Terkeltaub, R.A. *et al.* Bone morphogenetic proteins and bFGF exert opposing regulatory effects on PTHrP expression and inorganic pyrophosphate elaboration in immortalized murine endochondral hypertrophic chondrocytes (MCT cells). *J. Bone Miner. Res.* **13**, 931–941 (1998).
29. Alves, R.D., Eijken, M., Bezstarosti, K., Demmers, J.A. & van Leeuwen, J.P. Activin A suppresses osteoblast mineralization capacity by altering extracellular matrix composition and impairing matrix vesicle production. *Mol. Cell. Proteomics* **12**, 2890–2900 (2013).
30. Zhang, M. *et al.* Osteoblast-specific knockout of the insulin-like growth factor (IGF) receptor gene reveals an essential role of IGF signaling in bone matrix mineralization. *J. Biol. Chem.* **277**, 44005–44012 (2002).
31. Kyono, A., Avishai, N., Ouyang, Z., Landreth, G.E. & Murakami, S. FGF and ERK signaling coordinately regulate mineralization-related genes and play essential roles in osteocyte differentiation. *J. Bone Miner. Metab.* **30**, 19–30 (2012).
32. Hatch, N.E., Nociti, F., Swanson, E., Bothwell, M. & Somerman, M. FGF2 alters expression of the pyrophosphate/phosphate regulating proteins, PC-1, ANK and TNAP, in the calvarial osteoblastic cell line, MC3T3E1(C4). *Connect. Tissue Res.* **46**, 184–192 (2005).
33. Wang, H. *et al.* Overexpression of fibroblast growth factor 23 suppresses osteoblast differentiation and matrix mineralization *in vitro*. *J. Bone Miner. Res.* **23**, 939–948 (2008).
34. Liu, S., Tang, W., Zhou, J., Vierthaler, L. & Quarles, L.D. Distinct roles for intrinsic osteocyte abnormalities and systemic factors in regulation of FGF23 and bone mineralization in Hyp mice. *Am. J. Physiol. Endocrinol. Metab.* **293**, E1636–E1644 (2007).
35. Le, L.Q. & Parada, L.F. Tumor microenvironment and neurofibromatosis type I: connecting the GAPs. *Oncogene* **26**, 4609–4616 (2007).
36. Wang, W. *et al.* Local low-dose lovastatin delivery improves the bone-healing defect caused by Nf1 loss of function in osteoblasts. *J. Bone Miner. Res.* **25**, 1658–1667 (2010).
37. Wang, W. *et al.* Mice lacking Nf1 in osteochondroprogenitor cells display skeletal dysplasia similar to patients with neurofibromatosis type I. *Hum. Mol. Genet.* **20**, 3910–3924 (2011).
38. Ono, K. *et al.* The Ras-GTPase activity of neurofibromin restrains ERK-dependent FGFR signaling during endochondral bone formation. *Hum. Mol. Genet.* **22**, 3048–3062 (2013).
39. Lecanda, F., Avioli, L.V. & Cheng, S.L. Regulation of bone matrix protein expression and induction of differentiation of human osteoblasts and human bone marrow stromal cells by bone morphogenetic protein-2. *J. Cell. Biochem.* **67**, 386–396 (1997).
40. Schindeler, A. *et al.* Modeling bone morphogenetic protein and bisphosphonate combination therapy in wild-type and Nf1 haploinsufficient mice. *J. Orthop. Res.* **26**, 65–74 (2008).
41. Schindeler, A. *et al.* Distal tibial fracture repair in a neurofibromatosis type 1-deficient mouse treated with recombinant bone morphogenetic protein and a bisphosphonate. *J. Bone Joint Surg. Br.* **93**, 1134–1139 (2011).
42. Whyte, M.P. *et al.* Enzyme-replacement therapy in life-threatening hypophosphatasia. *N. Engl. J. Med.* **366**, 904–913 (2012).
43. Whyte, M.P. Physiological role of alkaline phosphatase explored in hypophosphatasia. *Ann. NY Acad. Sci.* **1192**, 190–200 (2010).
44. Yadav, M.C. *et al.* Enzyme replacement prevents enamel defects in hypophosphatasia mice. *J. Bone Miner. Res.* **27**, 1722–1734 (2012).
45. Yadav, M.C. *et al.* Dose response of bone-targeted enzyme replacement for murine hypophosphatasia. *Bone* **49**, 250–256 (2011).
46. Rodda, S.J. & McMahon, A.P. Distinct roles for Hedgehog and canonical Wnt signaling in specification, differentiation and maintenance of osteoblast progenitors. *Development* **133**, 3231–3244 (2006).
47. Zhu, Y. *et al.* Ablation of NF1 function in neurons induces abnormal development of cerebral cortex and reactive gliosis in the brain. *Genes Dev.* **15**, 859–876 (2001).
48. Sohn, P., Crowley, M., Slattery, E. & Serra, R. Developmental and TGF-β-mediated regulation of Ank mRNA expression in cartilage and bone. *Osteoarthritis Cartilage* **10**, 482–490 (2002).
49. Cailotto, F., Sebillaud, S., Netter, P., Jouzeau, J.Y. & Bianchi, A. The inorganic pyrophosphate transporter ANK preserves the differentiated phenotype of articular chondrocyte. *J. Biol. Chem.* **285**, 10572–10582 (2010).
50. Larizza, L., Gervasini, C., Natacci, F. & Riva, P. Developmental abnormalities and cancer predisposition in neurofibromatosis type 1. *Curr. Mol. Med.* **9**, 634–653 (2009).
51. Anticevic, D., Jelic, M. & Vukicevic, S. Treatment of a congenital pseudarthrosis of the tibia by osteogenic protein-1 (bone morphogenetic protein-7): a case report. *J. Pediatr. Orthop. B* **15**, 220–221 (2006).
52. Lee, F.Y. *et al.* Treatment of congenital pseudarthrosis of the tibia with recombinant human bone morphogenetic protein-7 (rhBMP-7). A report of five cases. *J. Bone Joint Surg. Am.* **88**, 627–633 (2006).
53. Fabeck, L., Ghafil, D., Gerroudj, M., Baillon, R. & Delince, P. Bone morphogenetic protein 7 in the treatment of congenital pseudarthrosis of the tibia. *J. Bone Joint Surg. Br.* **88**, 116–118 (2006).

ONLINE METHODS

Animals and drugs. All procedures were approved by the Vanderbilt University Medical Center Institutional Animal Care and Use Committee (IACUC). WT and *Col2-Nf1* KO mice were generated by crossing *Nf1*$^{flox/flox}$ mice and *Nf1*$^{flox/+}$; α1(II) collagen-Cre breeders[47,54]. *Nf1*$^{flox/flox}$ mice and *Nf1*$^{flox/flox}$ mice; α1(II) collagen-Cre mice were used as WT and KO, respectively. *Osx-Nf1* KO mice were generated by breeding doxycycline-fed *Osx-cre*; *Nf1*$^{flox/flox}$ mice with *Nf1*$^{flox/flox}$ breeders[47]. All mice were on a C57BL/6 background. Bone analyses were performed in 18-d-old or 2-month-old male and female mice, as indicated in figure legends. sALP-FcD10 (Asfotase Alfa, Alexion Pharmaceuticals) was described previously[55]. Briefly, mineral-targeting recombinant tissue-nonspecific alkaline phosphatase (ALP, sALP-FcD10) was produced in CHO cells by modifying the coding sequence of human *ALPL*. The GPI anchor sequence of the hydrophobic C-terminal domain of human ALPL was removed to generate a soluble, secreted enzyme (sALP). Then the human *ALPL* ectodomain sequence was extended with the coding sequence encoding the Fc region of human IgG1 (Fc). Finally the C terminus of the Fc region was extended with ten aspartic acid residues (D10). The dose of 8.2 mg kg^{-1} per day was selected because it was previously shown to be efficacious in short-term (16 days) efficacy study in *Alpl*$^{-/-}$ mice[55]. The specific activity of the lot used in the present study was 878 U mg^{-1}. sALP-FcD10 was administered subcutaneously for the periods of time indicated in the text.

Human subjects. The study was approved by the Institutional Review Board of the University of Texas Southwestern Medical Center, of the Rizzoli Orthopaedic Institute (Bologna, Italy) and of Vanderbilt University. The parents of the subjects provided informed consent. Bone tissues were obtained from 9 patients with NF1 and tibial pseudarthrosis (aged between 7 months and 18 years), and control samples were obtained from 6 children without NF1 who underwent surgery for congenital dysplasia of the hip without any other coexisting pathology (n = 3)[56] or scoliosis (n = 3) (aged between 3.3 and 17 years). Diagnosis of pseudarthrosis was based on radiographic and clinical findings. Diagnosis of NF1 was performed according to the criteria presented at the National Institutes of Health Consensus Development Conference on Neurofibromatosis (http://consensus.nih.gov/1987/1987Neurofibramatosis064html.htm).

Cell culture. Mouse BMSCs were extracted from long bones by spinning down diaphyses at 1,500 r.p.m. for 3 min. Cells were then counted, plated at a density of 1 × 10^6 cells/well (12-well plates) or 2 × 10^6 cells/well (6-well plates) and grown for 7 days in αMEM supplemented with 10% FBS, 100 IU ml^{-1} penicillin, 100 μg/ml streptomycin (Cellgro, Manassas, VA, USA). At day 7, differentiation and mineralization was induced by the addition of 50 μg/ml ascorbic acid and 10 mM β-glycerophosphate, and the medium was refreshed every 2–3 days. BMSC differentiation and mineralization were assessed by ALP activity and Alizarin red S staining, respectively, using standard protocols.

Primary chondrocytes were extracted from 4-day-old pup rib bones. The cartilaginous part of the rib was dissected and soft tissues removed, then digested by collagenase D (3 mg/ml, Roche, USA) and 0.25% trypsin/EDTA (EDTA) (Gibco, USA) in DMEM for 3 h. At confluence, 5 × 10 μl drops of concentrated cells (2 × 10^7 cells/ml) were plated in 6 wells. After 2 h of incubation, 2 ml of complete cell culture medium was delicately added. Cells were differentiated in DMEM supplemented with 10% FBS, 100 IU ml^{-1} penicillin, 100 μg ml^{-1} streptomycin, 50 μg ml^{-1} of ascorbic acid and 10 mM β-glycerophosphate.

Human cells extracted from bone marrow[56] or bone tissue were maintained in alpha MEM supplemented with 10% FBS, 100 U ml^{-1} penicillin, 0.1 mg ml^{-1} streptomycin at 37 °C in a 5% CO_2-humidified atmosphere. Cells from bone tissues were digested overnight with collagenase before plating. After 4 days, nonadherent cells were removed, and adherent bone cells were grown until confluence or passaged before RNA extraction.

Adenovirus infection of bone marrow stromal cells. BMSCs were isolated from *Nf1*$^{flox/flox}$ mice and seeded at a density of 1 × 10^6 cells/well in 12-well plates. At 40% confluence, cells were incubated in complete culture medium (α-MEM, 10% FBS and 100 IU ml^{-1} penicillin) containing either Ad5-CMV-GFP or Ad5-CMV-Cre (Vector development lab, Baylor College of Medicine) at 2.5 × 10^9 PFUs. After 2 days of incubation, the medium was refreshed with complete culture medium. *Nf1* recombination efficiency was determined according to Wang *et al.*[37].

Serum vitamin D, calcium and phosphate assays. Blood samples were collected from WT and *Osx-Nf1* KO mice at sacrifice. Vitamin D, phosphate and calcium concentration in mouse serum was determined using a 25OH-Vitamin-D ELISA Assay kit (Eagle Biosciences, cat# VID31-K01), a Phosphate Assay kit (BioVision, cat # k410-500) and a Calcium Assay kit (BioVision, cat# k380-250), respectively, according to the manufacturer's instructions.

PP_i and PC-1 assays. PP_i release in cell-conditioned medium (ePP_i) was measured radiometrically using differential adsorption on activated charcoal of uridine-diphospho-D-glucose [6-^{3}H] (Cat #NET1163250UC, PerkinElmer) as previously described[49,57,58]. Forty microliters of conditioned medium (or blank control) and 120 μl of assay solution (57 nM of Tris acetate, pH 7.6; 5.2 mM MgAc; 18.6 μM glucose 1,6-diphosphate (G1,6DP); 9 μM uridine-diphosphoglucose (UDPG); 4 μM β-nicotinamide adenine dinucleotide (NAD+); 0.136 U uridine-diphosphoglucose pyrophosphorylase (UDPGPP); 0.5 U phosphoglucomutase; 0.5 U glucose-6-phosphate dehydrogenase (G6PD); 0.02 μCi ^{3}H-UDPG) were incubated at 37 °C for 1 h and then adsorbed on 200 μl of charcoal for 10 min on ice. After centrifugation at 14,000 r.p.m. for 10 min, 100 μl of the supernatant was transferred into a vial containing 5 ml of Bio-safe II for radioactivity count. PP_i levels were normalized by protein concentration in cell lysates in each well. Measurements were performed in triplicate and similar results were obtained from at least 3 independent experiments.

ENPP1 activity was determined using 1.5 mM of the synthetic chromogenic substrate thymidine 5′-monophosphate *p*-nitrophenyl ester in reaction buffer (100 mM Tris/HCl, pH 8.0, 130 mM NaCl, and 15 mM $MgCl_2$) incubated at 37 °C for 30 min. The reaction was terminated by the addition of 50 μl 4 N NaOH. Product formation was monitored by measurement of absorbance at 405 nm. ENPP1 activity in each well was normalized by cell number. Measurements were performed in triplicate and from at least 3 independent experiments.

RT-qPCR and genomic PCR. Total RNA was extracted using TRIzol (Invitrogen, Grand Island, NY, USA), and cDNAs were synthesized from 1 μg of RNA following DNase I treatment using the high-capacity cDNA reverse-transcription kit (Applied Biosystems, USA). Quantitative PCR (qPCR) was performed by using TaqMan or SYBR green gene expression assays. The probe and primer sets for mouse *Runx2* (Mm00501578_m1); *Alpl* (Mm00475834_m1); *Ank* (Mm00445047_m1); *Enpp1* (Mm00501097_m1); *Spp1* (Mm00436767_m1), *Igf1* (Mm01228180_m1), human *ANKH* (Hs00219798_m1) and human *ENPP1* (Hs01054040_m1) and the normalizers *Hprt* (Mm00446968_m1); human *GAPDH* (Hs99999905_m1) were obtained from Applied Biosystems (Foster City, CA, USA). The SYBR green primers were *Spp1* (forward; CTCCTTGCGCCACAGAATG, reverse; TGGGCAACAGGGATGACA), *Nf1* (forward; GTATTGAATTGAAGCACC TTTGTTTGG, reverse; CTGCCCAAGGCTCCCCCAG); *Bglap* (forward; ACCCTGGCTGCGCTCTGTCTCT, reverse; GATGCGTTTGTAGGCGGTC TTCA) and *Col1a1* (forward; GACATCCCTGAAGTCAGCTGC, reverse; TCCCTTGGGTCCCTCGAC). Specificity of amplification was verified by the presence of a single peak on the dissociation curve. Amplification conditions are available upon request. Measurements were performed in triplicate and from at least 3 independent experiments.

For genotyping, genomic DNA was isolated from tail tips by sodium hydroxide digestion, and PCR was performed using primers P1, P2 and P4, as described by Zhu *et al.*[47]. The *Col2a1-cre* transgene was detected using the fwd: GAGTT GATAGCTGGCTGGTGGCAGATG and reverse: TCCTCCTGCTCCTAGGG CCTCCTGCAT primers.

Western blot analyses. Whole cell lysates were separated by SDS-PAGE electrophoresis according to standard protocols. Nitrocellulose membranes were probed with the indicated antibody using standard protocols (monoclonal anti-β-actin antibody (Sigma cat# AC-74, dilution 1:5,000), anti-pSmad1/5 antibody (Cell Signaling cat#9516S, dilution 1:1,000), anti-Smad1/Smad5 antibody (Abcam cat# ab75273, dilution 1:1,000), anti ENPP1/PC-1 (Aviva Systems Biology,

cat# OAEB02445, dilution 1:500) and anti-ANK (Origen, cat# TA325111, dilution 1:1,000).

Histology. Static histomorphometry measurements were performed as previously described in accordance with standard nomenclature[59], using the Bioquant Analysis System (Nashville, TN, USA) on 5 μm undecalcified methymethacrylate sections. Calcified cartilage BV/TV was measured in the growth plate hypertrophic region following von Kossa and van Gieson staining.

X-rays and μCT analyses. Radiographs were obtained using a digital cabinet X-ray system (LX-60, Faxitron X-Ray, USA). μCT analyses were performed using a Scanco μCT 40 system (Scanco Medical, Bassersdorf, Switzerland). Tomographic images were acquired at 55 kVp and 145 mA with an isotropic voxel size of 12 μm and at an integration time of 250 ms with 500 projections collected per 180° rotation.

Raman spectroscopy. Sensitive to the vibrational modes of chemical bonds, Raman spectroscopy (RS) characterizes the biochemical properties of bone tissue, namely mineral-to-collagen ratio (MCR) and crystal structure. Using midshaft vessel perforations as landmarks, spectra were obtained from cortical bone of the femur with 5 accumulations of 20 s exposures to a 20-mW, near-infrared laser (785 nm) at a spot size of ~1.5 μm in diameter. Spectra were processed via least-squares modified polynomial fit to suppress background fluorescence[60] and smoothed for noise using a second-order Savitsky-Golay filter[61]. Raman shift calibration was accomplished using a neon lamp and a silicon standard. Silicon standard measurements before and after data acquisition ensured wave number consistency across bones. Spectral intensities for known Raman peaks and peak ratios were extracted using custom Matlab software (Mathworks, Natick, MA) to measure mineralization as ν1 phosphate (symmetrical stretching at ~960 cm^{-1}) per proline (ring at ~854 cm^{-1}) and crystallinity (crystal grain size and perfection) as the inverse full width at half maximum intensity of the ν1 phosphate peak).

Biomechanical testing. Hydrated samples were tested in three-point bending with a span of 8 mm at a rate of 3 mm min^{-1} (ref. 62). Force and displacement were measured from a 100 N load cell and from the linear variable displacement transformer of the material testing system (Dynamight 8841, Instron, Canton, OH). Structural properties were extracted from force-displacement curves by custom Matlab algorithms (Mathworks, Natick, MA). Material properties were calculated by accounting for structure by using cross-sectional area and moment of inertia as measured by μCT.

Statistical analyses. Depending on whether data per group passed the Shapiro-Wilk normality test or whether standard deviations were not different among the groups (Bartlett's test), one-way analysis of variance (ANOVA) or the Kruskal-Wallis Test (nonparametric) was used to determine whether differences existed in μCT -, Raman- and biomechanical-derived properties among the experimental groups. When differences existed at $P < 0.05$, *post hoc* pair-wise comparisons were tested for significance in which the P value was adjusted ($P_{adj} < 0.05$) by Holm-Sidak's method or Dunn's method (nonparametric). Statistical analysis was performed using GraphPad PRISM (v6.0a, La Jolla, CA). Data are provided as mean ± s.d. No statistical method was used to predetermine sample size. The investigators were blinded to allocation during experiments and outcome assessment. The experiments were not randomized.

54. Ovchinnikov, D.A., Deng, J.M., Ogunrinu, G. & Behringer, R.R. Col2a1-directed expression of Cre recombinase in differentiating chondrocytes in transgenic mice. *Genesis* **26**, 145–146 (2000).
55. Millán, J.L. *et al.* Enzyme replacement therapy for murine hypophosphatasia. *J. Bone Miner. Res.* **23**, 777–787 (2008).
56. Granchi, D. *et al.* Biological basis for the use of autologous bone marrow stromal cells in the treatment of congenital pseudarthrosis of the tibia. *Bone* **46**, 780–788 (2010).
57. Terkeltaub, R., Rosenbach, M., Fong, F. & Goding, J. Causal link between nucleotide pyrophosphohydrolase overactivity and increased intracellular inorganic pyrophosphate generation demonstrated by transfection of cultured fibroblasts and osteoblasts with plasma cell membrane glycoprotein-1. Relevance to calcium pyrophosphate dihydrate deposition disease. *Arthritis Rheum.* **37**, 934–941 (1994).
58. Cailotto, F. *et al.* Inorganic pyrophosphate generation by transforming growth factor-β-1 is mainly dependent on ANK induction by Ras/Raf-1/extracellular signal-regulated kinase pathways in chondrocytes. *Arthritis Res. Ther.* **9**, R122 (2007).
59. Parfitt, A.M. *et al.* Bone histomorphometry: standardization of nomenclature, symbols, and units. Report of the ASBMR Histomorphometry Nomenclature Committee. *J. Bone Miner. Res.* **2**, 595–610 (1987).
60. Lieber, C.A. & Mahadevan-Jansen, A. Automated method for subtraction of fluorescence from biological Raman spectra. *Appl. Spectrosc.* **57**, 1363–1367 (2003).
61. Maher, J.R., Takahata, M., Awad, H.A. & Berger, A.J. Raman spectroscopy detects deterioration in biomechanical properties of bone in a glucocorticoid-treated mouse model of rheumatoid arthritis. *J. Biomed. Opt.* **16**, 087012 (2011).
62. Makowski, A.J. *et al.* The loss of activating transcription factor 4 (ATF4) reduces bone toughness and fracture toughness. *Bone* **62**, 1–9 (2014).

doi:10.1038/nm.3583

Queries for Author

Journal: Journal of Medical Genetics
Paper: jmedgenet-2014-102815
Title: Evaluation of somatic mutations in tibial pseudarthrosis samples in neurofibromatosis type 1

The proof of your manuscript appears on the following page(s).

It is the responsibility of the corresponding author to check against the original manuscript and approve or amend these proofs.

Please read the proofs carefully, checking for accuracy, verifying the reference order and checking figures and tables. When reviewing your page proof please keep in mind that a professional copyeditor edited your manuscript to comply with the style requirements of the journal.

This is not an opportunity to alter, amend or revise your paper; it is intended to be for correction purposes only. The journal reserves the right to charge for excessive author alterations or for changes requested after the proofing stage has concluded.

During the preparation of your manuscript for publication, the questions listed below have arisen (the query number can also be found in the gutter close to the text it refers to). Please attend to these matters and return the answers to these questions when you return your corrections.

Please note, we will not be able to proceed with your article if these queries have not been addressed.

A second proof is not normally provided.

Query Reference	Query
Q1	IMPORTANT: Corrections at this stage should be limited to those that are **essential**. Extensive corrections will delay the time to publication and may also have to be approved by the journal Editor.
Q2	Please note that alterations cannot be made after you have approved for publication, irrespective of whether it is Online First.
Q3	Author SURNAMES (family names) have been highlighted - **please check that these are correct**.
Q4	Please check all names are spelt correctly, and check affiliation and correspondence details, including departments.
Q5	The resolution of figure 4 is too low. Please resupply the figure in a resolution of at least 300 dpi. Guidelines on figure preparation can be found here: http://group.bmj.com/products/journals/instructions-for-authors/Figure_preparation.pdf
Q6	Please ensure that your trial registration number (if relevant for your article type) appears at the end of the abstract. If not, please provide and we will insert.
Q7	Please check MAPK has been spelt out correctly; if not, please amend accordingly
Q8	Please check TE has been spelt out correctly; if not, please amend accordingly
Q9	Please check IGV has been spelt out correctly; if not, please amend accordingly
Q10	Please spell out CV the first time it appears.

Author query sheet

Query Reference	Query
Q11	The abbreviation NS has been change to Noonan syndrome. Please confirm this is OK, or amend if necessary
Q12	Please provide ethics approval statement.
Q13	Please provide genus name for 'H. sapiens'

If you are happy with the proof as it stands, please email to confirm this. Minor changes that do not require a copy of the proof can be sent by email (please be as specific as possible).
Email: **production.jmg@bmj.com**

If you have any changes that cannot be described easily in an email, please mark them clearly on the proof using the annotation tools and email this by reply to the eProof email.

We will keep a copy of any correspondence from you related to the author proof for six months. After six months, correspondence will be deleted.

Please respond within 48 hours

ORIGINAL ARTICLE

Evaluation of somatic mutations in tibial pseudarthrosis samples in neurofibromatosis type 1

David W Sant,[1] Rebecca L Margraf,[1] David A Stevenson,[2,3,5] Allie H Grossmann,[1,4] David H Viskochil,[3] Heather Hanson,[3] Melanie D Everitt,[3] Jonathan J Rios,[6,7,8,9] Florent Elefteriou,[10,11,12,13] Theresa Hennessey,[4] Rong Mao[1,4]

For numbered affiliations see end of article.

Correspondence to
Dr Rong Mao, Department of Pathology, University of Utah, ARUP Institute for Clinical and Experimental Pathology, 500 Chipeta Way, MS-115, Salt Lake City, UT 84108, USA; rong.mao@aruplab.com

DWS and RLM contributed equally.

Received 8 October 2014
Revised 4 December 2014
Accepted 18 December 2014

ABSTRACT

Background Tibial pseudarthrosis is associated with neurofibromatosis type 1 (NF1) and there is wide clinical variability of the tibial dysplasia in NF1, suggesting the possibility of genetic modifiers. Double inactivation of *NF1* is postulated to be necessary for the development of tibial pseudarthrosis, but tissue or cell of origin of the 'second hit' mutation remains unclear.

Methods Exome sequencing of different sections of surgically resected NF1 tibial pseudarthrosis tissue was performed and compared to germline (peripheral blood).

Results A germline *NF1* splice site mutation (c.61-2A>T, p.L21 M68del) was identified from DNA extracted from peripheral blood. Exome sequencing of DNA extracted from tissue removed during surgery of the tibial pseudarthrosis showed a somatic mutation of *NF1* (c.3574G>T, p.E1192*) in the normal germline allele. Further analysis of different regions of the tibial pseudarthrosis sample showed enrichment of the somatic mutation in the soft tissue within the pseudarthrosis site and absence of the somatic mutation in cortical bone. In addition, a germline variant in *PTPN11* (c.1658C>T, p.T553M), a gene involved in the RAS signal transduction pathway was identified, although the clinical significance is unknown.

Conclusions Given that the *NF1* somatic mutation was primarily detected in the proliferative soft tissue at the pseudarthrosis site, it is likely that the second hit occurred in mesenchymal progenitors from the periosteum. These results are consistent with a defect of differentiation, which may explain why the mutation is found in proliferative cells and not within cortical bone tissue, as the latter by definition contains mostly mature differentiated osteoblasts and osteocytes.

INTRODUCTION

Neurofibromatosis type 1 (NF1, OMIM #162200) is an autosomal dominant genetic disorder affecting 1 in 3000–4000 individuals. It is caused by mutations in *NF1* found on chromosome 17q11.2, which encodes for the protein neurofibromin and is involved in regulation of the RAS-MAPK (mitogen-activated protein kinases) pathway. Individuals with NF1 have multisystem manifestations (eg, café au lait macules, neurofibromas, learning disabilities, short stature, malignancies, distinctive osseous lesions), but there is a high degree of clinical variability.

Noonan syndrome (OMIM #163950) is an autosomal dominant genetic disorder affecting between 1 in 1000 and 2500 live births.[1] It is clinically characterised by short stature, congenital heart defects, pectus anomalies, and abnormal facial features. Individuals with Noonan syndrome have some overlapping traits of NF1, such as short stature, mild intellectual disability, similar facial gestalt, skeletal defects, and skin abnormalities such as café au lait spots.[1 2] Noonan syndrome and NF1 are caused by mutations in genes involved in the RAS signal transduction pathway. Mutations causing Noonan syndrome were found in multiple genes involved in the RAS/MAPK signalling pathway,[3] but half of the reported cases have a mutation in *PTPN11*.[2] Most individuals who fulfil NF1 diagnostic criteria and have features of Noonan syndrome have germline mutations in *NF1*, but some individuals have a second germline mutation in *PTPN11*.[4–7]

Orthopaedic complications affect approximately 38% of individuals with NF1,[8] including tibial dysplasia. Tibial dysplasia typically presents as anterolateral bowing progressing to fracture and non-union (ie, pseudarthrosis) and is almost always unilateral.[9] However, the degree of bowing is variable and not all individuals with tibial dysplasia progress to pseudarthrosis. Biopsies have shown proliferation of a fibrous tissue between the fractured bone segments.[10] In the general population tibial pseudarthrosis is extremely rare, occurring in only 1 in 140 000 live births,[8] but 3–4% of patients with NF1 have tibial pseudarthrosis.[11] Fracture of the bowed tibia frequently occurs in early childhood.[8]

It is postulated that bi-allelic inactivation of the *NF1* locus is necessary for the development of pseudarthrosis in NF1 and this has been documented in several instances in human biopsies,[9 10 12–14] and further supported by the phenotype of mouse models characterised by biallelic *Nf1* loss of function in osteoprogenitors.[15] However, the tissue or cell of origin of the 'second hit' mutation in human individuals remains unclear. In addition, not all individuals with tibial pseudarthrosis have NF1 and there is wide clinical variability of the tibial dysplasia in NF1, suggesting the possibility of additional genetic causes and/or modifiers. To elucidate the tissue of origin harbouring a somatic 'second hit' mutation associated with tibial pseudarthrosis, exome sequencing in one pseudarthrosis sample (c.3574 G>T, p.E1192*) (previously reported in Paria *et al*[12]) was performed in different sections of tibial pseudarthrosis from an individual with NF1.

To cite: Sant DW, Margraf RL, Stevenson DA, *et al*. *J Med Genet* Published Online First: [*please include* Day Month Year] doi:10.1136/jmedgenet-2014-102815

MATERIALS AND METHODS

Samples and DNA extraction

Peripheral blood and tissues from the tibial pseudarthrosis region were collected from a patient with a clinical diagnosis of NF1 and tibial pseudarthrosis under a University of Utah institutional review board approved protocol.

Three pseudarthrosis samples were cut from the amputated limb of a patient with tibial pseudarthrosis (figure 1A). Two tissue samples were from the pseudarthrosis fracture site; one sample had no appreciable hard tissue and the other had a mixture of soft and hard tissue. The third sample was from tibial cortex near the pseudarthrosis site (figure 1B). The discarded tissue was stored in a freezer at −80°C. For convenience these three samples are labelled as follows: 'PA' (soft fibrous tissue from the pseudarthrosis/fracture site that did not grossly contain any compact bone), 'Mixed' (tissue from the pseudarthrosis/fracture site that grossly contained a mixture of soft fibrous tissue and compact bone), and 'Bone' (tibial cortical bone). Before DNA extraction, a small adjacent portion of the 'Mixed' specimen was cut and removed and sent for histology (figure 2). Formalin-fixation, paraffin embedding, sectioning, and haematoxylin and eosin (H&E) staining were performed by the Biorepository and Molecular Pathology Core at the Huntsman Cancer Institute of the University of Utah.

DNA was extracted from peripheral blood samples using the Puregene DNA Extraction automated system (Qiagen, Venlo, Netherlands).

For DNA isolation from tibial tissue, samples from frozen tissue ('PA', 'Mixed', 'Bone') were mechanically broken into small pieces. Fragmented sample pieces were lysed by incubation for 18 h at 56°C in lysis buffer provided in the Chemagic Tissue 10 kit (Chemagen/Perkin-Elmer, Waltham, Massachusetts, USA). Following lysis, DNA was extracted using the Chemagic Tissue 10 kit (PerkinElmer Chemagen Technologie Gmbh, Baesweiler, Germany) according to the manufacturer's instructions. Briefly, DNA in the lysis buffer was bound to magnetic beads, subjected to multiple washes, and then a final incubation of the beads in TE (Tris-EDTA) buffer pH 8.0 eluted the DNA from the beads. To maximise DNA yield, the original DNA/lysis buffer solution was saved after the first incubation with the magnetic beads and processed through a second round of DNA extraction with a new aliquot of beads. Also, the final elution of the DNA from the beads was performed twice on each bead set for maximum DNA yield. Extracted DNA was then further purified and concentrated using the Qiagen PCR Purification Kit (Qiagen, Venlo, Netherlands).

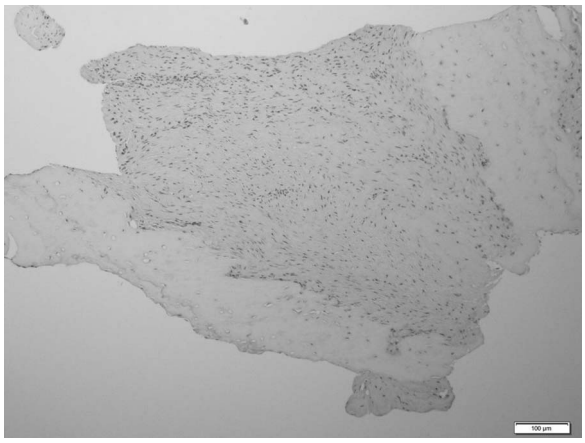

Figure 2 Image of haematoxylin and eosin stain (100× magnification) of a frozen tissue section sampled from the region of the tibial fracture and pseudarthrosis site adjacent to the 'Mixed' sample that grossly had both soft fibrous tissue and hard tissue. Image shows fragments of bone with an adjacent reactive/reparative fibroblastic proliferation. Size marker located in lower right quadrant.

DNA was quantified on the Qubit 2.0 fluorometer using the Qubit dsDNA HS assay kit (Invitrogen, Life Technologies, Carlsbad, California, USA). Equivalent quantity of DNA from peripheral blood and the tibial pseudarthrosis samples was run on a 2% agarose gel to assess sample quality.

Exome sequencing and variant discovery

Exome sequencing was performed on DNA from the patient's blood and one of the tibial pseudarthrosis samples which included soft tissue and bone ('Mixed' sample). Exons were captured with the SeqCap EZ Human Exome Library V.3.0 (Roche NimbleGen Inc, Madison, Wisconsin, USA) and sequenced with 2×100 bp paired-end reads on HiSeq 2500 Instrument (Illumina, San Diego, California, USA) according to the manufacturer's recommendations. Sequence was aligned to the human reference genome (GRCh37) using Burrows-Wheeler Aligner (V.0.5.11) and variants from the reference were called

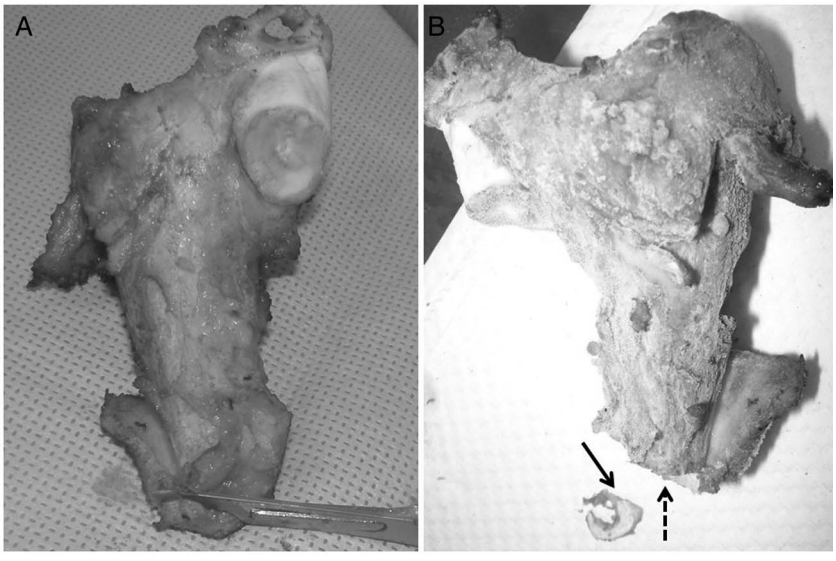

Figure 1 (A) Photo of amputated distal tibia (on left) with residual fibular section (upper right). The lower region shows the fracture site and pseudarthrosis region. The scalpel marks the region of the pseudarthrosis where samples were obtained right after surgery for DNA extraction. (B) Segment of frozen cortical tibial bone (on right indicated by solid black arrow) subsequently cut from the adjacent tibial section near the fracture site (far right region of the large sample indicated by dotted black arrow). The adherent soft tissue from the small tibial sample was later dissected away from the fragment shown on the right (labelled by the black solid arrow) and the bone was then utilised for DNA extraction.

with Samtools and Genome Analysis Toolkit (V.1.6). After the first alignment, a second refined alignment was done which removed PCR duplicate reads, identified read bias, and realigned around deletions and insertions. Variant lists were in vcf file format or csv format with annotation. Variants with a low variant quality score <10 and total read coverage <8× were removed from further analysis. Variants were analysed using the Golden Helix SVS software (Quintiles, Durham, North Carolina, USA) and also the VarBin method.[16] The exome data were filtered by location (exon ±100 positions) and also by eliminating variants of higher population frequency (>2% minor allele frequency) using the 1000 Genomes data,[17] and the Exome Sequencing Project (ESP 6500) dataset.[18] Silent changes not close to splice sites were also filtered.

Rare germline variants (present in both the patient's blood and tibial pseudarthrosis 'Mixed' sample) or somatic variants (only in the tibial pseudarthrosis 'Mixed' sample) were initially investigated specifically for *NF1* and 15 other genes involved in the RAS/MAPK pathway: *SPRED1*, *RASA1*, *RAF1*, *HRAS*, *BRAF*, *KRAS*, *MEK1/MAP2K1*, *MEK2/MAP2K2*, *PTPN11*, *SOS1*, *PTEN*, *KIT*, *MAPK1/ERK2*, *SPRED2*, and *TP53*. Furthermore, variant investigation was expanded to the entire exome-captured regions. One analysis was to look at somatic mutations present in the 'Mixed' sample by subtraction of germline variants present in the blood sample, and then filtering out variants using Varbin method data (to eliminate most false positives) and visualisation of reads in Integrative Genomics Viewer (IGV) (table 1).

Variants confirmation by Sanger sequencing

All four samples (blood, PA, mixed, and bone) were Sanger sequenced for the three variants found in *NF1* and *PTPN11*. Sanger sequencing used BigDye Terminator Cycle Sequencing Kit (Applied Biosystems, Carlsbad, California, USA) on an Applied Biosystems 3730 DNA Analyzer. Primer sequences are available upon request.

RESULTS

Clinical findings

This report describes a young girl who fulfils clinical diagnostic criteria for NF1. The child was referred for genetics evaluation at 5 years of age due to multiple café au lait macules and tibial/fibular pseudarthrosis. A family history was positive for her father, who was clinically diagnosed with NF1 without tibial dysplasia, pulmonic stenosis or pectus anomaly. The child had >5 café au lait macules and freckling of the axillae and bilateral groin. There was no history of Lisch nodules or optic pathway tumours, and no evidence of dermal or plexiform neurofibromas. A very mild pectus excavatum was present. She had a history of an infantile haemangioma on her chest that resulted in surgical excision. Her left leg was noted to have anterolateral bowing at birth and radiographs at 3 months of age showed tibial and fibular fracture. Casting and bracing was performed until 2 years of age but the pseudarthrosis persisted. Three surgical attempts to achieve union, including open reduction, shortening with excision of abnormal bone and internal fixation with bone grafting, were not successful (figure 3). Following the third attempt, there appears to have been progressive healing followed by rapid bone resorption and increasing pain and limp. Below the knee amputation through the pseudarthrosis was performed at 4 years of age and she was fitted for a prosthesis. Discarded tissue from the surgical procedure was collected and stored at −80°C.

The child was re-evaluated at 7 years of age and had excellent function with her prosthesis. Growth parameters at that time showed a height of 127 cm (~75th centile), weight of 33.4 kg (~95th centile), and head circumference of 53 cm (~95th centile). She had a history of mild speech and motor delays and learning problems. On physical examination she had an increase in café au lait macules, but still no dermal neurofibromas or Lisch nodules. Based on the findings of a *PTPN11* variant (see results below), she was referred to cardiology and an echocardiogram was performed. She was found to have coarctation of the aorta with a peak velocity of 2.88 m/s, and the distal aorta measured 0.61 cm (z-score of −3.55). Systolic blood pressure measurements were borderline elevated (95th centile), but there was not a significantly abnormal arm–leg gradient by blood pressure measurement. Imaging of the renal arteries was normal.

The child inherited NF1 from her father who also fulfils diagnostic criteria for NF1 without tibial pseudarthrosis, report of pulmonic stenosis, or pectus anomaly. He was also found to harbour the same *PTPN11* variant.

Quality of DNA extracted from pseudarthrosis tissue

Due to potential difficulties in extracting high-quality DNA from bone, several experiments were done to assess and compare the quality of DNA generated using the protocols described in the Methods section. The DNA extracted from all three tibial pseudarthrosis samples ('PA', 'Mixed', 'Bone') had equivalent low to no DNA degradation/fragmentation as compared to the DNA extracted from blood (data not shown). All

Table 1 Next generation sequencing detected somatic variants in the pseudarthrosis sample, sorted by variant quality

chr: position	Gene	cDNA change	Zygosity	Protein change	Function	Total read coverage*	Variant % reads†	Variant quality‡	Transcript
17:29 560 097	*NF1*	c.3574G>T	Het	p.E1192*	Nonsense	260	16	551	NM_000267
11:397 063	*PKP3*	c.562C>A	Het	p.P188T	Missense	9	33	123	NM_007183
6:31 239 051	*HLA-C*	c.418T>G	Het	p.S140A	Missense	47	13	29	NM_002117
19:47 960 350	*SLC8A2*	c.1177G>C	Het	p.A393P	Missense	15	47	27	NM_015063
9:131 939 417	*IER5L*	c.915C>A	Het	p.Y305*	Nonsense	5	40	25	NM_203434
14:101 004 615	*BEGAIN*	c.1473C>A	Het	p.C491*	Nonsense	10	20	13	NM_020836
4:3 768 346	*ADRA2C*	c.13G>T	Het	p.A5S	Missense	11	18	11	NM_000683
1:3 414 968	*MEGF6*	c.3319C>A	Het	p.P1107T	Missense	10	20	11	NM_001409

*Total read coverage for the variants >8×.
†Total reads containing the variant as a percentage of total read coverage for that position (variant allele frequency).
‡Variant quality score: Phred-scaled quality score for the non-reference allele. Higher score indicates high confidant in variant calls. Variant quality scores <10 are likely false positives and were filtered out of this dataset. Table was sorted from high to low variant quality.

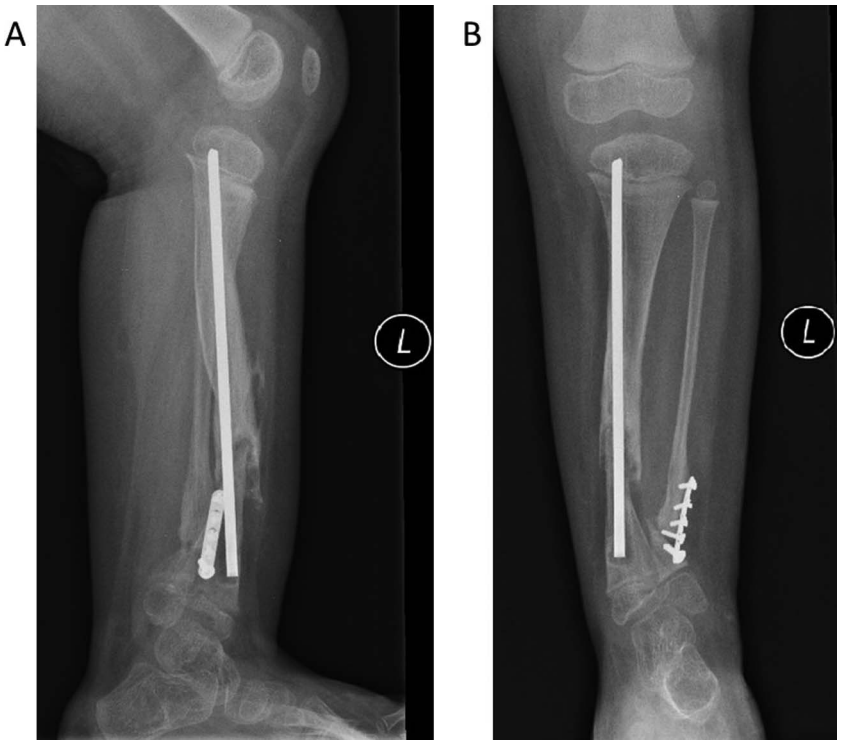

Figure 3 Radiographs of the leg (A, lateral view; B, anteroposterior view) showing the tibial and fibular pseudarthrosis just before amputation.

samples contained DNA of large fragment sizes and were successfully used to amplify long range PCR amplicons over 12 000 base pairs (data not shown). When DNA samples from blood and the three tibial samples were all sonicated on the Covaris Sonicator, all samples yielded the expected average fragment size between 340–350 bp (0.7% CV, data not shown).

Variant discovery

DNA from blood and one pseudarthrosis sample which contained a mixture of hard and soft tissues ('Mixed') was used for exome sequencing. The patient was found to have a deleterious germline mutation in *NF1*. This *NF1* mutation is a known pathogenic splice site mutation at genomic position chr17:29 482 999 (GRCh37 reference); c.61-2 A>T. This splice site mutation will cause skipping of exon 2 and result in a deletion of 48 amino acids in neurofibromin (predicted protein variation p.L21 M68del, HGMD CS # 086346, *NF1* gene reference: NM_000267).[19] The variant was confirmed present in all four patient samples by Sanger sequencing (figure 4A). A germline variant was also found in *PTPN11*, a gene related to the RAS/MAPK pathway. This variant was at genomic position chr12:112 940 006; c.1658C>T, p.T553M (HGMD CS090465, dbSNP NCBI rs148176616, NM_002834.3). This germline variant was also confirmed by Sanger sequencing in all four patient samples (figure 4B). The *PTPN11* protein product is conserved across many species at the mutation location (figure 4D). The child inherited NF1 from her father who also fulfils diagnostic criteria for NF1, and he was also found to harbour the same *PTPN11* variant.

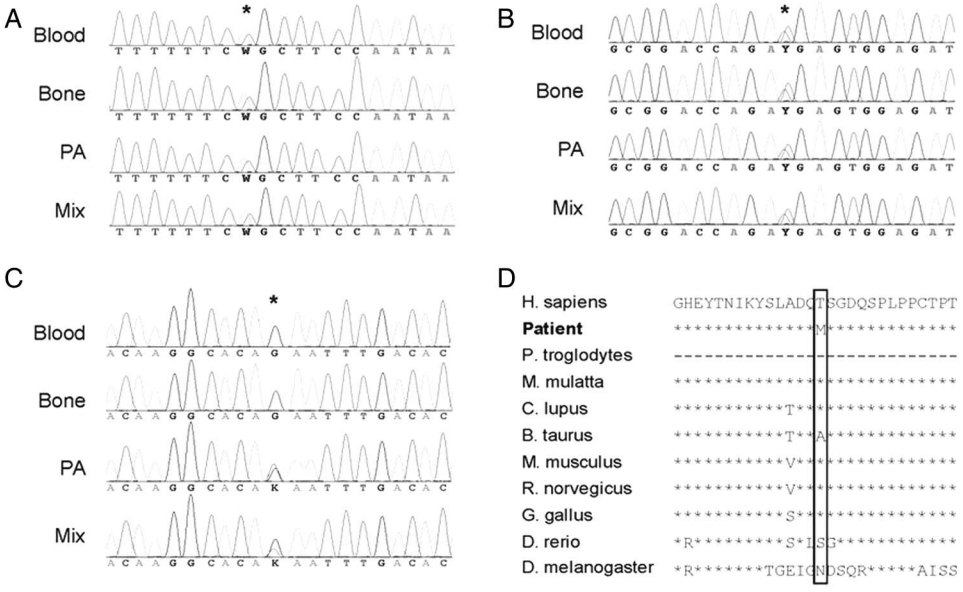

Figure 4 (A–C) Sanger sequencing traces for peripheral blood sample ('Blood'), tibial compact bone without soft tissue slightly away from the immediate fracture site ('Bone'), soft tissue sample from the tibial fracture and pseudarthrosis site without appreciable bone ('PA'), and tissue from the tibial fracture and pseudarthrosis site containing soft tissue and bone ('Mix'). The position of the variant is starred in each panel: (A) the *NF1* germline variant c.61-2A>T; (B) the *PTPN11* germline variant c.1658C>T; (C) the *NF1* somatic variant c.3574G>T; (D) PTPN11 protein multiple sequence alignment. Amino acids that match the *H sapiens* reference are starred, mismatched amino acids are shown, and absent sequence is dashed (*P troglodytes*). The position of the patient's variant is marked with a box.

A novel *NF1* somatic variant was found at genomic location chr17: 29 560 097; c.3574 G>T (NM_000267.3), p.E1192* (nonsense mutation) in exon 27. The read coverage for the tibial pseudarthrosis sample ('Mixed') was 263x, where the *NF1* somatic variant had 16% read frequency (41x variant containing reads which came from both directions). No reads in the blood sample contained the *NF1* variant (91× coverage at this location) (previously reported in Paria *et al*[12]). Data from 50 other exomes were analysed, and no other samples had reads containing this *NF1* variant. Despite the low percentage of reads with the somatic *NF1* variant (16%), Sanger sequencing confirmed the presence of this somatic variant in the tibial pseudarthrosis sample ('Mixed'), while this variant was absent in the blood sample (figure 4C). The relatively low percentage of reads with the somatic *NF1* mutation indicates that not all cells in the extracted tissue contained this variant, indicating an expected mosaicism in the tissue. Before DNA extraction, visual inspection indicated this 'Mixed' tibial sample consisted of both hard and soft tissues (figure 2). To determine if this *NF1* somatic variant could be localised to a specific tissue type, Sanger sequencing of the variant was performed on DNA from a pseudarthrosis sample that contained only the soft tissue ('PA') and DNA from only hard tissue ('Bone' sample, with apparent cortical bone from the tibia), and then compared it to the tibial pseudarthrosis sample that was used for the exome sequencing ('Mixed' sample, containing a combination of soft and hard tissues). Sanger sequencing showed that the presence of the somatic *NF1* variant was higher in the 'PA' sample (only soft tissue) than in the 'Mixed' sample (soft and hard tissue), and entirely absent in both the sample with only hard tissue and the blood sample (figure 4C).

No germline or somatic variants, except for the above described *PTPN11* and *NF1* variants, were identified in the list of 14 other genes involved in the RAS/MAPK pathway. A list of putative somatic variants throughout the genome identified from the entire exome captured region for the 'Mixed' sample is shown in table 1.

DISCUSSION

Even though pseudarthrosis tissue in individuals with NF1 has been shown to be caused by double inactivation of NF1,[10 12] it is not known which specific cell type(s) is the originator of the somatic *NF1* variant that drives the tibial dysplasia and pseudarthrosis. Once a somatic *NF1* variant was identified in this patient's pseudarthrosis sample, further analysis by Sanger sequencing showed that this somatic variant was present in the soft tissue adjacent to the cortical bone at the fracture/pseudarthrosis site but was not present in the compact cortical bone. The tissue harbouring the mutation shows a fibroblastic proliferation. Because an important source of osteoprogenitors contributing to callus formation and bone union comes from the periosteum, it is possible that the *NF1* somatic mutation detected in the proliferative soft tissue at the pseudarthrosis site originally occurred in mesenchymal progenitors from the periosteum. However, the origin of these proliferative cells is still unknown. These results are also consistent with the defect of differentiation observed in *Nf1* deficient osteoprogenitors,[15] which may explain why the mutation is found in proliferative cells and not within cortical bone tissue, as the latter by definition contains mostly mature differentiated osteoblasts and osteocytes.

Since not all NF1 individuals with tibial bowing develop pseudarthrosis and there is wide clinical variability in the degree of bowing, it is possible that there are genetic modifiers of the tibial dysplasia phenotype (germline and/or somatic). In addition, although a recent study showed that the large majority of NF1-associated tibial pseudathrosis samples show double inactivation of *NF1*, a 'second hit' was not uniformly identified in all samples.[12] We initially examined *NF1* and 15 additional genes associated with the RAS/MAPK signalling pathway (see gene list in the Materials and methods section), but no mutations were detected in these genes except for the described *NF1* and *PTPN11* variants. The entire exome captured region for the 'Mixed' sample was analysed for somatic variants by subtracting the germline variants present in the blood sample, and no significant variant/gene except for the second hit in *NF1* was identified (somatic variants, see table 1). However, it is notable that this patient had a germline variant in a *PTPN11*, the gene that encodes the non-receptor protein tyrosine phosphatase SHP2.[20 21] Most mutations in this gene known to cause Noonan syndrome occur in exons 3, 7, 8, and 13.[22] Exon 3 codes for part of N-SH2, and exons 7, 8, and 13 code for the PTP domain.[20] The mutations in these exons are involved in inhibiting the interaction between the N-SH2 and PTP domains.[22] The variant found in our patient (p.T553M) is located within exon 14, at the C-terminus of the protein but close to the PTP domain. This *PTPN11* variant is of unknown significance, in particular because the patient lacks some of the findings of Noonan syndrome (eg, short stature, webbed neck, pulmonic stenosis). This variant has a SIFT (sorting intolerant from tolerant) score of 0.08 and is predicted to be tolerated,[23] but a PolyPhen-2 score of 0.939 and is predicted to be possibly damaging.[24] The multiple protein alignment shows that the amino acid encoded by this triplet is highly conserved across species (figure 4D). The variant chr12:112 940 006; c. 1658C>T, p.T553M (HGMD ID:CS090465, rs148176616) is a rare mutation, found in only six alleles of 13 000 analysed in the 6500 exomes project.[18]

Despite the non-pathogenic prediction of SIFT, the p.T553M *PTPN11* variant has previously been associated with Noonan syndrome, and was found in a fetus that was screened for *PTPN11* mutations upon suspicion of Noonan syndrome in utero. The fetus had an increased nuchal translucency at 15 weeks gestation.[25] This variant was also detected in a lymphoid neoplasm of a patient with T cell acute lymphoblastic leukaemia without Noonan syndrome, but it was not determined whether the variant was of germline or somatic origin.[26 27] Another *PTPN11* variant (p. L560F), in the same region of the protein as p.T553M, was reported in a patient with Noonan syndrome and hypertrophic cardiomyopathy.[21]

It is likely that this mutation is not pathogenic for Noonan syndrome based on the lack of some of the classic clinical features of Noonan syndrome in the child and father. However, a modifying effect of this *PTPN11* variant on the clinical phenotype, including the congenital heart defect and tibial dysplasia, cannot be ruled out.

Additional studies of other NF1 pseudarthrosis cases looking at microdissected sections of the pseudarthrosis region will be insightful to help identify the cellular origin of the initiating 'second hit' or modifiers that lead to tibial pseudarthrosis. Part of the difficulty with identifying somatic mutations in skeletal tissue is due to the complications of extracting high quality DNA from bone, without extracting enzymatic inhibitors (such as calcium), in enough quantities to be used for next generation sequencing. Multiple methods have been employed for extracting DNA from compact bone;[28–31] however, subsequent performance with next generation sequencing has not been reported. The use of the Chemagen Tissue 10 kit (Chemagen, Germany) with a modified extraction procedure allowed us to extract large quantities of high quality DNA from compact bone along with soft tissue from

a pseudarthrosis site, usable for next generation sequencing. Our data show that these methods can be used in future studies involving skeletal tissue in NF1, to identify the affected cell type(s) causing the bony abnormalities seen in NF1.

Author affiliations
[1]ARUP Laboratories, ARUP Institute for Clinical and Experimental Pathology, Salt Lake City, Utah, USA
[2]Department of Pediatrics, Division of Medical Genetics, Stanford University, Stanford, California, USA
[3]Departments of Pediatrics, Division of Medical Genetics, University of Utah, School of Medicine, Salt Lake City, Utah, USA
[4]Department of Pathology, University of Utah, School of Medicine, Salt Lake City, Utah, USA
[5]Shriners Hospital for Children Salt Lake City, Salt Lake City, Utah, USA
[6]Sarah M. and Charles E. Seay Center for Musculoskeletal Research, Texas Scottish Rite Hospital for Children, Dallas, Texas, USA
[7]Department of Pediatrics, UT Southwestern Medical Center, Dallas, Texas, USA
[8]Eugene McDermott Center for Human Growth and Development and UT Southwestern Medical Center, Dallas, Texas, USA
[9]Department of Orthopaedic Surgery, UT Southwestern Medical Center, Dallas, Texas, USA
[10]Vanderbilt Center for Bone Biology; Vanderbilt University Medical Center, Nashville, Tennessee, USA
[11]Departments of Medicine, Vanderbilt University Medical Center, Nashville, Tennessee, USA
[12]Departments of Pharmacology, Vanderbilt University Medical Center, Nashville, Tennessee, USA
[13]Department of Cancer Biology, Vanderbilt University Medical Center, Nashville, Tennessee, USA

Acknowledgements The authors thank the Shriners Hospital for Children (Salt Lake City, Utah, USA) and their clinicians and coordinators including John Carey, Stephen Santora, Jacque D'Astous, Michael Pond, Janice Davis, Jeanne Siebert, Susan Geyer, and Austin Stevens for their role in consenting and collecting surgical tissues and for their input. This work was supported by grants from the Department of Defense (award W81XWH-11-1-250), and Shriners Hospital for Children (Salt Lake City). Portions of the research were supported by the University of Utah Clinical Genetics Research Program (CGRP) and the National Center for Research Resources and National Center for Advancing Translational Sciences at the National Institutes of Health (UL1RR025764). The authors would like to thank the NHLBI GO Exome Sequencing Project and its ongoing studies which produced and provided exome variant calls for comparison: the Lung GO Sequencing Project (HL-102923), the WHI Sequencing Project (HL-102924), the Broad GO Sequencing Project (HL-102925), the Seattle GO Sequencing Project (HL-102926), and the Heart GO Sequencing Project (HL-103010).

Contributors DAS and RM were responsible for the overall content; DWS, RLM, DAS, and RM designed the study, performed the experiments, and wrote and edited the manuscript; AHG performed histologic analysis and interpretation, and edited the manuscript; DHV designed the study and edited the manuscript; HH performed consenting, collected data and samples, and edited manuscript; MDE and TH provided clinical data and samples, and edited the manuscript; JJR and FE performed data analysis and interpretation, and edited the manuscript.

Competing interests None.

Patient consent Obtained.

Ethics approval

Provenance and peer review Not commissioned; externally peer reviewed.

REFERENCES

1 Allanson JE. Noonan syndrome. *J Med Genet* 1987;24:9–13.
2 Van der Burgt I. Noonan syndrome. *Orphanet J Rare Dis* 2007;2:4.
3 Lepri F, Scavelli R, Digilio M, Gnazzo M, Grotta S, Dentici ML, Pisaneschi E, Sirleto P, Capolino R, Baban A, Russo S, Franchin T, Angioni A, Dallapiccola B. Diagnosis of Noonan syndrome and related disorders using targeted next generation sequencing. *BMC Med Genet* 2014;15:14.
4 Bertola DR, Pereira AC, Passetti F, De Oliveira PS, Messiaen L, Gelb BD, Kim CA, Krieger JE. Neurofibromatosis-Noonan syndrome: molecular evidence of the concurrence of both disorders in a patient. *Am J Med Genet Part A* 2005;136A:242–5.
5 Nyström AM, Ekvall S, Strömberg B, Holmström G, Thuresson AC, Annerén G, Bondeson ML. A severe form of Noonan syndrome and autosomal sominany café-au-lait spots—evidence for different genetic origins. *Acta Paediatr* 2009;98:693–8.
6 Thiel C, Wilken M, Zenker M, Sticht H, Fahsold R, Gusek-Schneider GC, Rauch A. Independent NF1 and PTPN11 mutations in a family with neurofibromatosis-Noonan syndrome. *Am J Med Genet Part A* 2009;149A:1263–7.
7 Prada CE, Zarate YA, Hagenbuch S, Lovell A, Schorry KE, Hopkin RJ. Lethal presentation of neurofibromatosis and Noonan syndrome. *Am J Med Genet Part A* 2011;155A:1360–6.
8 Crawford AH, Schorry EK. Neurofibromatosis in children: the role of the orthopaedist. *J Am Acad Orthop Surg* 1999;7:217–30.
9 Stevenson DA, Little D, Armstrong L, Crawford AH, Eastwood D, Friedman JM, Greggi T, Schindeler A, Schorry EK, Wilkes D, Viskochil DH, Yang FC, Elefteriou F. Approaches to treating NF1 tibial pseudarthrosis: consensus from the Children's Tumor Foundation NF1 Bone Abnormalities Consortium. *J Pediatr Orthop* 2013;33:269–75.
10 Stevenson DA, Zhou H, Ashrafi S, Messiaen LM, Carey JC, D'Astous JL, Santora SD, Viskochil DH. Double inactivation of NF1 in tibial pseudarthrosis. *Am J Hum Genet* 2006;79:143–8.
11 Friedman JM, Birch PH. Type 1 neurofibromatosis: a descriptive analysis of the disorder in 1728 patients. *Am J Med Genet* 1997;70:138–43.
12 Paria N, Cho TJ, Choi IH, Kamiya N, Kayembe K, Mao R, Margraf RL, Obermosser G, Oxendine I, Sant DW, Song MH, Stevenson DA, Viskochil DH, Wise CA, Kim HK, Rios JJ. Neurofibromin deficiency-associated transcriptional dysregulation suggests a novel therapy for tibial pseudoarthrosis in NF1. *J Bone Miner Res* 2014;29:2636–42.
13 Sakamoto A, Yoshida T, Yamamoto H, Oda Y, Tsuneyoshi M, Iwamoto Y. Congenital pseudarthrosis of the tibia: analysis of the histology and the NF1 gene. *J Orthop Sci* 2007;12:361–5.
14 Leskelä HV, Kuorilehto T, Risteli J, Koivunen J, Nissinen M, Peltonen S, Kinnunen P, Messiaen L, Lehenkari P, Peltonen J. Congenital pseudarthrosis of neurofibromatosis type 1: impaired osteoblast differentiation and function and altered NF1 gene expression. *Bone* 2009;44:243–50.
15 de la Croix Ndong J, Makowski AJ, Uppuganti S, Vignaux G, Ono K, Perrien DS, Joubert S, Baglio SR, Granchi D, Stevenson DA, Rios JJ, Nyman JS, Elefteriou F. Asfotase-α improves bone growth, mineralization and strength in mouse models of neurofibromatosis type-1. *Nat Med* 2014;20:904–10.
16 Durtschi J, Margraf RL, Coonrod EM, Mallempati K, Voelkerding KV. VarBin, a novel method for classifying true and false positive variants in NGS data. *BMC Bioinformatics* 2013;14(Suppl 13):S2.
17 1000 Genomes Project Consortium, Abecasis GR, Altshuler D, Auton A, Brooks LD, Durbin RM, Gibbs RA, Hurles ME, McVean GA. A map of human genome variation from population-scale sequencing. *Nature* 2010;467:1061–73.
18 Exome Sequencing Project (ESP 6500). Exome Variant Server, NHLBI GO Exome Sequencing Project (ESP), Seattle, WA. http://evs.gs.washington.edu/EVS/ (accessed Jun 2014).
19 Pros E, Gómez C, Martin T, Fábregas P, Serra E, Lázaro C. Nature and mRNA effect of 282 different NF1 point mutations: focus on splicing alterations. *Hum Mutat* 2008;29:E173–93.
20 Hof P, Pluskey S, Dhe-Paganon S, Eck MJ, Shoelson SE. Crystal structure of the tyrosine phosphatase SHP-2. *Cell* 1998;92:441–50.
21 Sarkozy A, Conti E, Seripa D, Digilio MC, Grifone N, Tandoi C, Fazio VM, Di Ciommo V, Marino B, Pizzuti A, Dallapiccola B. Correlation between PTPN11 gene mutations and congenital heart defects in Noonan and LEOPARD syndromes. *J Med Genet* 2003;40:704–8.
22 Tartaglia M, Mehler EL, Goldberg R, Zampino G, Brunner HG, Kremer H, van der Burgt I, Crosby AH, Ion A, Jeffery S, Kalidas K, Patton MA, Kucherlapati RS, Gelb BD. Mutations in PTPN11, encoding the protein tyrosine phosphatase SHP-2, cause Noonan syndrome. *Nat Genet* 2001;29:465–8.
23 Kumar P, Henikoff S, Ng PC. Predicting the effects of coding non-synonymous variants on protein function using the SIFT algorithm. *Nat Protoc* 2009;4:1073–81.
24 Adzhubei IA, Schmidt S, Peshkin L, Ramensky VE, Gerasimova A, Bork P, Kondrashov AS, Sunyaev SR. A method and server for predicting damaging missense mutations. *Nat Methods* 2010;7:248–9.
25 Lee KA, Williams B, Roza K, Ferguson H, David K, Eddleman K, Stone J, Edelmann L, Richard G, Gelb BD, Kornreich R. PTPN11 analysis for the prenatal diagnosis of Noonan syndrome in fetuses with abnormal ultrasound findings. *Clin Genet* 2009;75:190–4.
26 COSMIC Catalogue of Somatic Mutations in Cancer Server Link. http://cancer.sanger.ac.uk/cancergenome/projects/cosmic/ (accessed Sep 2014).
27 Atak ZK, Gianfelici V, Hulselmans G, De Keersmaecker K, Devasia AG, Geerdens E, Mentens N, Chiaretti S, Durinck K, Uyttebroeck A, Vandenberghe P, Wlodarska I, Cloos J, Foà R, Speleman F, Cools J, Aerts S. Comprehensive analysis of transcriptome variation uncovers known and novel driver events in T-cell acute lymphoblastic leukemia. *PLoS Genet* 2013;9:e1003997.
28 Hänni C, Brousseau T, Laudet V, Stehelin D. Isopropanol precipitation removes PCR inhibitors from ancient bone extracts. *Nucleic Acids Res* 1995;23:881–2.
29 Jakubowska J, Maciejewska A, Pawlowski R. Comparison of three methods of DNA extraction from human bones with different degrees of degradation. *Int J Legal Med* 2012;126:173–8.
30 Loreille OM, Diegoli TM, Irwin JA, Coble MD, Parsons TJ. High efficiency DNA extraction from bone by total demineralization. *Forensic Sci Int Genet* 2007;1:191–5.
31 Vince A, Poljak M, Seme K. DNA extraction from archival Giemsa-stained bone-marrow slides: comparison of six rapid methods. *Br J Haematol* 1998;101:349–51.

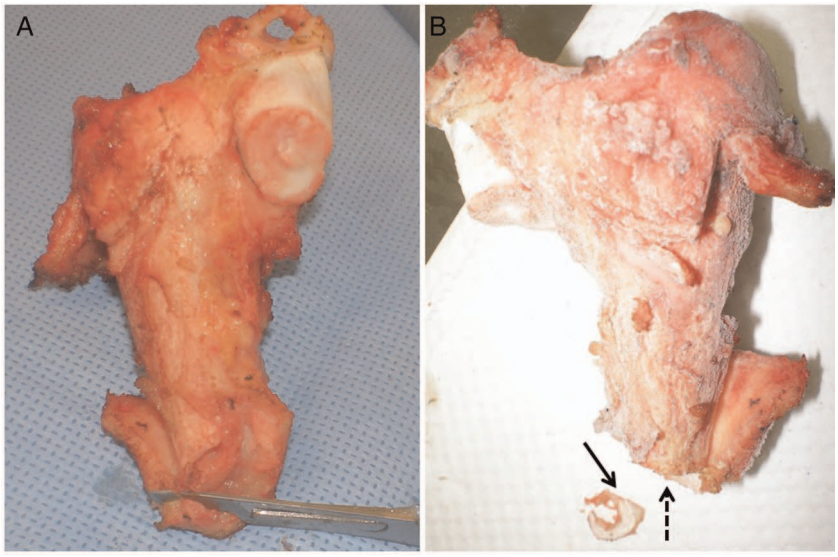
A
B